MASS. INST. OF TECHNOLOGY
APR 5 1966
LIBRARIES

NUCLEAR MAGNETIC RESONANCE IN CHROMIUM TRIBROMIDE

by

Stephen David Senturia
B. A., Harvard College
(1961)

SUBMITTED IN PARTIAL FULFILLMENT
OF THE REQUIREMENTS FOR THE
DEGREE OF DOCTOR OF
PHILOSOPHY

at the

MASSACHUSETTS INSTITUTE OF
TECHNOLOGY

June 1966

Signature of Author ... .
Department of Physics, March 8, 1966

Certified by .....
Thesis Supervisor

Accepted by ... .
Chairman, Departmental Committee
on Graduate Students

Nuclear Magnetic Resonance in Chromium Tribromide

by

Stephen David Senturia

Submitted to the Department of Physics on March 8, 1966 in partial fulfillment of the requirement for the degree of Doctor of Philosophy.

Abstract

This thesis is a study of ferromagnetic chromium tribromide (Curie temperature, Tc = 32.56°K) using the techniques of nuclear magnetic resonance (NMR). The frequencies of NMR lines due to Cr^{53}, Br^{79}, and Br^{81} nuclei located inside ferromagnetic domains were studied as functions of temperature.

The frequencies of the Cr^{53} triplet were measured between 4.2°K and 29.74°K (0.91 Tc). Analysis of this data yields (i) the magnitudes and temperature dependences of the components of the electric field gradient tensor at a chromium site; and (ii) the magnitude and temperature dependence of the magnetic hyperfine field at a chromium site set up by the aligned Cr^{3+} spin. The chromium site hyperfine field is proportional to the magnetization, enabling the temperature dependence of the magnetization to be determined up to 0.91 Tc. Above 29.74°K, the Cr^{53} lines faded out. It was possible, however, to extend the determination of the temperature dependence of the magnetization to higher temperatures with the bromine NMR lines.

We have discovered and identified Br^{79} and Br^{81} NMR lines in the ferromagnetic state of $CrBr_3$. These lines arise from the splitting of the pure quadrupole resonances by a magnetic hyperfine field. They were studied, together with two additional lines found by Gossard, et. al.,* in the temperature range 4.2°K - 32.35°K. The pure quadrupole resonance frequencies for the two bromine isotopes were measured at 34.5°K, just above the Curie temperature. Analysis of the bromine NMR data yields (i) the magnitudes and temperature dependences of the components of the electric field gradient tensor at the bromine sites; and (ii) the magnitude, direction, and temperature dependence of the magnetic hyperfine field at the bromine sites. Since the bromine hyperfine field, like the chromium hyperfine field, is proportional to the magnetization, the determination of the temperature dependence of the magnetization can be extended to 32.35°K (0.993 Tc).

The temperature dependence of the magnetization in the vicinity of the Curie point is fitted to various suggested theoretical forms. The most commonly used form is the simple power law: $M(T)/M(0) = D(1 - T/Tc)^{\beta}$.

In $CrBr_3$, it is found that $\beta = 0.365 \pm 0.015$, a significant departure from the very accurate 1/3 power law behavior previously observed in other magnetic materials. Two features of the Hamiltonian appropriate to the $CrBr_3$ spin system are suggested as possible origins of the unique critical behavior of the $CrBr_3$ magnetization.

An anisotropic thermal expansion anomaly at the $CrBr_3$ Curie point is postulated to explain the small observed temperature dependences in the components of the electric field gradient tensors at the bromine and chromium sites.

Finally, the NMR lines in ferromagnetic $CrBr_3$ are found to be ideally suited for use as highly accurate, reproducible thermometers between 1.5°K and 29°K. The sensitivity is estimated to be 2 millidegrees or better over this temperature range. A priliminary calibration above 4.2°K, good to ± 0.02°K, is provided.

* A. C. Gossard, V. Jaccarino, E. D. Jones, J. P. Remeika, and R. Slusher, Phys. Rev., 135, A1051 (1964).

Thesis Supervisor: George B. Benedek

Title: Professor of Physics

TABLE OF CONTENTS

Chapter I.	Introduction	9
Chapter II.	Experimental Methods	18
	A. Introduction	18
	B. Temperature Control and Measurement	18
	1. General Requirements	18
	2. Controlled Heat Leak Temperature Regulation	19
	3. Thermal Gradients	29
	4. Temperature Measurement and Thermometer Calibration	31
	C. NMR Detection	34
	1. Spectrometer	34
	2. Features of the Audio Detection System	38
Chapter III.	Experimental Data	41
	A. Introduction	41
	B. NMR Data	41
	1. Chromium NMR Frequencies	41
	2. Bromine NMR Frequencies	46
	3. NMR Linewidths	47
	C. Magnetic Resonance Thermometry Using $CrBr_3$	54
	1. Sensitivity	55
	2. Reproducibility	58

Chapter IV.	Interpretation of Experimental Data	60
	A. Introduction	60
	B. General I = 3/2 Hamiltonian	60
	1. Hyperfine Hamiltonian	61
	2. Quadrupole Hamiltonian	64
	3. Combined Hamiltonian	66
	C. Interpretation of the Chromium NMR Data	67
	D. Identification of the Bromine NMR Lines	70
	1. Origin of the Bromine Lines	70
	2. Identification of Transitions	86
	E. Detailed Analysis of the Bromine NMR Data	88
	1. Scope of the Problem	88
	2. Reverse Eigenvalue Problem Below 29.74°K	88
	3. Use of Constant Parameters Below 20°K	91
	4. Necessity of Using Temperature Dependent Parameters Above 20°K	94
	5. Thermal Expansion Anomaly - Suggested and Discussed	100
	6. Results of the Data Analysis	107
Chapter V.	Critical Behavior	117
	A. Introduction	117
	B. Critical Behavior of the Magnetization - Experimental	118
	1. Simple Power Law	118
	2. Buckingham's Function	125

C. Critical Behavior of the Magnetization - Discussion 126

1. The Heisenberg Exchange Hamiltonian and its Offspring 127

2. The $CrBr_3$ Hamiltonian 128

D. Maximum Loss Point 133

Chapter VI. Conclusions 136

References 138

Acknowledgements 141

Biographical Note 142

List of Illustrations

Illustration			Page
Fig.	1	$CrBr_3$ crystal structure.	11
Fig.	2	Dewar assembly.	22
Fig.	3	Block assembly.	23
Fig.	4	Heater control circuit.	27
Fig.	5	Kushida spectrometer.	35
Fig.	6	Block diagram of audio detection system.	39
Fig.	7	Low frequency NMR data; Cr^{53}, Br^{79}, and Br^{81}.	44
Fig.	8	Cr^{53} line shape.	45
Fig.	9	High frequency NMR data; Br^{79} and Br^{81}.	52
Fig.	10	Temperature dependence of the Cr^{53} linewidth.	53
Fig.	11	Sensitivity of NMR lines as thermometers.	57
Fig.	12	Cr^{53} energy levels.	69
Fig.	13	Bromine site - nearest neighbor geometry.	72
Fig.	14	Bromine site - ion locations for point charge calculations	74
Fig.	15	Typical bromine energy levels ($\eta = 0$).	80
Fig.	16	q^{79} as a function of temperature for several values of η.	93
Fig.	17	Symmetry of thermal expansion peak about T_c, illustrated with q^{79}.	106
Fig.	18	Final temperature dependent Hamiltonian parameters	110
Fig.	19	Simple power law fit to reduced magnetization - FULL solution.	121
Fig.	20	Simple power law fit to reduced magnetization - HALF solution.	122
Fig.	21	$CrBr_3$ simplified magnetic lattice.	130

List of Tables

Table			Page
Table	I	NMR Frequencies and Quadrupole Splitting for Cr^{53} Nuclei	42
Table	II	NMR Frequencies for Br^{79} and Br^{81} Nuclei - Low Frequency Lines	48
Table	III	NMR Frequencies for Br^{79} and Br^{81} Nuclei - High Frequency Lines	50
Table	IV	Comparison of Theory of Bromine Line Origin with Experiment	85
Table	V	Constant Hamiltonian Parameters	95
Table	VI	Final Temperature Dependent Hamiltonian Parameters	108
Table	VII	Temperature Dependence of the $CrBr_3$ Magnetization	
		a. Chromium Data	114
		b. Bromine Data	115
Table	VIII	Simple Power Law Fit to Reduced Magnetization in Critical Region	123

Chapter I

Introduction

This thesis is a study of ferromagnetic chromium tribromide using the techniques of nuclear magnetic resonance.

The most significant characteristic of a ferromagnet is the existence of a spontaneous magnetization below the Curie temperature. This magnetization, decreasing gradually with increasing temperature, vanishes comparatively suddenly at the Curie temperature. A correct theory of ferromagnetism must be capable of explaining not only the existence of the magnetization, but also its observed temperature dependence.

Until recently, it has not been possible to test precisely the proposed theoretical models of ferromagnetism. All the theories assumed that the magnetic moments which interact and become aligned at low temperatures are localized at lattice points. The familiar ferromagnets, though, iron, cobalt, nickel and their alloys are metals, electrical conductors with free or nearly-free electrons. Furthermore, the classical techniques for measuring the magnetization do not determine directly the microscopic spontaneous magnetization inside a ferromagnetic domain. Rather they measure a macroscopic sample magnetization in a large external field. The effects of the susceptibility of the sample and the demagnetizing field are always included in the measured magnetization.

Within the last decade, two major advances have occurred which enable us to make detailed comparisons between theory and experiment:

1. The development of nuclear magnetic resonance (NMR) techniques in magnetic systems permits the temperature dependence of the magnetization to be measured with unprecedented accuracy. NMR experiments can provide directly the time average alignment of each spin in the absence of an external field. The nucleus probes the microscopic spontaneous magnetization, and this magnetization is not altered by the presence of external and demagnetizing fields.

2. Ferromagnetic materials have been discovered which are electric insulators. The insulating property assures that the magnetic moments are localized, making these materials ideal systems in which to test theories of ferromagnetism.

$CrBr_3$ was one of the first insulating ferromagnets in which an NMR line was identified which could be related to the magnetization.[1, 2] The fruitfulness of previous NMR studies of antiferromagnetic manganese fluoride[3-8] led us to undertake a detailed NMR study of $CrBr_3$. The primary goal was to measure with precision the temperature dependence of the magnetization from low temperatures to the Curie point (32.56°K).

The crystal structure[9] of $CrBr_3$ is shown in Fig. 1. The chromium atoms are arranged in honeycomb layers, each layer of chromium atoms being sandwiched between two layers of nearly close-packed bromine atoms. The macroscopic properties of the material reflect this structure. The crystallites are flaky and slip easily in the plane of the hexagonal layers. The flakes are very plastic, deforming easily, and care must be taken to avoid straining the samples.

$CrBr_3$ was observed to be a ferromagnet by Tsubokawa[1] in 1960.

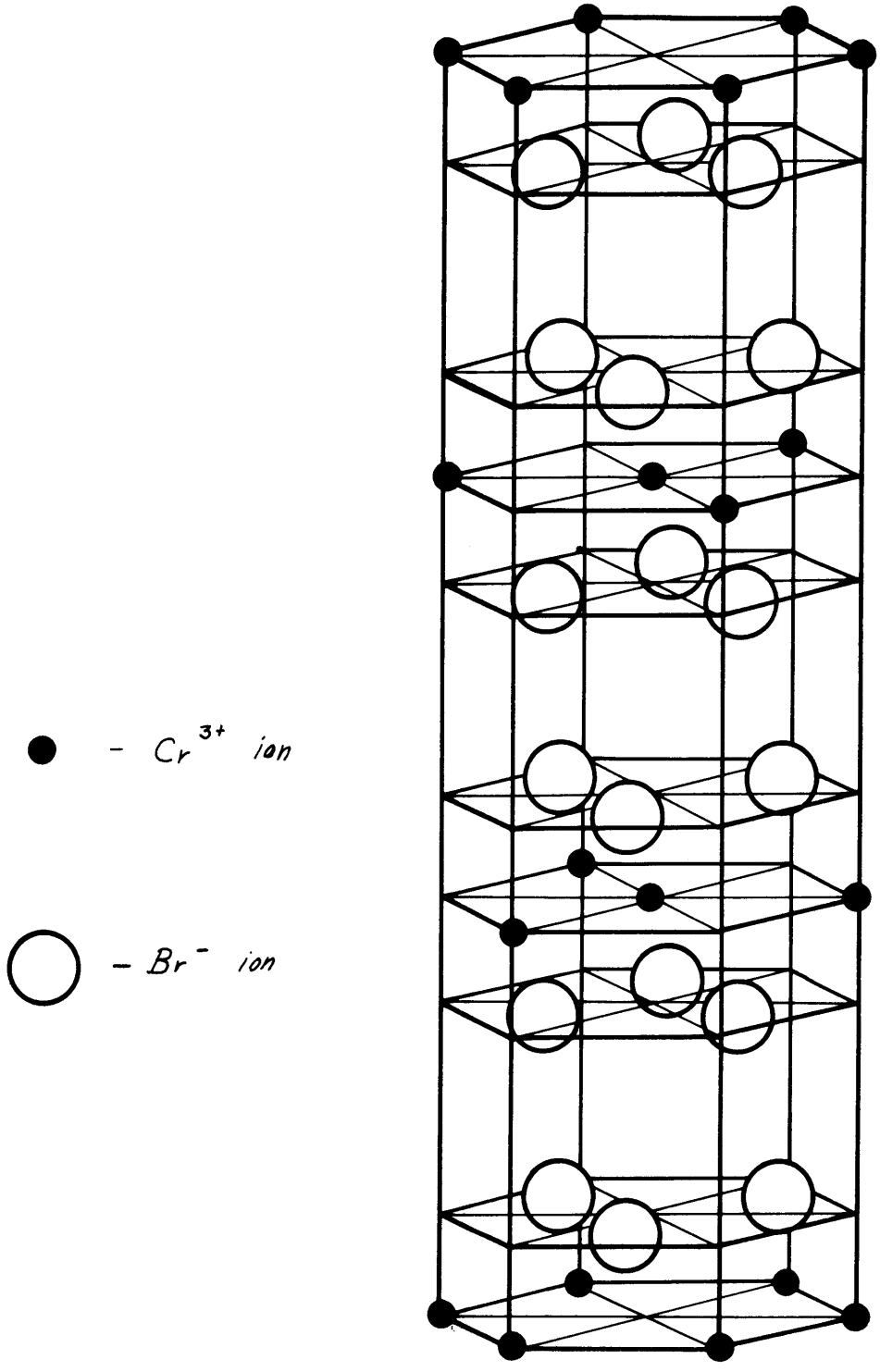

Fig. 1 $CrBr_3$ Crystal Structure

He measured the saturation magnetization at absolute zero to be 3 Bohr magnetons per chromium atom, indicating that the magnetic moment of the Cr^{3+} ions comes entirely from the spins of the three unpaired electrons. This material, then, has localized spin magnetic moments which exhibit parallel long range order at low temperatures. It is very close to an ideal system for comparison with theoretical calculations. The only departure from ideality lies in the marked anisotropy of the crystal lattice. The anisotropy is reflected in the model for the super-exchange coupling which has been used to account for the ferromagnetic behavior of $CrBr_3$.[1, 2] In this model, the exchange coupling of a spin to its nearest neighbors within a hexagonal plane is about sixteen times as strong as the coupling to the nearest spins in adjacent layers.[10] One pictures the ferromagnetic state as consisting of strongly ordered sheets of spins which have a weak tendency to line up parallel to one another.

The utility of NMR in studying the magnetization of an ordered spin system depends on the accuracy with which an NMR frequency can be related to the magnetization. In virtually every magnetic material studied thus far by NMR techniques, the relation between the particular NMR frequency under study and the magnetization has been quite simple. The presence of a large unpaired electron spin on an ion tends to break up the closed shells of the core electrons, modifying the spatial wave functions for electrons which differ only in their spin state. This results in a slight unbalance in the core spin probability density which creates a large magnetic field at the nuclear site. This field, called the hyperfine field, is proportional to the electron spin and fluctuates at frequencies

characteristic of exchange energies. Since the fluctuations in the hyperfine field are very rapid compared to the nuclear Larmor frequency, the nucleus can only respond to the time-average hyperfine field, which has a value proportional to the magnetization. If the hyperfine interaction is the only significant interaction involving the nuclear spin states, then the NMR frequency (ν) of the nucleus in question will be proportional to the magnetization (M):

$$\nu(T) = A\ M(T) \qquad (1-1)$$

The coupling constant A depends only on the occupied electronic wave functions of the ion, and therefore in an insulator can be expected to be independent of temperature except for a possible contribution due to thermal expansion of the lattice.

In 1961, Gossard, Jaccarino, and Remeika[2] found the Cr^{53} resonance in ferromagnetic $CrBr_3$ at low temperatures. The Cr^{53} nuclei interact with a large hyperfine field (about 240 kG at 4.2°K) due to the aligned Cr^{3+} spins. The only other interaction involving the nuclear moment is a very weak electric quadrupole coupling between the nuclear quadrupole moment and a small electric field gradient due to a departure from octahedral point symmetry at the chromium site.[2] The quadrupole coupling causes a splitting of what would be a single NMR line into a triplet, the central member of which is unshifted from the value it would have in the absence of the quadrupole interaction. Thus, the central Cr^{53} NMR frequency is proportional to the magnetization, and is an appropriate resonance for making direct measurements of the temperature

dependence of the magnetization.

The temperature dependence of the Cr^{53} NMR frequency has already been used to study the validity of spin wave theory. Gossard, Jaccarino and Remeika[2] fit their low temperature Cr^{53} NMR data to a theoretical expression based on non-interacting spin wave theory. Davis and Narath,[10] using Cr^{53} NMR data up to 60% of the Curie temperature showed that a spin wave theory in which interactions between spin waves are taken into account by a renormalization procedure applied to the spin wave dispersion relation could satisfactorily represent the temperature dependence of the magnetization throughout the temperature range over which they had data.

In the present work, we report measurements of the temperature dependence of the triplet of Cr^{53} NMR lines from 4.2°K to 29.74°K, overlapping and extending previous work. From this data we obtain directly the temperature dependence of the magnetization from the low temperature spin-wave region up to 91% of T_c, where the effects of the sudden vanishing of the magnetization at T_c are beginning to appear. In addition, we observe a small temperature dependence in the quadrupole splitting of the Cr^{53} triplet. This effect had not been seen by the previous workers.

We would have liked to continue the measurements of the Cr^{53} NMR frequencies closer to the Curie temperature, but the resonances faded out above 29.74°K. The hope of extending the measurements of the temperature dependence of the magnetization closer to T_c was revived by the accidental discovery of a pair of very strong NMR lines which had

temperature dependences quite similar to the Cr^{53} lines.[11] We proved that these lines came from the two isotopes of bromine nuclei Br^{79}, and Br^{81}.

Like the chromium nuclei, the bromine nuclei experience a hyperfine field due to the aligned chromium spins on neighboring ions. What happens in this case is that the large unpaired spin on the chromium ion causes the closed shell Br^- ion to be polarized in much the same way as the spin density unbalance developes in the chromium ionic core. This effect, called the transferred hyperfine interaction, has been observed and carefully studied in MnF_2.[3-6]

In addition to the magnetic hyperfine interaction, a strong electric field gradient at the bromine site interacts with the nuclear quadrupole moment. This quadrupole interaction has a magnitude comparable to the hyperfine interaction and produces strong mixing of the simple Zeeman spin eigenstates. As a result, the bromine NMR frequencies do not measure directly the time average alignment of the Cr^{3+} spins.

The existence of the bromine quadrupole interaction above the Curie temperature had been demonstrated by Barnes and Segel in 1959.[12] The temperature dependence of the Br^{81} pure quadrupole resonance between 77°K and room temperature has since been measured by van de Vaart.[13] In spite of these experiments, very little was known about the details of the quadrupole interaction Hamiltonian, details such as the direction of the principal axes of the electric field gradient tensor and the size of the asymmetry parameter. Furthermore, since the bromine nuclear resonances below T_c were new, nothing was known about the

magnitude, direction, and temperature dependence of the hyperfine field at a bromine site. The task of sorting out these details was greatly aided by the subsequent report of a second pair of bromine resonances by Gossard and co-workers.[14]

In the present work we report the results of a thorough NMR study of these four new bromine resonances. We have measured the temperature dependences of the four bromine resonance frequencies in the ferromagnetic state from 4.2°K up to as high as 32.35°K for the strongest line of the four. We have also measured the pure quadrupole resonance frequencies for both Br^{79} and Br^{81} nuclei at 34.5°K, just above the Curie point. Analysis of this data yields the following information:

1. We have determined the magnitude, direction, and temperature dependence of the magnetic hyperfine field at a bromine site from 4.2°K to 32.35°K, or up to 0.993 T_c. As in the case of the chromium nucleus, the hyperfine field at a bromine nucleus is proportional to the magnetization; thus the bromine NMR data enable us to extend our determination of the temperature dependence of the magnetization up to 0.993 T_c.

2. We have determined the magnitude and temperature dependence of the components of the electric field gradient tensor at a bromine site.

3. We have shown that the temperature dependences of several of the NMR lines in ferromagnetic chromium tribromide can be used as sensitive, highly reproducible thermometers below 30°K.

4. We have examined the temperature dependence of the magnetization in the vicinity of the Curie point by fitting the data to various

suggested theoretical forms. The most commonly used form is the following, in which the magnetization M(T), normalized by its value at absolute zero, is expressed as a function of T/T_c:

$$\frac{M(T)}{M(O)} = D\left(1-\frac{T}{T_c}\right)^{\beta} \qquad (1-2)$$

Two previous measurements by Heller and Benedek of the exponent β in magnetic insulators yielded values of 0.333 ± 0.003 in antiferromagnetic MnF_2,[7,8] and 0.33 ± 0.015 in ferromagnetic EuS.[15] In the present work we find a definite departure from this 1/3 power law behavior. In $CrBr_3$, the best fit to the data occurs with $\beta = 0.365 \pm 0.015$. Furthermore, while the temperature above which Eq. 1-2 would fit the data was $0.90\ T_c$ in MnF_2 and $0.92\ T_c$ in EuS, we find that Eq. 1-2 can fit the $CrBr_3$ data only above $0.955\ T_c$, a very limited temperature range.

5. From the observed temperature dependences of the components of the electric field gradient tensor at a bromine site, we infer that there must be a rather large anomaly in the thermal expansion of $CrBr_3$ at its Curie point.

Finally, it should be mentioned that we have not attempted to apply theoretical models of ferromagnetism to the data away from T_c because the theories in this temperature range do not yield simple functional expressions which can be readily fit to our data. Nonetheless, our precise data on the temperature dependence of the magnetization is now available throughout the region where spin wave renormalization should apply.

Chapter II

Experimental Methods

A. Introduction

The experimental apparatus and techniques used in the investigations of this thesis will be discussed in two parts. The first part will deal with the methods used to obtain, regulate and measure sample temperatures in the range 4.2°K - 35°K. In the second part, the NMR spectrometer and associated NMR detection equipment will be described.

B. Temperature Control and Measurement

1. General Requirements

The general requirements for a temperature control system for this experiment were threefold:

a. The sample must be located in an isothermal environment whose temperature can be adjusted throughout the desired range.

b. It must be possible to stabilize the temperature to within a millidegree for long times (up to an hour), or to sweep the temperature at a slow, uniform rate.

c. A calibrated thermometer must be located in a position such that thermal gradients between the sample and thermometer are too small to introduce significant errors into the temperature measurements.

The particular range of temperature required for this experiment eliminated the possibility of pumping on cryogenic fluids to achieve temperature control. Therefore, a controlled heat leak system was

devised, using liquid helium as the basic cryogenic fluid. While both liquid hydrogen and liquid neon have boiling points closer to the $CrBr_3$ Curie temperature of 32.56°K, both were rejected for use, the former because of its extreme flammability, the latter because of its cost. The actual cryostat used in this experiment was a close copy of a system designed by Peter Heller.[18]

2. Controlled Heat Leak Temperature Regulation

The basic features of controlled heat leak temperature regulation are as follows: An isothermal environment for the sample is provided by enclosing the sample in a block, typically copper, which has a high thermal conductivity and also a large thermal mass (to damp out fast temperature fluctuations). This block is cooled by placing it in weak thermal contact with a cold, stable bath, usually a cryogenic fluid. The equilibrium temperature of the block is determined by a dynamic balance between a) the rate of heat loss by the block to the bath, and b) the rate of heat flux into the block from the experimental leads and from a heater. Regulation and sweeping of the sample temperature are provided by manual and/or servo control of the power supplied to the heater. The quality of temperature regulation which can be achieved by such a system depends primarily on the stability of the bath, the sensitivity and stability of the heater control system, and on the amount of thermal contact between room temperature and the block, and between the block and the bath.

Use of the Helium Vapor Column as a Bath A typical method for building controlled heat leak systems is to surround the block with a

vacuum jacket and submerge the entire assembly in the cryogenic fluid. In this case, temperature differences between block and bath of up to thirty degrees would have to be used. In order to support a thirty degree temperature gradient without a large flow of heat through the block (which would create undesired gradients between sample and thermometer), the design of the vacuum jacket would be critical.

Peter Heller considered the possibility of using the helium vapor above the boiling liquid helium as a bath in which to suspend the block. The advantage of doing so is readily apparent: between the liquid helium level and the top of the helium dewar, there is a large thermal gradient. By positioning the block at different heights in the vapor column, a wide range of equilibrium block temperatures is readily accessible.

The major difficulty of using the vapor column as a bath is poor temperature stability. While the temperature of the boiling liquid helium is quite steady, the temperature profile in the vapor column above the liquid depends on several factors: a) the level of the liquid helium, which is, of course, changing with time; b) the temperature at the top of the dewar flask; and c) the rate of flow of helium vapor through the dewar, i. e., the boiling rate of the liquid. If the vapor column is to serve as a useful bath for millidegree temperature control, these three factors must be brought under control. In our cryostat, described below, a design developed by Peter Heller which successfully solved the vapor stabilization problem, was employed.

Liquid Helium Cryostat Using a Vapor Bath. Schematic drawings

of the cryostat and block assemblies are shown in Figs. 2 and 3 respectively. The double walled dewars were made of glass; the helium dewar inner diameter was 1-7/8". The block was an OFHC copper cylinder, 1-1/4" in diameter and 3" long. Weak thermal contact with the bath was provided by the block insulation which consisted of a 1/4" thick styrofoam jacket and a 1" thick styrofoam cap. The transmission line connected the NMR coil to the spectrometer and also served to support the block.

Between the liquid helium level and the block was a copper platform which was thermally connected to the liquid helium by a tubular copper sleeve. Because of the high thermal conductivity of this sleeve, the temperature of the platform was close to 4.2°K and was not strongly dependent on the liquid helium level. If the flow rate of helium vapor past the platform was not too large, the vapor temperature at the platform would equal the platform temperature, and would be stable in time.

A second stable temperature point was provided by the arrangement of the brass dewar cap. This cap was insulated from room temperature by a 1" thick styrofoam cover, and insulated from the helium vapor by a 4" thick styrofoam plug. A large number of copper fingers were soldered to the cap and dipped into the liquid nitrogen surrounding the helium dewar. The nitrogen was maintained in contact with the fingers by an automatic filling system. The combined effect of the arrangement of styrofoam and copper was to maintain the dewar cap at a temperature near 77°K. If the flow of vapor out of the top of the dewar was sufficiently slow, the vapor at the top of the dewar would

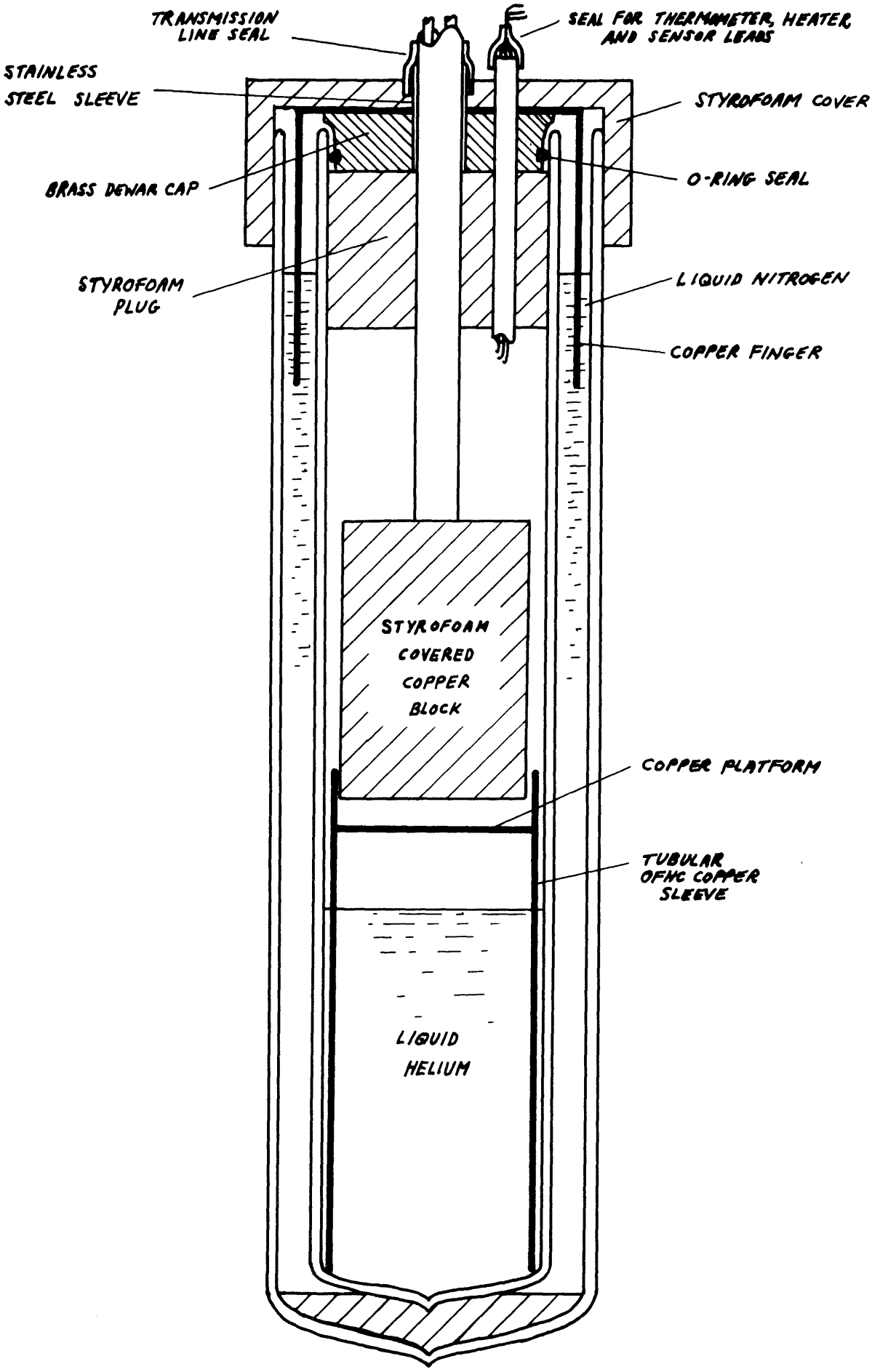

Fig. 2 Dewar Assembly

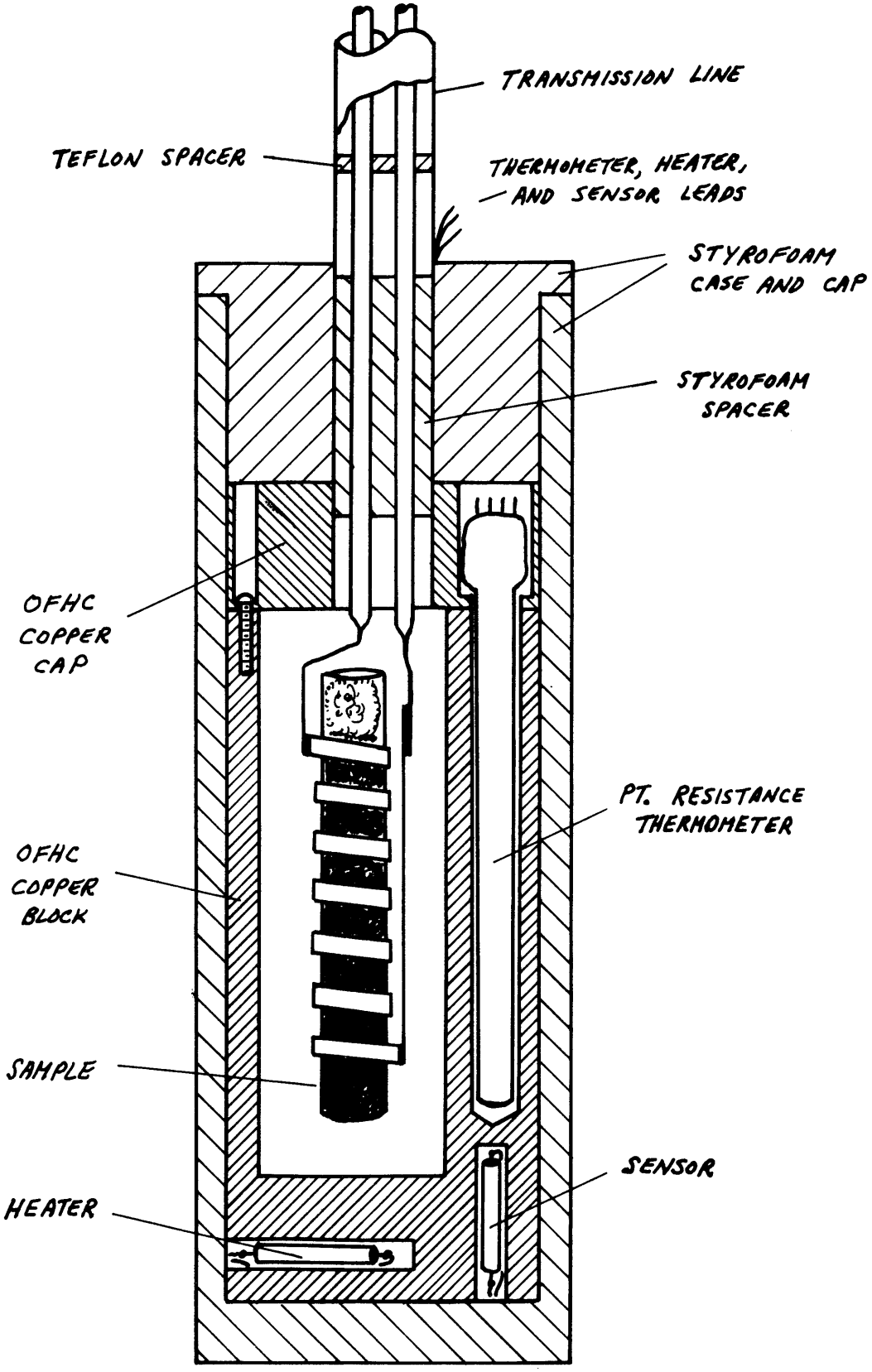

Fig. 3 Block Assembly

reach a stable temperature.

Few special precautions were required to assure a vapor flow rate within satisfactory limits. The silvered glass dewars, the liquid nitrogen jacket, and the brass dewar cap clamped near nitrogen temperature all served to isolate the liquid helium quite well. In the absence of block heater power, a full load of liquid helium (just over one liter) would last more than 24 hours.

The dewar was sealed to prevent convective turbulence in the vapor column and to prevent the accumulation of ice and solid air which would disrupt the temperature profile and impede the adjustment of block position. The dewar cap was sealed with an O-ring (See Fig. 2). The thermometer leads and other leads were brought out through a stainless steel tube at the end of which was a plastic tube pinched off tightly. The transmission line seal had to allow vertical movement of the block. A stainless steel tube, slightly larger than the transmission line, was brought up from the dewar cap to just above the styrofoam cover. A tapered plastic tube, cut from Meuller clip insulation, sealed the sleeve to the transmission line as shown. The lifetime of one of these seals was about eight runs. Egress for the helium vapor evolved by the slowly boiling liquid was provided by a loosely corked vent tube (not shown).

With the top and bottom temperatures and flow rate of the vapor column stabilized, the vapor temperature profile was steady enough to serve as a bath.

Regulation of Block Temperature. The rate of heat flow from the block to the bath was determined by the temperature difference between

the block and vapor, and by the thermal conductivity of the block's styrofoam jacket. Said another way, the equilibrium block temperature adjusted itself so that the heat flow to the bath through the styrofoam jacket exactly equalled the flow of heat into the block from the leads and the heater. In order for the heater to serve as an effective means of controlling the final block temperature, the heat leak down the leads and transmission line had to be small.

All leads were of #36 Nyclad copper wire. The transmission line consisted of two 1/8" OD thin wall stainless steel tubes inside a 7/16" OD thin wall stainless steel tube. The total length of the transmission line was about 13"; approximately half this length was actually inside the cold helium vapor. Teflon spacers served to support the inner conductors and to provide rough thermal contact from the inner conductors to the case. At the bottom of the transmission line, a 1" long styrofoam spacer prevented any convection between the interior of the transmission line and the cavity containing the NMR coil and sample. With these precautions, the heat leak to the block was within tolerable limits. It is very difficult to make a good estimate of the size of the heat leak; our best guess is that the total leak was less than 20 milliwatts.

The size of the block was sufficient to make the equilibrium vapor temperature profile somewhat dependent on the actual block position. This dependence was only important at the beginning of a run. During helium transfer, the block would rest on the platform. If the desired operating temperature required raising the block several inches after transfer, the establishment of an equilibrium temperature distribution in

the vapor column would take about 2 hours.

The range of block temperatures accessible by simply raising and lowering the block was entirely sufficient for the present experiment. In the absence of any heater power, the temperature varied from about $8^{o}K$ (with the block on the platform) to over $50^{o}K$ (with the block near the styrofoam plug). Equilibrium temperatures below $8^{o}K$ were obtained by slightly increasing the boiling rate of the liquid helium, thus cooling the vapor in the dewar. With as little as 20 milliwatts supplied to a resistor at the bottom of the helium reservoir, block temperatures below $5^{o}K$ could be reached.

In practice, the block was heated to maintain its temperature a few degrees above the temperature it would reach in the absence of heater power. The current through the heater resistor was then electronically regulated using a feedback signal from a sensor thermometer embedded in the block (See Fig. 3). The amount of heater power used ranged from 20 to 60 mw. The control system used was designed by Peter Heller and Lee Frank.

A schematic drawing of the feedback loop circuit is shown in Fig. 4. The block temperature is sensed by the sensor resistor (S) which is located in one arm of a d. c. Wheatstone bridge. The sensor is a 1/2 watt 240 Ω Allen-Bradley carbon resistor, and has a large temperature coefficient below $50^{o}K$. In the corresponding arm of the Wheatstone bridge is a set of dummy leads to cancel the sensor lead resistance and a resistance network made up of a precision decade resistor (D), a motor-driven ten turn potentiometer (P), and a coupling resistor (C). The error signal from the Wheatstone bridge is detected by a galvanometer (KinTel

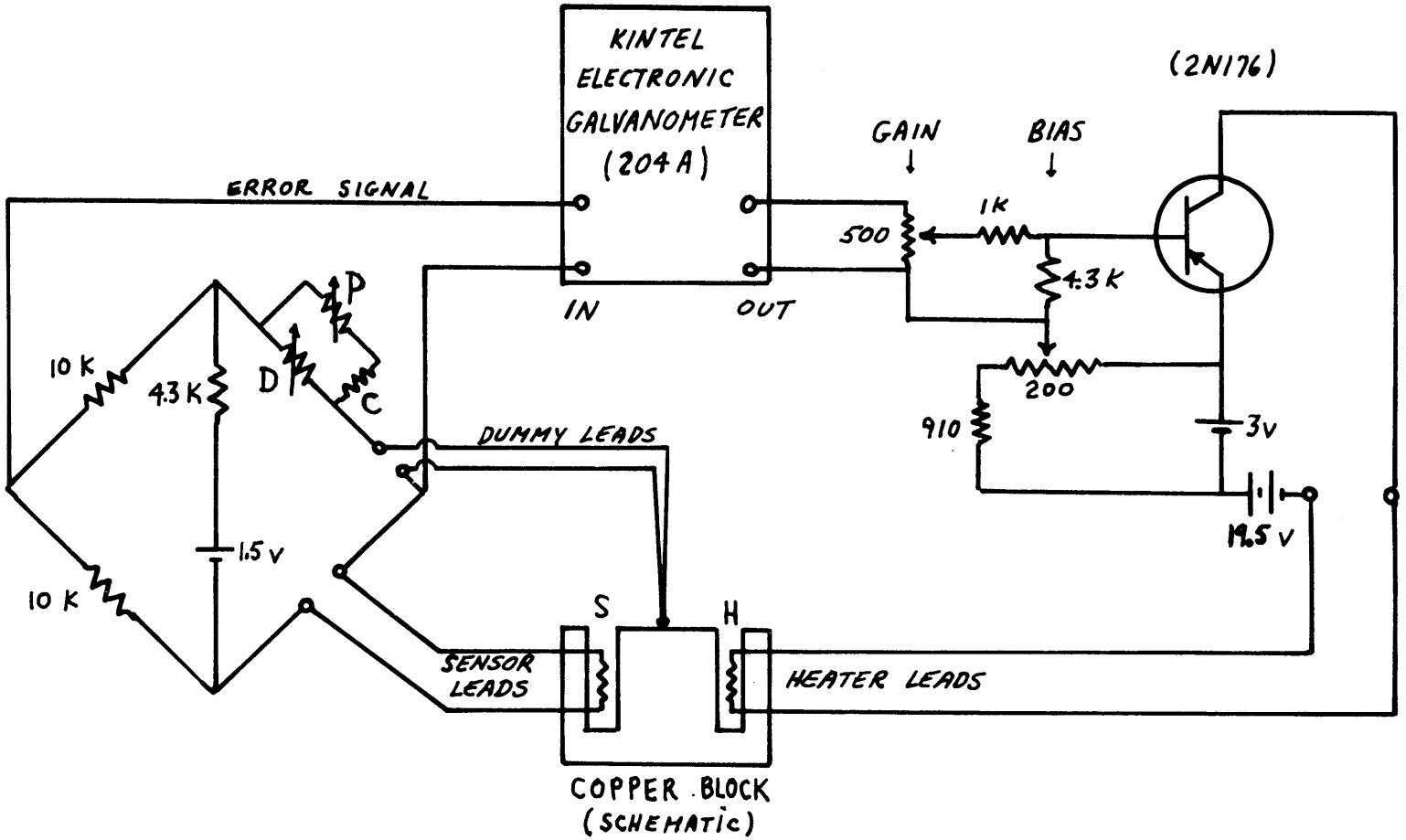

Fig. 4 Heater control circuit.

204A) which also serves to amplify the error signal. The amplified signal is applied through a gain control to the base of a 2N176 transistor connected in a common emitter configuration with the heater resistor (H) as a load. The manual bias on the transistor base controls the zero-error heater current. If the Wheatstone bridge goes out of balance due to a change either in the sensor temperature or in the setting of D and P, an error signal applied to the 2N176 changes the heater current so as to restore balance. Thus, a stable temperature is achieved by setting the bridge at the desired balance point while a swept temperature is achieved by turning the potentiometer with the motor. The purpose of C is to set the sweep range.

There was a time lag between a change in heater current and the corresponding change in sensor temperature due to the finite thermal conductivity of the intervening copper. Because of the lag, the amplifier gain could not be set too high; the heater current change would over-compensate for the temperature error before the sensor temperature had time to respond, and oscillation or "hunting" would set in. At low temperatures, this hunting provided the limitation on the degree of temperature regulation which could be obtained. Regulation to within a few tenths of a millidegree for several hours was typical below about $25^{\circ}K$.

At higher temperatures, the limitation came from the bath stability. In the vicinity of the Curie temperature, the automatic nitrogen filling system could not be used because the vibration caused by nitrogen transfer disrupted the observation of the weak NMR signals. As the

liquid nitrogen level dropped, the copper fingers warmed slightly causing drifts in the temperature of the brass cap and in the vapor column temperature profile. At the highest temperature used ($35^{o}K$), the resulting drift of the block temperature over 3/4 hour was about 4 millidegrees. As it turned out, this regulation was sufficient. Only about 10 minutes were spent on an NMR line during a sweep, during which time the temperature drifted by at most one millidegree. If closer regulation in this temperature range were needed, however, it would be easy to obtain by improving the amount of thermal contact between the brass cap and the liquid nitrogen.

3. Thermal Gradients

It was important to check whether the sample temperature was in fact equal to the block temperature. In particular, we needed to know whether a difference between sample and thermometer temperatures large enough to affect the inherent precision of the data might be present.

The primary reason for the concern over gradients was the fact that the sample could not be placed in rigid thermal contact with the block. The sample holder was a thin-walled polystyrene tube (5/16" O D) corked with a loose cotton plug (See Fig. 3). The NMR coil was made of copper ribbon, 1/8" wide and 0.015" thick, which was soldered to the flattened ends of the stainless steel conductors from the transmission line. The NMR spectrometer used a balanced tank curcuit, so no metal contact was permitted between the coil and the block. On the other hand, the stainless steel conductors provided a heat conduction path out of the block to the cooler vapor inside the transmission line. If the ends of the

conductors which protruded into the block cavity were not warmed to block temperature by the helium vapor inside the cavity, then some of the heater power would flow through the NMR coil and sample, up the transmission lines, and out to the bath. In this event, the sample temperature would be slightly lower than the block temperature.

To check this possibility, two series of measurements of the block temperature versus heater power levels were made at constant sample temperatures (18.00°K and 21.64°K). The constancy of the sample temperature was verified by the highly reproducible NMR frequencies, while the block temperature was measured with a platinum thermometer. For these measurements, the low frequency Br^{79} NMR line was displayed by sweeping temperature at fixed frequency. During the sweep, the block temperature as measured by the platinum thermometer was recorded as a function of time. The block temperature at which the resonance peak occurred could be located to 1 millidegree. In order to achieve the same sample temperature at a series of successively higher heater powers, the block position was lowered in steps until it rested on the platform, then increasing amounts of power were used to boil the liquid helium. Measurements were made with heater powers up to 200 mw (five times the normal amount). The results could be fit with the following formula:

$$T_{sample} = T_{block} - K I^2 \qquad (2\text{-}1)$$

Here, I represents the heater current in milliamps. Since the heater resistance was about 1000 ohms, I^2 is about equal to the heater power in milliwatts. The value for K obtained was 0.027 ± 0.005 millidegree/

milliamp^2. A correction of this form was applied to all the data presented in this thesis. In no instance did the correction exceed 3 millidegrees; the uncertainty in the correction was less than the experimental error from other sources.

In addition to the small steady temperature difference discussed above, there was a time lag in the response of the sample temperature to a change in block temperature. The time constant (τ) for this response varied from 0.25 minutes at the lowest temperatures to 0.50 minutes near the Curie point. With a typical sweep rate (r) of 25 millidegrees/minute, the sample temperature would lag the block temperature by an amount $r\tau$, which varied from 6 to 12 millidegrees. To correct for the lag, two temperature sweeps in opposite directions were always made, and their results averaged. The time lag then cancelled out to first order, and higher order corrections were shown to be unnecessary.

Another possible source of gradients was heating of the sample due to rf power absorption. No shift could be observed in the apparent resonance frequency with up to four times normal rf power. Therefore, this source of error was taken to be negligible.

4. Temperature Measurement and Thermometer Calibration

The block temperature was measured with a Leeds and Northrup type 8164 4-lead platinum resistance thermometer. The thermometer was embedded in the block as shown in Fig. 3, and the leads were wrapped around the block before being brought outside the styrofoam jacket to reduce undesired heat conduction from the thermometer.

The ratio of the thermometer resistance to a standard 4 ohm resistance was measured with a Leeds and Northrup type K3 potentiometer.

A 6 ma steady current was passed through the thermometer and the 4 ohm standard in series. The voltage drop across the 4 ohm resistor was used to standardize the current in the K3 bridge, and the voltage drop across the thermometer was then measured with the K3 bridge slidewire. The advantage of this system was that the standardization could be checked without disburbing the position of the slidewire, allowing repeated measurements on slow drifts to be made. Details of this method of using the K3 potentiometer may be found in the manufacturer's instruction manual.[19]

Bridge balance was detected with a Leeds and Northrup 2340-C galvanometer. The minimum temperature drift observable on the galvanometer depended on the temperature, varying from about 1.5 mdeg at 13°K to 0.3 mdeg at 35°K. The precision with which the slidewire setting could be read, however, was about a factor fo two worse. Thus the actual precision of a temperature measurement varied from 3 mdeg at 13°K to 0.6 mdeg at 35°K.

The resistance ratio measurements were converted to temperatures with the Z-function, tabulated by White[15] as typical for high quality platinum resistance thermometers.

The Z-function is defined as follows:

$$Z(T) = \frac{R_T - R_4}{R_{273} - R_4} \qquad (2\text{-}2)$$

Here R_T, R_4, and R_{273} are the thermometer resistances at the operating temperature, the helium point, and the ice point respectively. They could equally well represent resistance ratios to our 4 ohm standard; thus we can

use the potentiometer slidewire readings directly in Eq. 2-2 to obtain Z(T). A more convenient way to use the Z-function is with the following formula, obtained from Eq. 2-2:

$$\frac{R_T}{R_{273}} = Z(T)\left\{1 - \frac{R_4}{R_{273}}\right\} + \frac{R_4}{R_{273}} \qquad (2\text{-}3)$$

Equation 2-3 permits us to calculate the ratio R_T/R_{273} as a function of temperature using White's tabulated Z-function and the experimental ratio R_4/R_{273}. For the thermometer we used (serial no. 1330894), this ratio was $R_4/R_{273} = 6.558 \times 10^{-4}$. Using Eq. 2-3 and the potentiometer reading at the ice point (R_{273}), we calculated a calibration table for the potentiometer reading R_T. Fourth order interpolation formulae were used to subtabulate White's Z-function table to obtain R_T versus temperature tabulated at 50 millidegree intervals between 13^oK and 39^oK. Note that this calculated table of R_T does not represent our own continuous calibration of the platinum thermometer. We used two fixed point readings and White's table (which is traceable to N. B. S.) to "define" our temperature scale.

Peter Heller checked the suitability of the Z-function for our particular thermometer by comparing the temperature obtained from the Z-function table to reproducible temperature standards. He made the comparison along the hydrogen vapor pressure curve and at the neon boiling and triple points. These points covered the range below 27.1^oK, and showed no discrepency larger than 0.02^oK. Comparisons at and above the freezing point of oxygen (55.5^oK) yielded agreement to 0.01^oK. On the

basis of these results, we expect the tabulated Z-function to be valid as an interpolation formula for our thermometer to an accuracy of ± 0.02°K.

C. NMR Detection

1. Spectrometer

The spectrometer used for all NMR measurements was a push-pull marginal oscillator of the Kushida type [16] (see Fig. 5). Several modifications of Kushida's original circuit have been employed, and they are described below.

The plate load in our spectrometer was essentially untuned. The radio frequency chokes were homemade, consisting of 35 turns of #36 Nyclad wire wound on 6.2 kΩ resistors. They were sufficiently broad-band in their response to be useful from 24 Mc/sec up to 130 Mc/sec, the entire frequency range of the measurements.

The transmission line, which has been described earlier, was also untuned. Kushida suggested that the spectrometer would work very well with an untuned line if it was made much shorter than a half-wave length. The 13" line used in this experiment met that requirement. Below 60 Mc/sec, a sample coil of the number of turns required to reach the desired frequency range was used. This number varied from 5 turns of 1/8" by 0.015" copper ribbon at higher frequencies to 24 turns of #20 Nyclad wire at the lowest frequencies. Above 60 Mc/sec, however, a different choice of sample coil was made because of the presence of the transmission line inductance. A coil was selected which had an inductance approximately equal to the series inductance of the transmission line (five

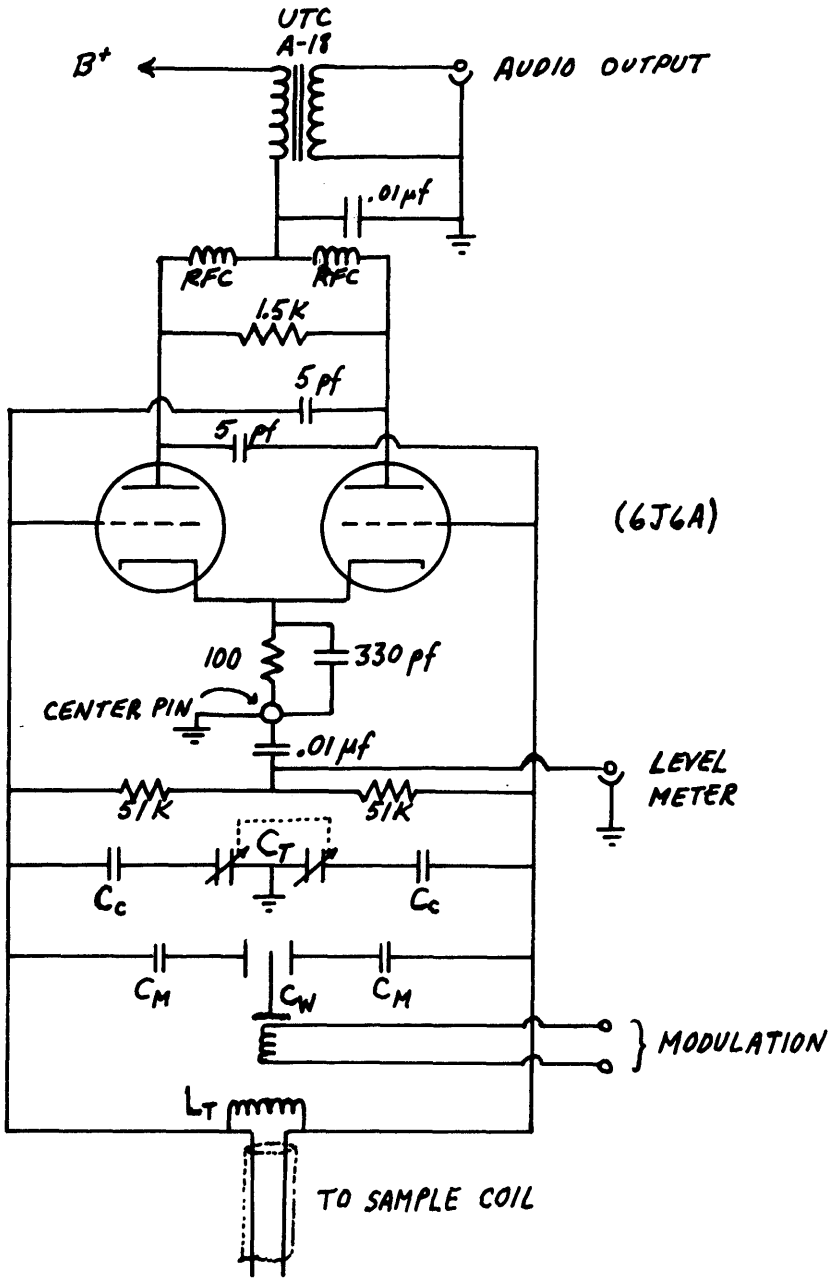

C_W - WOBBULATOR CAPACITOR, TEL INSTRUMENTS ELECTRONICS, #1800 B
C_T - JFD VC-18G SPLIT STATOR TUBULAR TRIMMER
C_C - 20 pf ABOVE 60 Mc/s ; ABSENT BELOW 60 Mc/s
C_M - 20 pf ABOVE 60 Mc/s ; 100 pf BELOW 60 Mc/s
L_T - SHUNT TUNING COIL, USED ABOVE 60 Mc/s
B^+ - 45 - 135 V AS NEEDED

Fig. 5 Kushida spectrometer.

turns of the ribbon were used, about 0.1μh). This choice provided near optimum spectrometer sensitivity to rf losses in the sample. Rough tuning to higher frequencies was then accomplished with the use of a shunt coil soldered to the top of the transmission line. Measurement of the frequency was done via a pickup wire near the oscillator tank circuit which was connected to a Hewlett-Packard 461A rf amplifier followed by a Hewlett-Packard 5245L cycle counter.

Fine tuning was obtained with the JFD trimmer capacitor. This trimmer could be motor driven to obtain a swept frequency. The frequency sweep was primarily used above 60 Mc/sec. At 100 Mc/sec, with the circuit components having the values indicated in Fig. 5, the total available sweep range was about 4 Mc/sec. A reasonably linear sweep could be obtained over about 1 Mc/sec. While it was necessary to change the shunt coil often in order to cover the wide frequency range of this experiment, no other changes in the spectrometer were required above 60 Mc/sec.

The level of oscillation was adjusted by changing the plate supply voltage. Except near the Curie point, where the sample losses loaded down the tank circuit, a plate supply of about 45 volts was used. As the level was lowered, the sensitivity to nuclear absorption improved while the noise of oscillation increased. The optimum level for operation was determined by a compromise between these effects.

Frequency modulation was done with a balanced wobbulator capacitor (Tel-Instrument Electronics, type 1800B) driven at 75 cps. The wobbulator introduced almost no incidental amplitude modulation of the spectrometer level at 150 cps, the frequency at which the NMR signals

were detected. Peak to peak modulations of up to 200 Kc/sec were achieved while operating at the lowest frequency of 24 Mc/sec without the introduction of excessive spurious signals. Above 24 Mc/sec, the usable modulation amplitude increased proportional to the frequency.

A few more words on spurious signals are in order. The plate circuit of the spectrometer detects changes in the level of oscillation; that is, any amplitude modulation of the level. In a frequency modulated spectrometer, such modulation can arise from several sources. Hopefully, the largest source is the nuclear absorption in the sample. Other spurious sources are frequency dependent electronic absorption in the sample, a dependence of the tank curcuit quality factor on the oscillation frequency, and non-linearities in the wobbulator response. The reason for using second harmonic detection is that the spurious signals are reduced more than the NMR signal when the detection frequency is doubled. We like to use an amount of frequency modulation which optimizes the NMR signal-to-noise ration; this amount is approximately a peak to peak modulation equal to the NMR linewidth. The use of the wobbulator made this possible by reducing to very manageable proportions that part of the second harmonic spurious signal not arising from electronic losses in the sample while still permitting quite large modulation amplitudes. The spurious signal due to electronic losses, however, was both a function of temperature and a function of frequency, particularly near the Curie point.

The low frequency NMR lines (below 60 Mc/sec) were displayed with a temperature sweep. Near T_c, the strongly temperature dependent

background signal from the electronic losses simply swamped the NMR signal. A frequency sweep was tried at low frequency without success, primarily because the broad sweep required (over 500 Kc/sec) necessarily involved large changes in circuit parameters which introduced new sources of spurious signals. Thus, the fading out of the low frequency bromine lines near T_c was not due to a vanishing signal-to-noise ratio per se; rather the lines disappeared into the electronic loss background.

The pair of high frequency NMR lines were displayed with a frequency sweep. At 100 Mc/sec with 200 Kc/sec peak to peak modulation, a 1 Mc/sec sweep width with no significant drift in spurious signal was easily achieved. At these higher frequencies, the electronic background loss near T_c, while still a strong function of temperature, was a weak function of frequency, so the spurious signal was not a serious impediment to the observation of the resonances.

2. Features of the Audio Detection System

The detection of an audio signal at 150 cps from the spectrometer was accomplished with standard lock-in detection techniques. A few features of the system used are worth noting.

A block diagram of the detection system is shown in Fig. 6. The central element is the lock-in amplifier, which was built from a circuit of J. D. Litster.[17] It incorporates telemetry filters (UTC-BMI-150) in a frequency selective amplifier with a voltage gain of about 10^5. Phase sensitive detection is done with a Sanders Model 2 phase comparator. The 150 cps reference signal is obtained by full wave rectification of a portion of the modulation signal followed by a 150 cps telemetry filter to

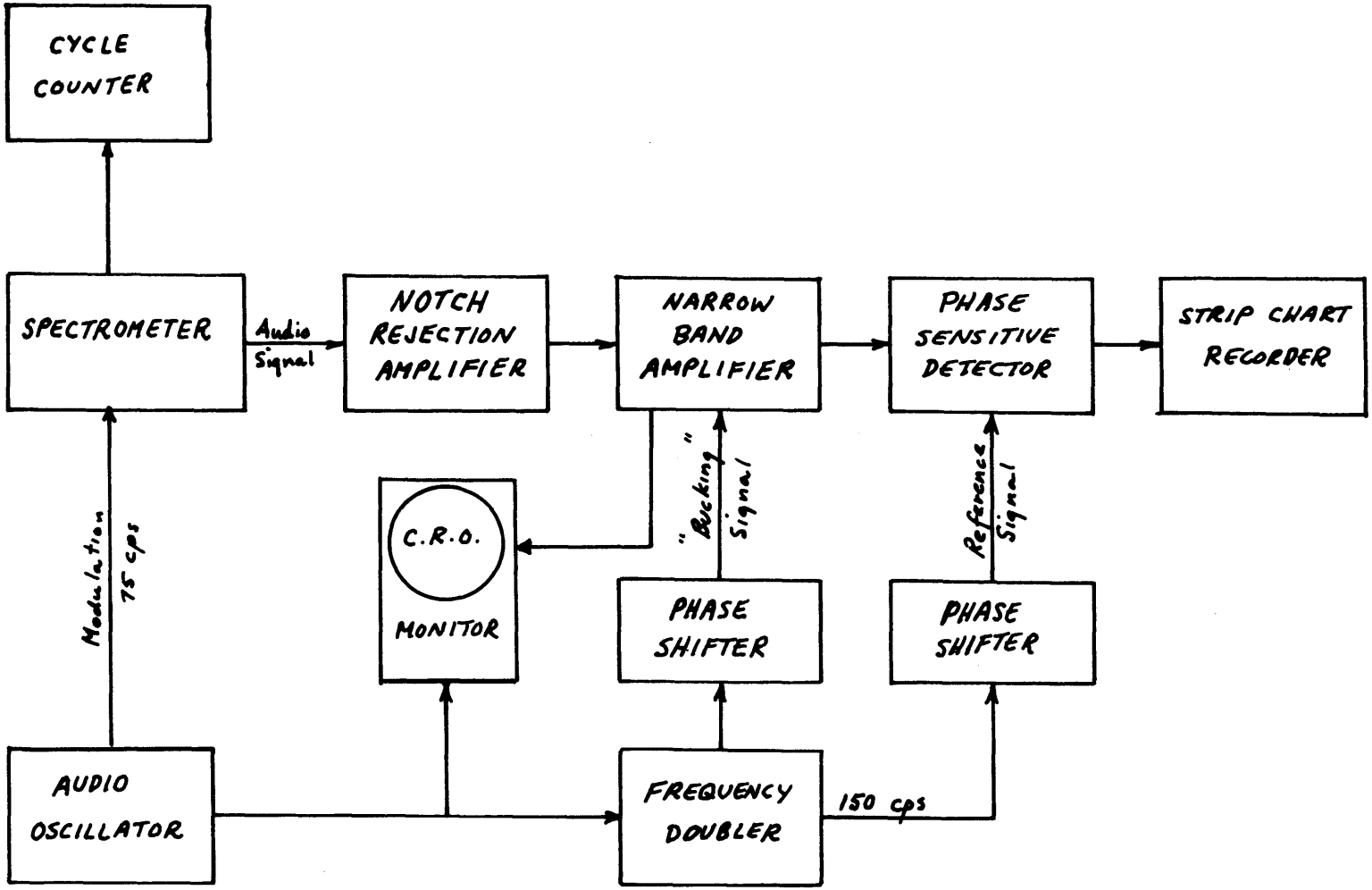

Fig. 6 Block diagram of audio detection system.

remove higher harmonics. Part of this doubled frequency signal is used to "buck out" the spurious signal from the spectrometer. The bucking out is successful only if the spurious signal does not change appreciably during a sweep through an NMR line. No attempt was made to "track" the spurious signal drifts during the temperature sweeps near T_c. A twin-tee notch rejection preamplifier was used to remove a large spurious signal at the 75 cps modulation frequency. Most of this first harmonic signal was due to the wobbulator, for reasons which are not understood. It was necessary to remove this signal explicitly with a notch amplifier because the skirt selectivity of the lock-in amplifier was not sufficient to prevent partial amplifier saturation by the 75 cps signal.

Finally, we mention a result of an investigation of the amplitude stability of various audio oscillators. We were concerned that drifts in the modulation signal from the audio oscillator would propagate through the spectrometer and appear as drifts in the spurious signal. We tested the amplitude stability of several oscillators. The best by far was a Hewlett-Packard 200 CD Wide Range Oscillator. Two different oscillators of this type were tested. If the oscillators were allowed to warm up for several hours and were not bumped, the amplitude at 75 cps was stable to 5 parts in 10^4 over a period of one hour.

Chapter III

Experimental Data

A. Introduction

The experimental data will be presented in two sections. In the first, we tabulate all the measurements of the NMR frequencies versus temperature. In the second part, we discuss the utility of the NMR lines as thermometric standards.

B. NMR Data

For purposes of analysis, it was desirable to measure the frequencies of the various chromium and bromine resonance lines at exactly the same temperature. This was extremely difficult to do, particularly for the low frequency resonances which were displayed with a swept temperature. Therefore, the measurements on different lines were made as close to the same temperature as possible (usually within ten millidegrees), and then the frequencies were interpolated to make the temperatures match up. This interpolation over small temperature intervals introduced no error into the data. The data presented here include the gradient correction to the sample temperature.

1. Chromium NMR Frequencies

We present here data from $4.2^{\circ}K$ to $29.74^{\circ}K$ on the triplet of Cr^{53} NMR lines which arise from nuclei inside ferromagnetic domains.[2] The spacing of the two satellite lines of the triplet is symmetric about the central line. The data is presented in Table I in terms of the frequency of the central line and the average observed quadrupole splitting as obtained

Table I

NMR Frequencies and Quadrupole Splitting for Cr^{53} Nuclei

Temperature T (^{o}K)		Central Frequency ν^{53} (Kc/sec)				Quadrupole Splitting q^{53} (Kc/sec)		
4.21		57442.7	±	0.2		296.6	±	0.2
† 10.00		54966	±	5		297	±	5
13.000		53179	±	1		296	±	1
16.000		51038	±	1		295	±	1
18.000		49397	±	2		295	±	2
19.500		48035	±	1		295	±	1
21.000		46534	±	2	**	291	±	3
21.640		45842	±	3		293	±	3
22.500	*	44844	±	2		285	±	3
23.160	*	44035	±	4		290	±	6
24.360		42426	±	5	**	290	±	7
25.275		41060	±	5	**	288	±	7
26.095		39697	±	3		285	±	3
26.680		38624	±	4		284	±	4
26.975		38051	±	4		284	±	4
27.675		36558	±	5		281	±	5
28.125		35490	±	5		282	±	5
28.665		34123	±	6		276	±	6
29.090		32901	±	6		278	±	6
29.435		31818	±	9		278	±	10
29.740		30784	±	10		286	±	15

* Central line obscured by bromine resonance. Entry is average of two satellite frequencies.

** One satellite obscured by bromine resonance.

† The data at 10^{o}K were not available for inclusion in the detailed computer analysis of the NMR frequencies. The relatively large uncertainty in the data at this temperature is due to the poor sensitivity of the platinum resistance thermometer.

from the satellites. The frequency of the central line is plotted versus temperature in Fig. 7. Note the crossing with the Br^{81} line. Whenever the Br^{81} line was within 150 Kc/sec of a Cr^{53} line, the Cr^{53} line was obscured. Therefore, the data at five temperatures near the crossing region come from only two of the three members of the triplet. In particular, at 22.500°K and 23.160°K, the central line was unobservable. The central frequencies entered in Table I for these two temperatures come from the average of the frequencies for the two satellites.

The Cr^{53} line shape was found to be dependent on the rf level of the spectrometer, increasingly so as the temperature was raised. In Fig. 8 are shown four different sketches of the second derivative line shape observed for the chromium line. In a) we show the line shape at 4.2°K. When the level was raised at 4.2°K, the line simply weakened due to saturation with no appreciable change in shape. In b), c), and d), we show how the shape changed with increasing level at 18°K. The saturable peak at the low frequency end of the line was taken to represent the NMR line. Its position did not shift with increasing level. The origin of the negative going peak at higher frequency which increased in intensity with increasing level is not understood. At fixed frequency, the temperature difference between the maxima of the positive and negative going peaks amounted to as much as 20 millidegrees at the highest temperatures.

Our lowest temperature measurements on the Cr^{53} triplet duplicated a portion of the work of Davis and Narath, who measured the central frequency from 1.44°K to 19.68°K.[10] At 4.2°K, our frequency agrees with theirs, but at higher temperatures there is a systematic discrepancy. In

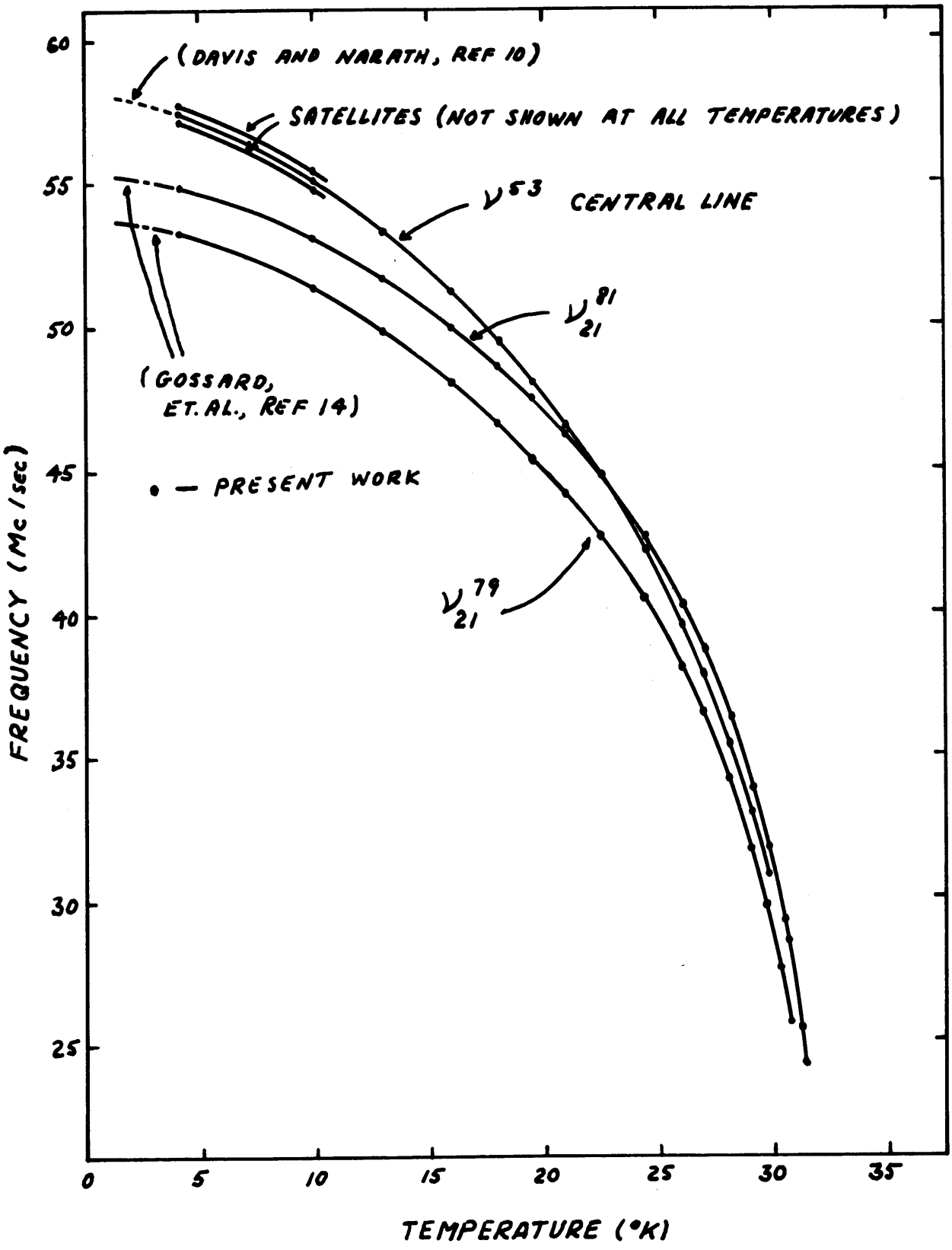

Fig. 7 Low frequency NMR data; Cr^{53}, Br^{79}, and Br^{81}.

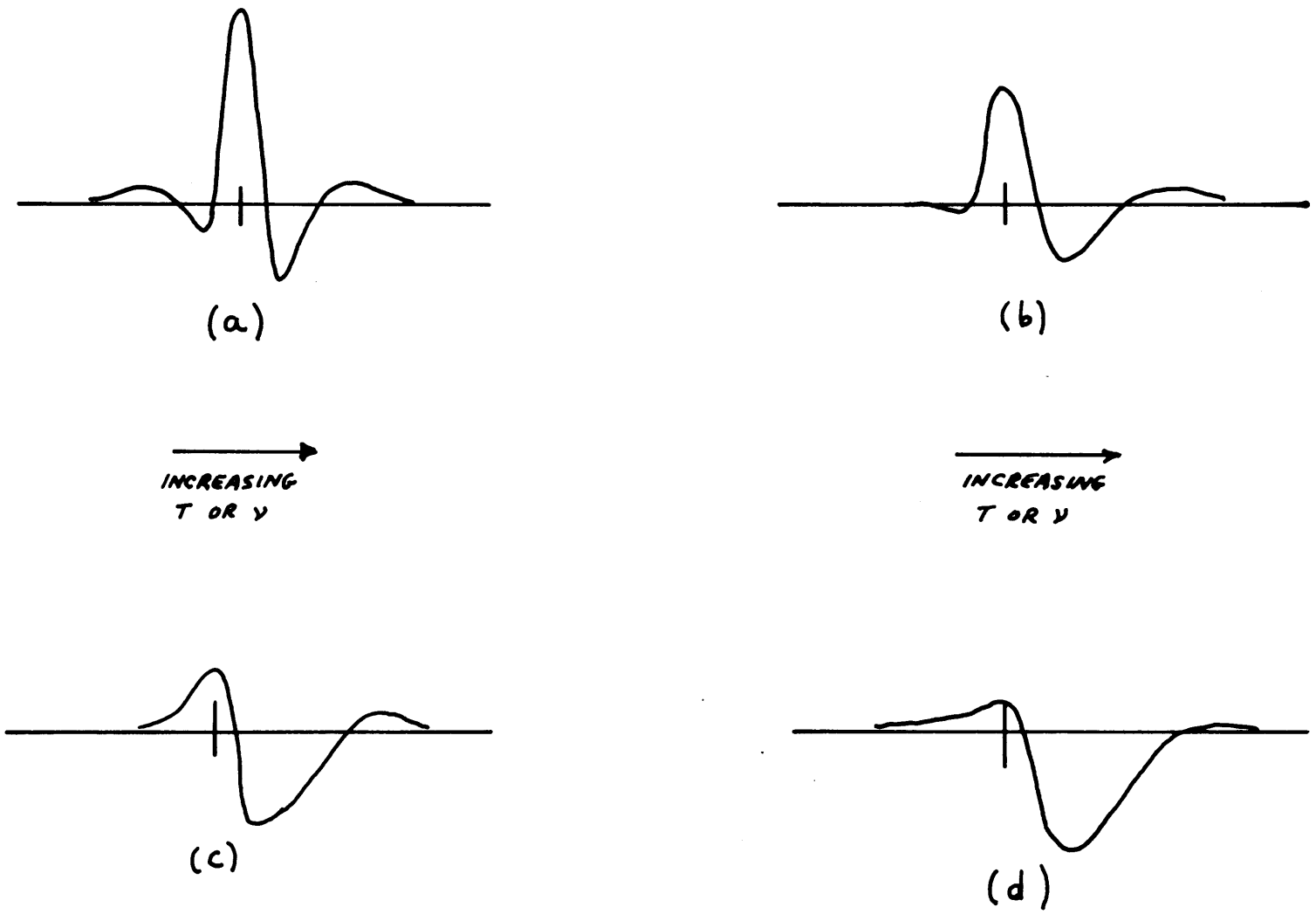

Fig. 8 Cr^{53} line shape (a) at 4.2°K; (b), (c), (d) at 18°K, as a function of increasing rf level.

particular, at $16^{o}K$, our temperature reading for a given resonance frequency is about $0.06^{o}K$ larger than theirs. We checked our thermometer calibration explicitly at $16.30^{o}K$ by measuring the vapor pressure of normal liquid hydrogen which was freshly condensed into a OFHC copper vessel in which the platinum resistance thermometer was embedded. The Z-function conversion of the platinum resistance to temperature agreed with the vapor pressure scale to $0.01^{o}K$, well within our expected accuracy of $\pm\ 0.02^{o}K$.

Davis and Narath used a manostat regulated bath of equilibrium liquid hydrogen for their temperature scale in the range 14^{o} - $20^{o}K$. They claim a calibration accuracy of $\pm\ 0.02K$. Clearly, the discrepancy of $0.06^{o}K$ cannot be explained solely on the basis of an unfortunate combination of calibration uncertainties. There are two further sources which may contribute to the disagreement: i) Davis and Narath's sample may have been slightly warmer than their liquid hydrogen bath; and ii) the liquid hydrogen they used may have not completely reached equilibrium composition. It is conceivable that a combination of i) and ii) might account for the remaining $0.02^{o}K$ discrepancy, but we emphasize that this is a speculation on our part.

2. Bromine NMR Frequencies

We present here data from $4.2^{o}K$ up to $32.35^{o}K$ on the frequencies of four bromine NMR lines which arise from the splitting of the pure quadrupole resonances of Br^{79} and Br^{81} by a magnetic hyperfine field. The low frequency pair of lines (identified by ν_{21}^{79} and ν_{21}^{81}) were displayed with a swept temperature; the high frequency pair of lines

(labelled by ν_{42}^{79} and ν_{42}^{81}) were displayed with a swept frequency. Not all the lines could be seen to the maximum temperature of 32.35°K. The frequency versus temperature data is given in Table II (low frequency) and Table III (high frequency); the maximum temperature for each line is indicated in the Tables. At the end of Table III, we also present data on the pure quadrupole resonance frequencies for both isotopes of bromine, measured just above the Curie point where the hyperfine field is zero.

The low frequency data is shown graphically in Fig. 7; the high frequency data is plotted in Fig. 9.

3. NMR Linewidths

No precise measurements of linewidths were made. We do, however, have estimates of the dependence of the linewidths on temperature for both chromium and bromine resonances.

The width of the Cr^{53} lines is about 10 Kc/sec at 4.2°K, and increases rapidly with temperature. At 29.74°K, the triplet of lines is barely resolvable, indicating that the linewidth of each component has increased to something on the order of 250 Kc/sec. Thus, between 4.2°K and 29.74°K, the Cr^{53} linewidth has increased by a factor of 25. The triplet is no longer visible at 29.97°K indicating that rapid broadening of each component continues and causes the triplet to merge into a single, weak line.

These results are shown graphically in Fig. 10. What is plotted is our best estimate of the Cr^{53} linewidth versus temperature. It must be emphasized that because of the large amplitude of frequency modulation used to detect the NMR lines, the numerical linewidth scale may not be

Table II

NMR Frequencies for Br^{79} and Br^{81} Nuclei - Low Frequency Lines

Temperature T (^{o}K)	Br^{79} Frequency ν_{21}^{79} (Kc/sec)	Br^{81} Frequency ν_{21}^{81} (Kc/sec)
4.21	53265 ± 1	54885 ± 1
† 10.00	51259 ± 5	53025 ± 5
13.000	49780 ± 2	51643 ± 2
16.000	47984 ± 2	49944 ± 2
18.000	46592 ± 2	48616 ± 2
19.500	45423 ± 2	47491 ± 2
21.000	44118 ± 2	46228 ± 2
21.640	43510 ± 2	45637 ± 2
22.500	42647 ± 2	44787 ± 2
23.160	41919 ± 3	44079 ± 2
24.360	40498 ± 3	42666 ± 3
25.275	39267 ± 3	41444 ± 3
26.095	38040 ± 3	40211 ± 3
26.680	37060 ± 4	39225 ± 4
26.975	36540 ± 4	38696 ± 4
27.675	35176 ± 4	37312 ± 4
28.125	34220 ± 10	36309 ± 5
28.665	32932 ± 5	35016 ± 5
29.090	31795 ± 6	33844 ± 6
29.435	30789 ± 9	32804 ± 7
29.740	29812 ± 10	31792 ± 10
29.970	28996 ± 11	30956 ± 10
30.085	28587 ± 12	30520 ± 11
30.360	27502 ± 12	29389 ± 12
30.550	26697 ± 13	28551 ± 14
30.760	25721 ± 17	27516 ± 15

Table II (Continued)

NMR Frequencies for Br^{79} and Br^{81} Nuclei - Low Frequency Lines

Temperature $T(^{o}K)$	Br^{79} Frequency ν_{21}^{79} (Kc/sec)	Br^{81} Frequency ν_{21}^{81} (Kc/sec)
30.915	—	26705 ± 16
30.946	—	26540 ± 17
31.003	—	26215 ± 17
31.039	—	26005 ± 18
31.085	—	25732 ± 18
31.140	—	25400 ± 20
31.188	—	25100 ± 20
31.234	—	24800 ± 20
31.279	—	24500 ± 20
31.323	—	24200 ± 20

† The data at $10^{o}K$ were not available for inclusion in the detailed computer analysis of the NMR frequencies. The relatively large uncertainty in the data at this temperature is due to the poor sensitivity of the platinum resistance thermometer.

Table III

NMR Frequencies for Br^{79} and Br^{81} Nuclei - High Frequency Lines

Temperature T (^{o}K)	Br^{79} Frequency ν_{42}^{79} (Kc/sec)	Br^{81} Frequency ν_{42}^{81} (Kc/sec)
4.21	130216 ± 3	121016 ± 3
†10.00	128340 ± 10	118445 ± 10
13.000	126980 ± 3	116660 ± 3
16.000	125444 ± 3	114587 ± 3
18.000	124301 ± 3	113051 ± 3
19.500	123374 ± 3	111810 ± 4
21.000	122375 ± 3	110485 ± 5
21.640	121923 ± 3	109864 ± 5
22.500	121283 ± 3	109021 ± 3
23.160	120775 ± 3	108329 ± 3
24.360	119776 ± 3	107012 ± 6
25.275	118947 ± 4	105919 ± 5
26.095	118132 ± 7	104862 ± 5
26.680	117530 ± 5	104047 ± 7
26.975	117200 ± 5	103624 ± 7
27.675	116380 ± 7	102551 ± 5
28.125	115796 ± 7	101805 ± 7
28.665	115060 ± 7	100857 ± 10
29.090	114452 ± 10	100037 ± 10
29.435	113886 ± 6	99341 ± 8
29.740	113373 ± 10	98683 ± 8
29.970	112959 ± 6	98151 ± 8
30.360	112206 ± 8	97189 ± 6
30.760	111353 ± 8	96114 ± 10
31.085	110584 ± 8	95140 ± 10
31.279	110069 ± 6	—
31.350	—	94229 ± 10

Table III (Continued)

NMR Frequencies for Br^{79} and Br^{81} Nuclei - High Frequency Lines

Temperature T(^{o}K)	Br^{79} Frequency ν_{42}^{79} (Kc/sec)	Br^{81} Frequency ν_{42}^{81} (Kc/sec)
31.797	108452 ± 10	—
31.898	108085 ± 10	—
31.996	107698 ± 10	—
32.046	107518 ± 10	—
32.098	107280 ± 15	—
32.147	107035 ± 15	—
32.198	106788 ± 10	—
32.245	106540 ± 30	—
32.294	106280 ± 20	—
32.349	105955 ± 15	—

Pure Quadrupole Resonance Frequencies

T	Br^{79}	Br^{81}
34.50	102750 ± 10	85850 ± 10
35.00	102750 ± 10	—

† The data at 10^{o}K were not available for inclusion in the detailed computer analysis of the NMR frequencies. The relatively large uncertainty in the data at this temperature is due to the poor sensitivity of the platinum resistance thermometer.

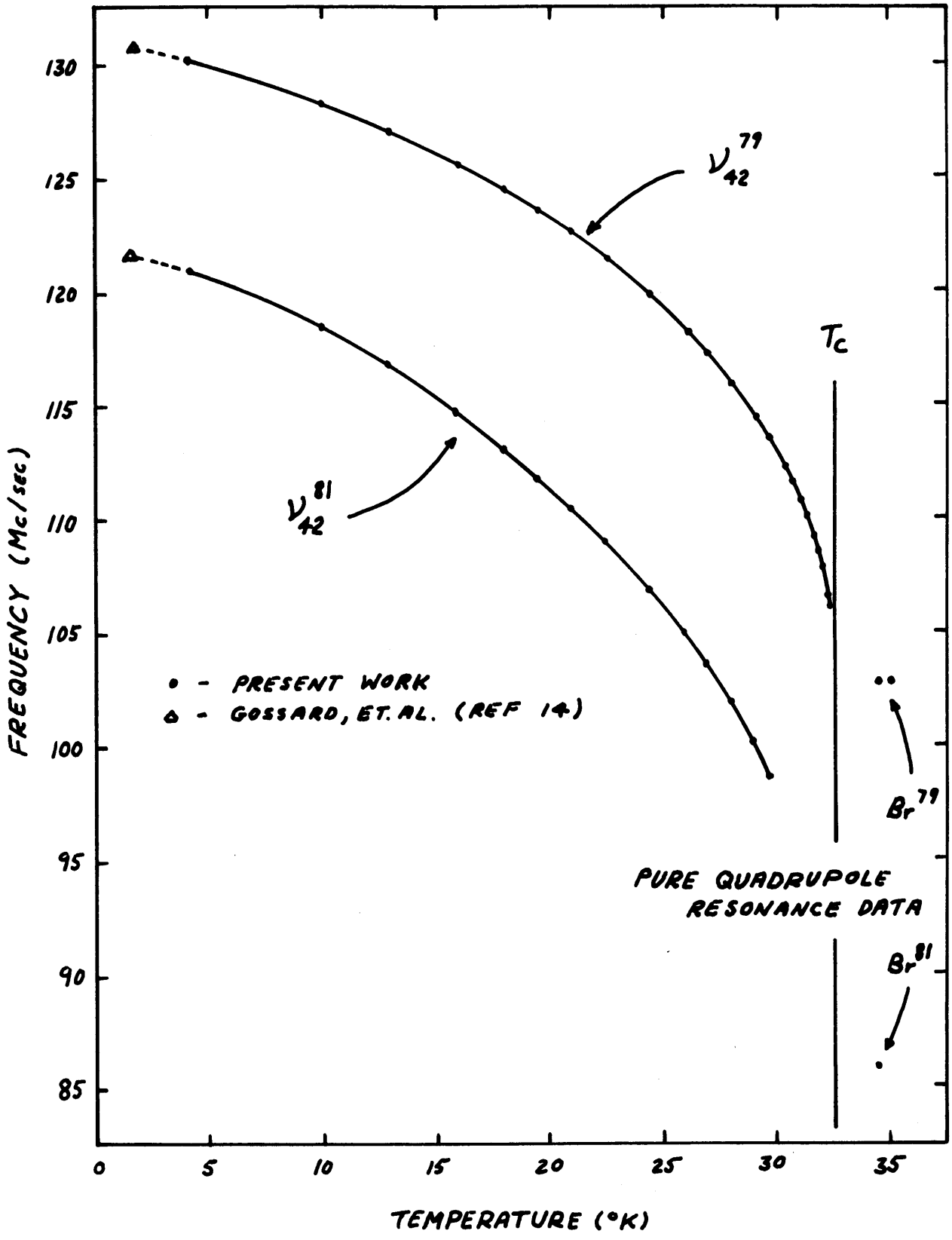

Fig. 9 High frequency NMR data; Br^{79} and Br^{81}.

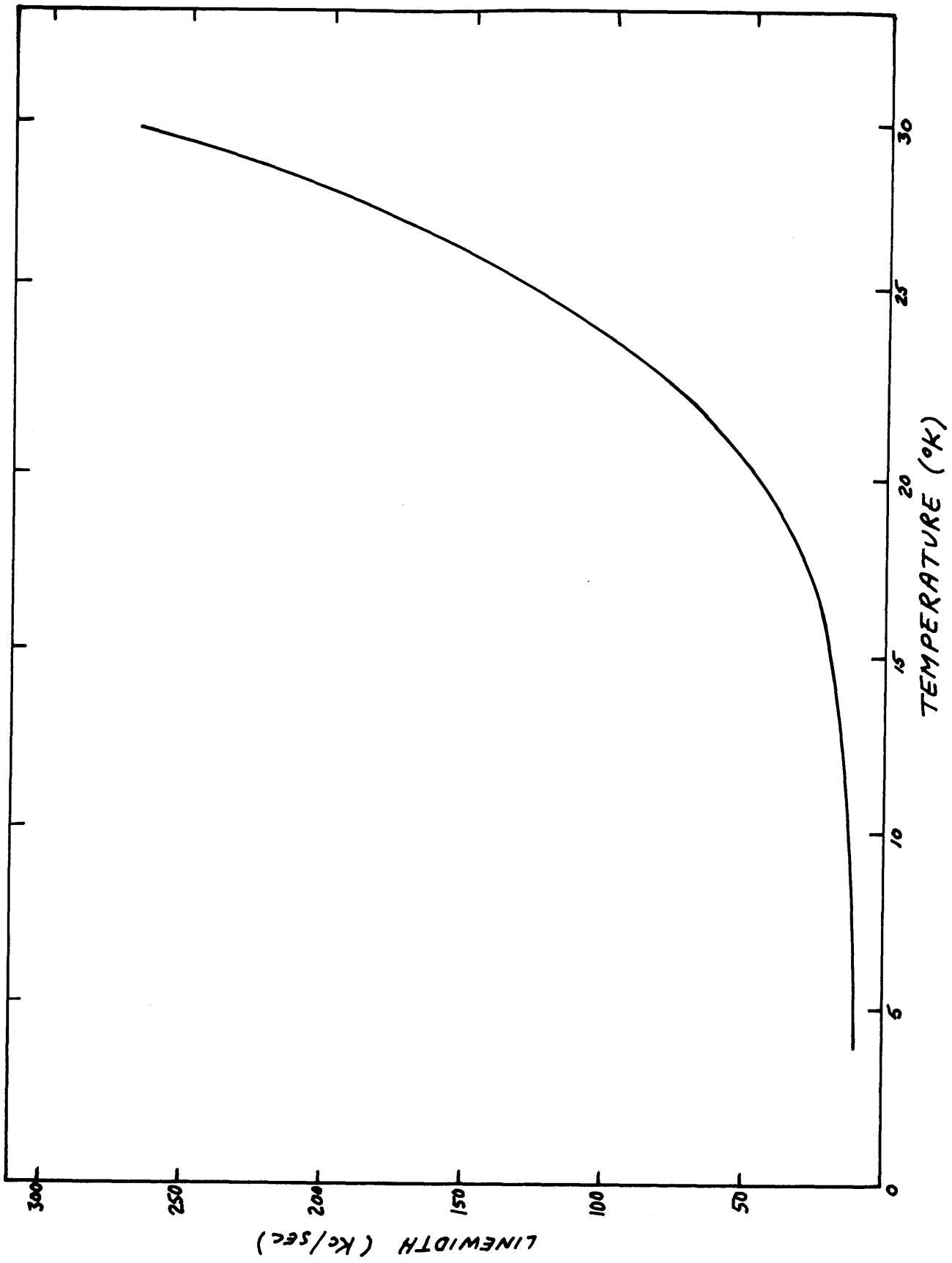

Fig. 10 Temperature dependence of the Cr^{53} linewidth.

very accurate. Nevertheless, the basic feature of very rapid broadening as T approaches T_c is correctly represented in the graph.

The low frequency bromine resonances have a width of about 45 Kc/sec at 4.2°K and, unlike the chromium lines, do not exhibit a catastrophic increase in width at higher temperatures. At the highest temperature at which a low frequency resonance was observed (31.324°K), the width had only increased to about 180 Kc/sec, and was not showing signs of rapid increase with temperature. The relative increase in width here was only a factor of 4.

The widths of the high frequency bromine resonances show even less dependence on temperature. At 4.2°K, both lines have widths of about 100 Kc/sec. At the highest temperature (32.35°K), the width had only doubled, and was about 200 Kc/sec. There was no evidence of catastrophic line broadening. Just above the Curie point (34.5°K), the pure quadrupole resonance linewidths were about 200 Kc/sec.

C. Magnetic Resonance Thermometry Using $CrBr_3$

The use of a temperature dependent NMR frequency as a thermometer has been investigated by several workers for the Cl^{35} pure quadrupole resonance frequency in $KClO_3$.[20, 21, 22] The primary advantage of this type of thermometer is that it possesses a universal calibration curve; that is, the pure quadrupole resonance frequency is a fundamental property of the solid and for pure enough material has a highly reproducible temperature dependence in all samples. The Cl^{35} pure quadrupole resonance in $KClO_3$ can be used as a precise, reproducible

thermometer above $20^{o}K$.[20, 21]

The bromine and chromium NMR lines in $CrBr_3$ also possess the universal calibration curve property; the magnetic hyperfine field is as much a fundamental property of the solid as the quadrupole interaction. In addition, the magnetic hyperfine field below the Curie point is a very rapid function of temperature. As a result, the $CrBr_3$ NMR frequencies below T_c are much more sensitive to temperature changes than is the $KClO_3$ line. In fact, we shall show that the $CrBr_3$ NMR lines can be used as precise thermometers from $30^{o}K$ down to $1^{o}K$.

Of the seven NMR lines studied in this thesis, two are most suitable as thermometers: the Cr^{53} central line and the low frequency Br^{81} resonance. The Cr^{53} line is most sensitive below $15^{o}K$; the Br^{81} line is best between $15^{o}K$ and $30^{o}K$. We discuss first the sensitivity of these NMR lines, and then present our results on the reproducibility of the resonance frequencies.

1. Sensitivity

We use the term "sensitivity" to mean the accuracy with which the temperature can be determined; it depends on several factors. For an NMR line, the sensitivity ΔT is given by

$$\Delta T = \frac{\Delta \nu}{\left| \frac{d\nu}{dT} \right|} \qquad (3\text{-}1)$$

where $\Delta\nu$ is the uncertainty in the determination of the resonance frequency, and $\frac{d\nu}{dT}$ is the slope of the NMR frequency with temperature.

The quantity $\Delta \nu$ depends on two factors, the NMR linewidth and the signal-to-noise ratio. Thus, the sensitivity of an NMR thermometer depends in effect on the type of detection system used. In the estimates of sensitivity to be presented below, we specify a slowly swept detection system similar to the one used in this experiment. The value of $\Delta \nu$ which we used to obtain the sensitivity was that which we were able to achieve experimentally; i. e., 2% of the linewidth except at the temperatures above 25° where the signal-to-noise ratio becomes small. At the higher temperatures, $\Delta \nu$ was as much as 10% of the linewidth. Vanier[21] has shown that in the case of $KClO_3$ an improvement of up to a factor of 10 in sensitivity can be obtained if a self-locked spectrometer is used to lock the spectrometer frequency to the center of the NMR line. We see no reason why a similar improvement is not possible in the sensitivity figures which we present here.

In Fig. 11 we plot the expected sensitivity of the Cr^{53} central line and the low frequency Br^{81} line versus temperature. Note that the combination of the two lines yields a sensitivity of $\pm$ 2 millidegrees or better from about $1.5^{\circ}K$ up to $29^{\circ}K$. If a self-locking spectrometer is used, the anticipated improvement in this figure makes $CrBr_3$ a superbly sensitive thermometer.

A few comments on the sensitivity estimates are in order. The dashed portion of the Cr^{53} curve below $4.2^{\circ}K$ is obtained from Davis and Narath's data together with our result for the accuracy with which the line center can be located at $4.2^{\circ}K$ ($\Delta \nu = 0.0002$ Mc/sec). Between $4.2^{\circ}K$ and about $18^{\circ}K$, the sensitivities shown are better than the actual experimental

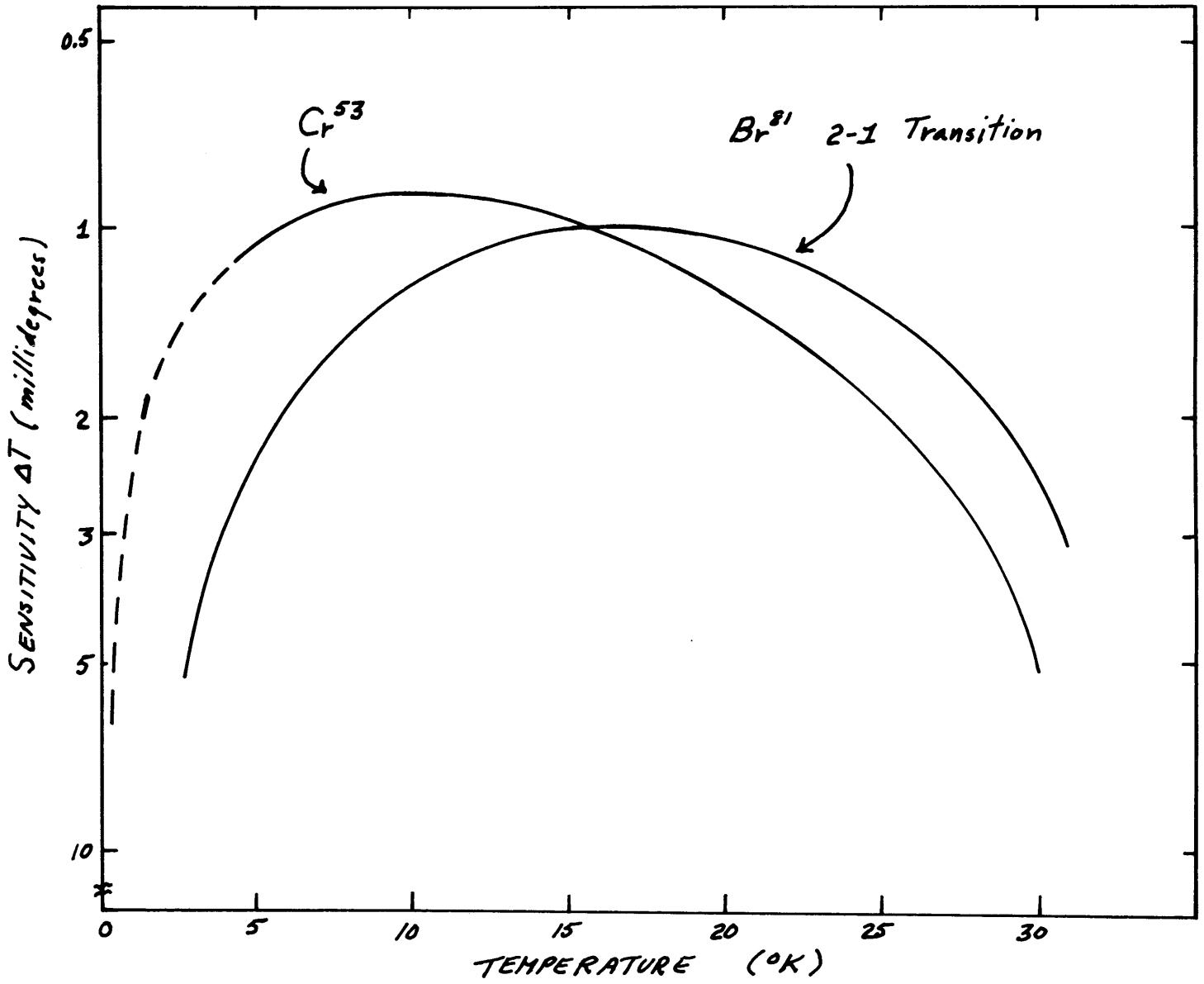

Fig. 11 Sensitivity of NMR lines as thermometers.

uncertainty we obtained. The reason for this apparent discrepancy is that our experimental uncertainty includes an uncertainty in the determination of the temperature as read from the relatively insensitive platinum resistance thermometer.

2. Reproducibility

To within our experimental error, the reproducibility of the NMR frequencies was exact. We used a total of three samples of loosely packed flakes over the course of 2-1/2 years of measurements. The first sample was provided by Dr. J. I. Harrison of Harwell; the remaining two came from Professor Smakula at MIT. Each of these samples was subjected to many thermal cyclings between room temperature and liquid helium temperature. The second Smakula sample was used more than the others. It was cycled at least 25 times over a period of six months. No effects of hysteresis were observed.

The best way to illustrate the reproducibility of our results is to give two measurements of the Cr^{53} central NMR frequency at liquid helium temperature:

i. 4/26/63 - Harrison sample, the second time it was cooled to liquid helium temperature: $\nu^{53} = 57.443 \pm 0.001$ Mc/sec.

ii. 6/4/65 - Smakula sample #2, after at least ten thermal cyclings: $\nu^{53} = 57.4427 \pm 0.0002$ Mc/sec.

The smaller experimental error in (ii) reflects an improved detection scheme rather than a change in linewidth.

In summary, the NMR lines in $CrBr_3$ can be used as very sensitive, reproducible thermometers between $1^{o}K$ and $30^{o}K$. The data presented in

this chapter provide a preliminary calibration of the NMR thermometers above 4.2°K to an accuracy of ± 0.02°K. The extensive Cr^{53} NMR measurements of Davis and Narath[10] provide additional calibration data between 1.5°K and 19.7°K.

Chapter IV

Interpretation of Experimental Data

A. Introduction

The main subject of this chapter is the development of a quantitative model to account for the frequencies and temperature dependences of the bromine NMR lines below the $CrBr_3$ Curie point. We also present an interpretation of the Cr^{53} NMR data. A summary of the results of our data analysis, including our determination of the temperature dependence of the magnetization from $4.2^{o}K$ to $32.35^{o}K$, comprises the final section of this chapter.

B. General I = 3/2 Hamiltonian

It is a curious coincidence that the three different Hamiltonians used to describe the Cr^{53}, Br^{79}, and Br^{81} NMR lines all have the same form. The three nuclei are subject to the same types of interactions, and all three nuclei happen to have the same nuclear spin (I = 3/2). In the case of Cr^{53}, the coincidence is of no particular value, but for the two isotopes of bromine, it has great usefulness. It is precisely because we could hypothesize a Hamiltonian which differed for the two bromine isotopes only in the numerical values of the nuclear moments that we were able to provide the first positive identification of the low frequency bromine NMR lines.

This general Hamiltonian is the sum of two terms.

$$\mathcal{H} = \mathcal{H}_{hf} + \mathcal{H}_{Q} \tag{4-1}$$

The first term, $\mathcal{H}_{hf}$, contains the magnetic hyperfine and dipole interactions of the nuclear magnetic moment with the surrounding Cr^{3+} spins. The second term, $\mathcal{H}_Q$, contains the electrostatic interaction of the nuclear quadrupole moment with the local electric field gradient.

1. Hyperfine Hamiltonian

The hyperfine Hamiltonian can be written as a Zeeman interaction between the nuclear magnetic moment, $\vec{\mu}$, and an effective internal field, $\vec{H}$.

$$\mathcal{H}_{hf} = -\vec{\mu} \cdot \vec{H} \tag{4-2}$$

The magnitude of the internal field, whether measured at a bromine or chromium nuclear site, is proportional to the magnetization, as we shall now explain.

The sources of the internal field at a given nuclear position are the spins on the surrounding Cr^{3+} ions. The magnitude and direction of this field are determined primarily by the hyperfine interaction, but there is also a small dipole contribution.

The instantaneous internal fields at the i^{th} bromine site, $\vec{H}_i(t)$, and at the j^{th} chromium site, $\vec{H}'_j(t)$, can be written as follows:

Bromine Site

$$\vec{H}_i(t) = \sum_n \overleftrightarrow{A}_{in}(t) \cdot \vec{S}_n(t) + \sum_k \overleftrightarrow{D}_{ik}(t) \cdot \vec{S}_k(t) \tag{4-3}$$

Chromium Site

$$\vec{H}'_j(t) = A'(t)\ \vec{S}_j(t) + \sum_p \overleftrightarrow{D}'_{jp}(t) \cdot \vec{S}_p(t)$$

$\vec{S}_n(t)$ is the Cr^{3+} spin on the n^{th} chromium ion, A'(t) is the direct hyperfine constant for the field at a chromium nucleus, $\overleftrightarrow{A}_{i,n}(t)$ is the transferred hyperfine tensor for the field at a bromine nucleus, and $\overleftrightarrow{D}_{ik}(t)$ and $\overleftrightarrow{D}'_{jp}(t)$ are the dipole-dipole tensors for the i^{th} bromine and j^{th} chromium sites, respectively. The sum index, n, in the bromine hyperfine interaction runs over the two nearest neighbor Cr^{3+} ions. The dipole sums over k and p should in theory run over all the spins in the crystal. In practice, however, they need run only over the spins in the nearest domains; the dipole effects of spins in far removed domains average out to zero. The bromine hyperfine tensor, the chromium hyperfine constant, and the two dipole tensors are written as functions of time because of the effects of lattice vibrations.

The fluctuation rate of each spin is much faster than the nuclear Larmor frequency. Therefore, the nuclear magnetic moments can only respond to the time average of the instantaneous fields of Eqs. 4-3. In taking the time averages, we note that in general, the lattice vibrations and the spin fluctuations are not correlated. Therefore, the effective internal field at a chromium site can be written

$$\vec{H}_{Cr} = \langle \vec{H}'_j(t) \rangle = \langle A'(t) \rangle \langle \vec{S}_j(t) \rangle + \sum_p \langle \overleftrightarrow{D}'_{jp}(t) \rangle \cdot \langle \vec{S}_p(t) \rangle \qquad (4\text{-}4)$$

A similar expression results for the effective internal field at a bromine site, $\vec{H}_{Br}$.

The time average spin $\langle \vec{S}_j(t) \rangle$ is directly proportional to the magnetization per atom. Therefore, the magnitude of the average internal field is proportional to the magnetization, M(T).

$$H_{Cr} = \lambda_{Cr} M(T)$$
$$H_{Br} = \lambda_{Br} M(T) \qquad (4\text{-}5)$$

The coupling constants, λ_{Cr} and λ_{Br}, contain the time averages of the appropriate hyperfine and dipole coefficients; they may therefore be slightly temperature dependent because of small contributions from the mean square amplitude of the thermally excited lattice vibrations. They might also depend on temperature implicitly through the effects of thermal expansion. We shall in fact show from our data analysis that λ_{Cr} and λ_{Br} are not temperature dependent below the $CrBr_3$ Curie point. Thus we may write $\mathcal{H}_{hf}$ in the form of Eq. 4-2 where the magnitude of $\vec{H}$ therein is proportional to the magnetization.

We now discuss the eigenvalues of the hyperfine Hamiltonian. We re-express the general hyperfine term, representing the magnetic moment $\vec{\mu}$ with the nuclear gyromagnetic ratio, γ_N, and the nuclear spin, $\vec{I}$.

$$\mathcal{H}_{hf} = -\hbar \gamma_N \vec{I} \cdot \vec{H} \qquad (4\text{-}6)$$

The coordinate system to which the $\vec{I}$ and $\vec{H}$ vectors are referred is arbitrary, but in the present case it is convenient to use a coordinate system determined by the lattice structure. Having selected such a system, if the internal field happens to lie along the z coordinate axis, the eigenstates of this Hamiltonian for I = 3/2 are the four spin states $|m\rangle$ for which the z-component of the spin is the good quantum number. The eigenvalues in this case are given by

$$E_m = -\hbar \gamma_N H m \qquad m = \pm 1/2, \pm 3/2 \qquad (4\text{-}7)$$

and the frequency of radiation needed to induce a transition between adjacent levels is

$$\nu = \frac{\gamma_N}{2\pi} H \qquad (4\text{-}8)$$

Note, however, that if we use the $|\ m\ \rangle$ states as the basis for a 4 x 4 matrix representation of $\mathcal{H}_{hf}$ but H does not lie along the z coordinate axis, then $\mathcal{H}_{hf}$ is not diagonal. There will be non-zero matrix elements between $|\ m\ \rangle$ states which differ by one unit in m.

2. Quadrupole Hamiltonian

The second term in the general Hamiltonian contains the interaction between the nuclear electric quadrupole moment and the electric field gradient (EFG) at the nuclear site. In general, the part of the electric field gradient which contributes to the nuclear quadrupole interaction is a real, symmetric, traceless tensor, φ_{ij}, the components of which are the second derivatives of the electrostatic potential evaluated at the nuclear position.[42] Such a tensor is diagonal in its principal axis coordinate system. We shall always choose our coordinates to be the principal axis frame of the EFG tensor.

In the principal axis frame, the quadrupole Hamiltonian is written

$$\mathcal{H}_Q = \frac{e^2 Qq'}{4I(2I-1)} \left\{ 3I_z^2 - I(I+1) + \frac{\eta}{2}(I_+^2 + I_-^2) \right\} \qquad (4\text{-}9)$$

In this expression, e is the electronic charge, Q is the nuclear quadrupole moment and I_z, I_+, and I_- are the familiar spin operators. The three

components of the diagonal EFG tensor appear in q' and η in the following way. The component with the largest magnitude is $q' = \varphi_{zz}$; this choice specifies the z axis of the coordinate system. The EFG tensor is traceless; that is,

$$\varphi_{xx} + \varphi_{yy} + \varphi_{zz} = 0 \tag{4-10}$$

Therefore, only one additional parameter is required to specify the EFG tensor. It is conventional to define the asymmetry parameter, η, by

$$\eta = \frac{\varphi_{xx} - \varphi_{yy}}{\varphi_{zz}} \tag{4-11}$$

Because of our choice of z axis

$$|\eta| \leq 1 \tag{4-12}$$

For $I = 3/2$, in particular, we can write

$$\mathcal{H}_Q = \frac{hq}{6} \left\{ 3I_z^2 - \frac{15}{4} + \frac{\eta}{2}(I_+^2 + I_-^2) \right\} \tag{4-13}$$

where h is Planck's constant and where

$$q = \frac{e^2 Q q'}{12h} \tag{4-14}$$

If the $|m\rangle$ states are used for a 4 x 4 matrix representation of $\mathcal{H}_Q$ the term proportional to η will produce off-diagonal matrix elements between states which differ by two units in m. The four eigenvalues of this Hamiltonian are doubly degenerate:

$$E = \pm \frac{hq}{2}\left(1 + \frac{\eta^2}{3}\right)^{1/2} \qquad (4\text{-}15)$$

Only one transition is possible, and has a frequency

$$\nu = q\left(1 + \frac{\eta^2}{3}\right)^{1/2} \qquad (4\text{-}16)$$

If the electric field gradient is axially symmetric ($\eta = 0$), the $| m \rangle$ state representation is diagonal; the energies are

$$E_{\pm 3/2} = + \frac{hq}{2}$$
$$E_{\pm 1/2} = + \frac{hq}{2} \qquad (4\text{-}17)$$

In general, the values of q and η can be expected to be temperature dependent[22] because of the effects of lattice vibrations and thermal expansion. We shall show from the data analysis that while the temperature dependences of these quantities are small, they are not negligible.

3. Combined Hamiltonian

Before putting the full Hamiltonian together, we insert one more definition. For notational convenience, we introduce a modified nuclear gyromagnetic ratio with the dimensions and units indicated:

$$\gamma = \frac{\gamma_N}{2\pi} \qquad ((\text{Mc/sec})/\text{KGauss})$$

In combining the two terms of our Hamiltonian, we divide all quantities by Planck's constant and express the Hamiltonian in frequency units (Mc/sec).

The total combined Hamiltonian, then, is

$$\mathcal{H}' = \frac{1}{h} \left(\mathcal{H}_{hf} + \mathcal{H}_Q \right)$$

$$= -\gamma \vec{I} \cdot \vec{H} + \frac{q}{6} \left\{ 3 I_z^2 - \frac{15}{4} + \frac{\eta}{2} \left(I_+^2 + I_-^2 \right) \right\} \qquad (4\text{-}18)$$

This Hamiltonian represents a physical model which will be used to interpret the frequencies and temperature dependences of the chromium and bromine NMR lines. Analysis of the data in terms of this model will yield information on the magnitudes, directions, and temperature dependences of the hyperfine fields at both chromium and bromine sites; we will also obtain the magnitudes and temperature dependences of the components of the electric field gradient tensors at the two sites. The temperature dependences of the EFG components which we find suggest a thermal expansion increase near the Curie point, while the temperature dependences of the two hyperfine fields provide detailed information on the temperature dependence of the magnetization all the way from $4.2^{\circ}K$ to $32.35^{\circ}K$, which is $0.993\ T_c$.

C. Interpretation of the Chromium NMR Data

The triplet of Cr^{53} lines was first found by Gossard, Jaccarino, and Remeika[2] and identified by them as coming from nuclei inside ferromagnetic domains. The large time average internal field at the chromium site (240 KGauss at $4.2^{\circ}K$) is parallel to the hexagonal c axis of the crystal, the easy magnetization direction. There is also a small

electric field gradient set up by the surrounding bromine ions. Because of the presence of axial symmetry around the chromium site, the z direction of the diagonal chromium EFG tensor also lies along the c axis, and the asymmetry parameter is zero.

The energy levels appropriate to the Cr^{53} nucleus are shown in Fig. 12. The Zeeman energies, $h\gamma^{53}H_{Cr}M$, are shifted by the quadrupole energies of Eq. 4-17. Since both the m = +1/2 and m = -1/2 levels are affected equally by the quadrupole interaction, the frequency of the $+1/2 \leftrightarrow -1/2$ transition is equal to $\gamma^{53}H_{Cr}$. The frequencies of the two satellite lines are $\gamma^{53}H_{Cr} \pm q^{53}$. Thus, for the data tabulated in Table I, the central Cr^{53} NMR frequency, $\nu^{53}(T)$, is proportional to $H_{Cr}(T)$, while the satellite splitting is equal to q^{53}.

The value of the quadrupole splitting, q^{53}, decreases from 296.6 Kc/sec at 4.2°K to 280 Kc/sec at 29.74°K, a total change of about 5%. This temperature dependence is one indication of the presence of a thermal expansion anomaly at the Curie temperature. A more detailed interpretation of this 5% shift in terms of a model for the thermal expansion anomaly will be presented later in the chapter.

The accuracy with which $H_{Cr}(T)$ can be related to the magnetization M(T) depends on the constancy of λ_{Cr}. We shall assume that λ_{Cr} is a constant; later we will show this assumption to be entirely consistent with our data. With a constant λ_{Cr}, the temperature dependence of the magnetization is obtained from $\nu^{53}(T)$ as follows:

$$\frac{M(T)}{M(0)} = \frac{H(T)}{H(0)} = \frac{\nu^{53}(T)}{\nu^{53}(0)} \qquad (4\text{-}19)$$

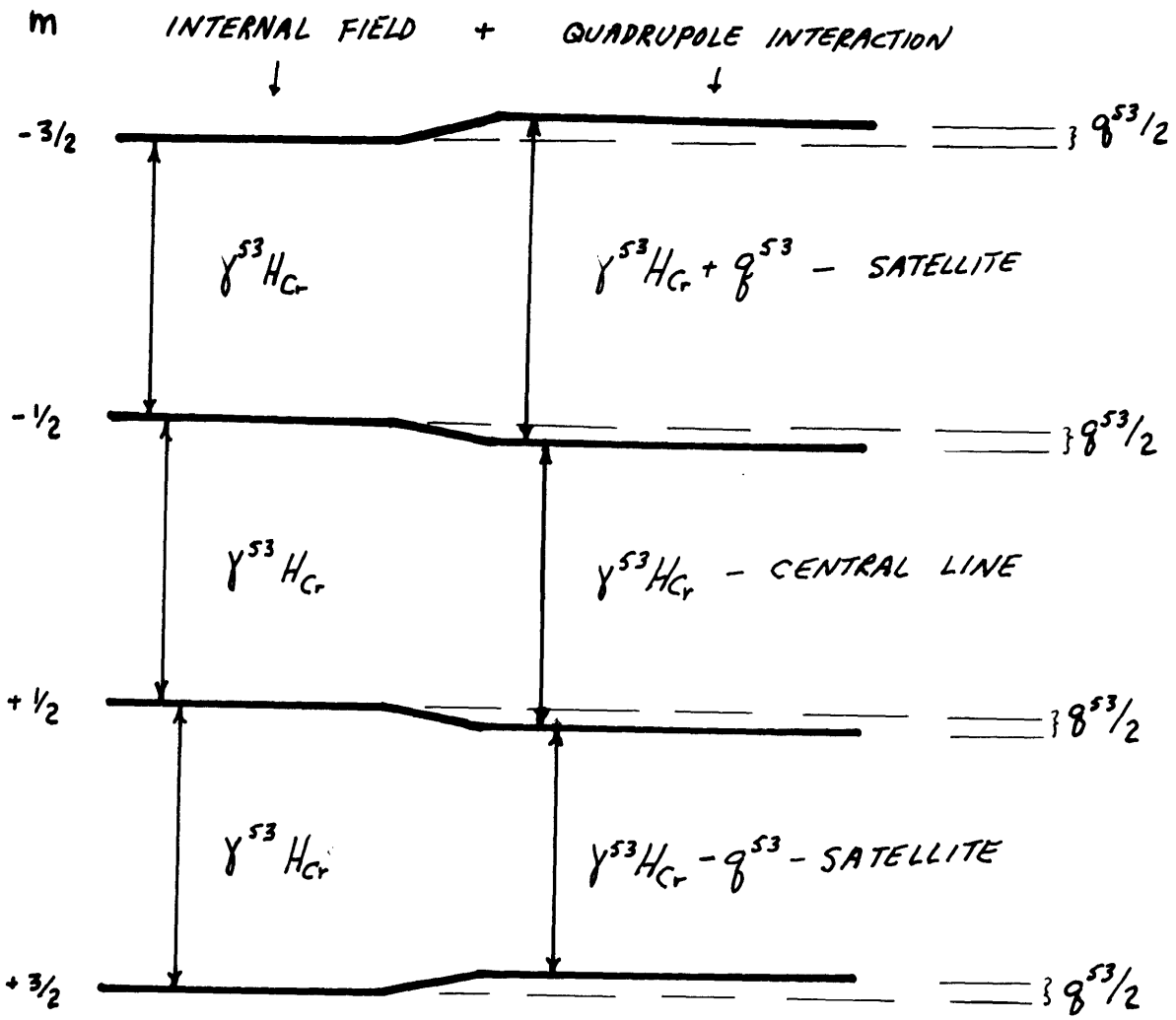

Fig. 12 Cr^{53} energy levels.

We use Davis and Narath's value,[10] $\nu^{53}(0) = 58.099$ Mc/sec, which they obtained by extrapolating to $0^{\circ}K$ their $\nu^{53}(T)$ data above $1.44^{\circ}K$. This frequency corresponds to a value of $H_{Cr}(0) = 241.48$ KGauss.

The temperature dependence of the magnetization from $4.2^{\circ}K$ to $29.74^{\circ}K$ is obtained from our $\nu^{53}(T)$ data using Eq. 4-19. The results are given in Table VIIa at the end of the chapter. Although the Cr^{53} NMR lines faded out above $29.74^{\circ}K$, we were able to use the bromine NMR lines to extend our determination of the temperature dependence of the magnetization to $32.35^{\circ}K$. Presentation of the results above $29.74^{\circ}K$ will follow the interpretation of the bromine NMR data.

D. Identification of the Bromine NMR Lines

1. Origin of the Bromine Lines

I discovered a strong absorption line quite by accident while sweeping temperature near $17^{\circ}K$ at 49.6 Mc/sec. A wide search revealed a second low frequency line near $13^{\circ}K$. The strong signals from these resonances seemed to indicate that they came from a nuclear species which had an abundance comparable to that of the chromium nuclei. This suggested the bromine nuclei as the origin of the new lines.

We knew of the bromine quadrupole interaction from the work of Barnes and Segel,[12] and we guessed that the new pair of resonances might be the result of the splitting of the pure quadrupole resonance by a transferred hyperfine field. In order to prove the validity of this

interpretation, we must first examine how the general Hamiltonian of Eq. 4-18 is to be applied to the bromine interactions.

The Electric Field Gradient Tensor We wish to determine the orientation of the bromine EFG principal axis coordinate system relative to the crystal axes. If we consider as a preliminary model the planar configuration of a bromine ion plus its two nearest neighbor chromium ions, we can use a simple symmetry argument to locate one of the principal axes. The bromine nearest neighbor geometry is shown in Fig. 13. The plane containing the crystal c axis and a line which bisects the Cr-Br-Cr angle, α, is a plane of local reflection symmetry, P. Because of this symmetry, one of the three EFG principal axes must be perpendicular to this plane, and must therefore lie in the hexagonal layer of bromine ions. We label this axis as the y axis. (For the moment, the naming of the coordinate axes can be considered an assumption. We will show that our specification of the z direction in Fig. 13 is correct in terms of the largest component of the diagonal EFG tensor.) The remaining two axes must lie in the symmetry plane; their orientation can be completely specified by the angle, ψ, between the crystal c axis and the EFG z axis. In the nearest neighbor model, specifically, the z axis is perpendicular to the Cr-Br-Cr plane and thus the crystal geometry leads to $\psi = 54.7^{o}$.

When we wish to include the effects of ions farther removed than the nearest neighbor chromium ions, a question arises concerning the applicability of this simple model. It involves the fact that the local reflection symmetry which we used to determine the direction of the y

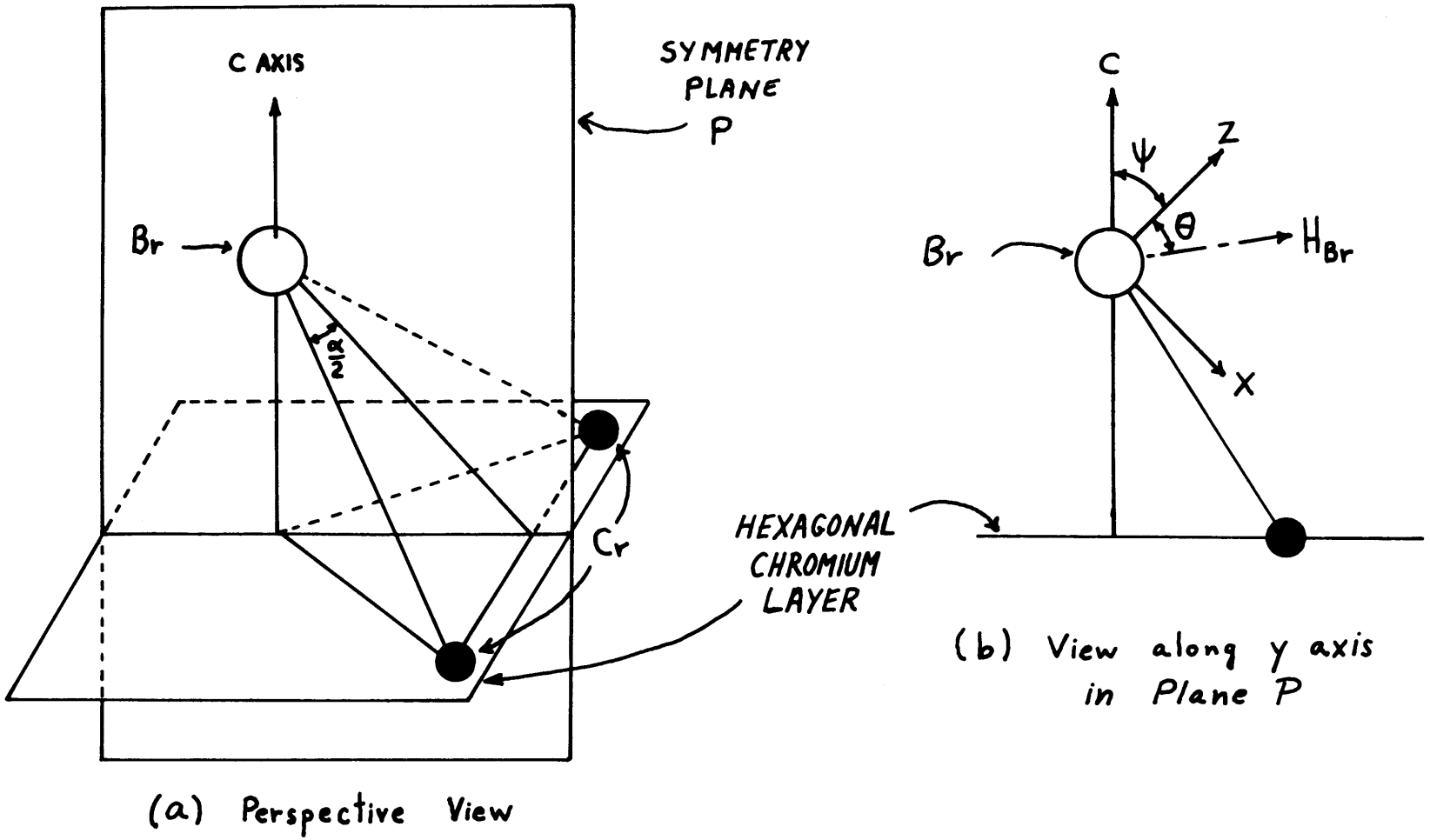

Fig. 13 Bromine site - nearest neighbor geometry.

axis does not extend throughout the entire crystal (the crystal structure is shown in Fig. 1). The layers of bromine atoms all possess this reflection symmetry relative to the plane P. And the layer of chromium ions containing the nearest neighbors has this reflection symmetry, as does every third layer of chromium ions above and below this nearest neighbor layer. But half of the ions in the remaining two-thirds of the chromium layers are located in sites for which the corresponding reflected sites are vacant (see Fig. 14). Therefore we cannot, using only a symmetry argument, be entirely sure that the x-z plane of the EFG principal axis system coincides with the local symmetry plane of Fig. 13. In the model which we shall use to analyze the NMR data, we shall assume, in effect, that the local symmetry plane, P, and the EFG x-z plane do coincide. In the discussion which follows, we present an estimate of the amount by which the two planes might differ.

A point charge model was used to study the principal axis geometry in more detail. The purpose of this calculation was to evaluate the relative contribution to the EFG tensor from those chromium ions not having reflection symmetry. In particular, we wished to know by what amount the x or z principal axes might be rotated out of the symmetry plane because of the contribution of these non-symmetrically located ions.

In the point charge model, each ion in the crystal is replaced by an equivalent point charge at the appropriate lattice site. The EFG tensor is calculated by simply summing the contributions from each ion. We have determined the point charge EFG tensor set up by 17 ions surrounding a central bromine site. The calculation was done in three

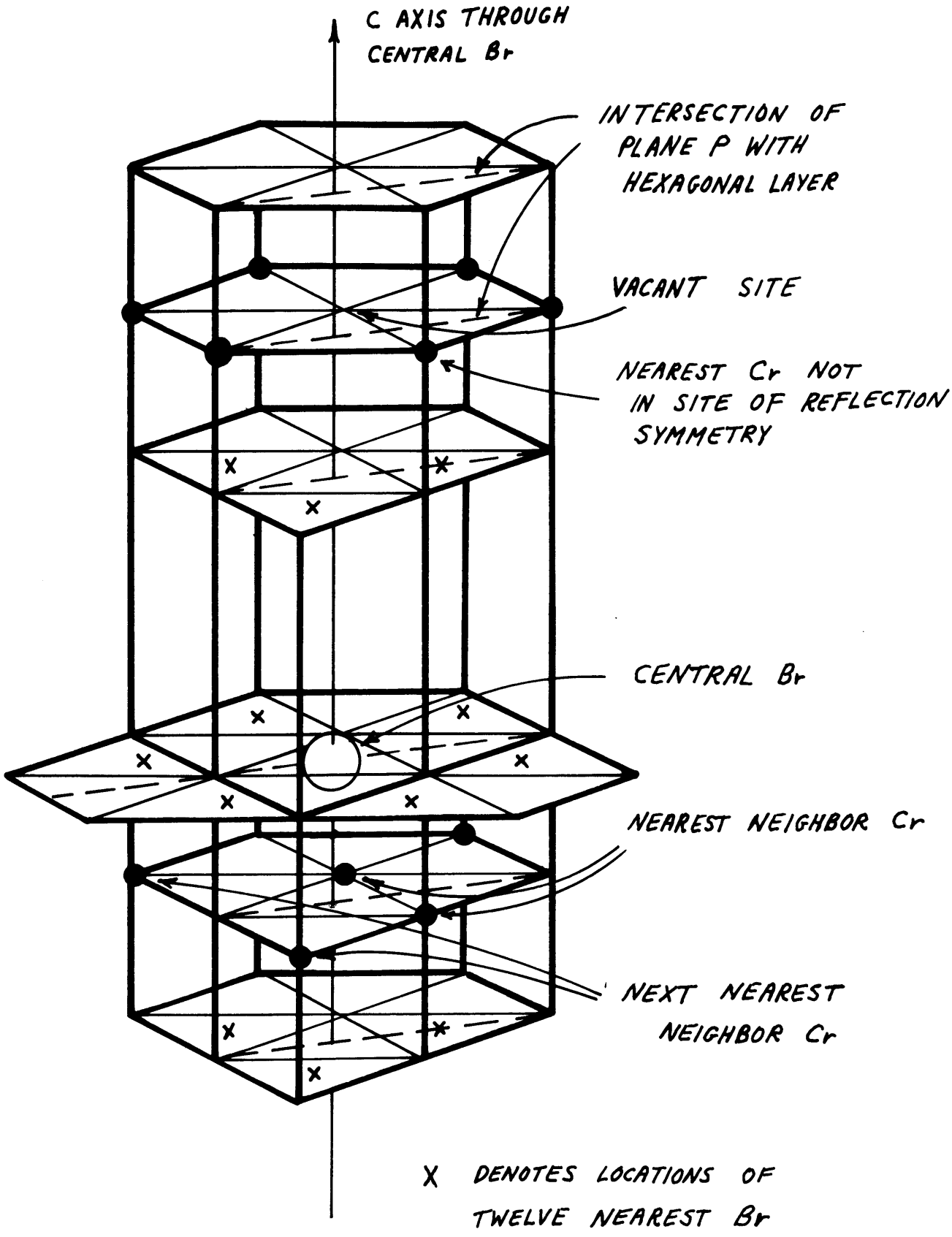

Fig. 14 Bromine site - ion locations for point charge calculation.

stages of increasing complexity:

(i) 2 nearest neighbor chromium ions only, as in Fig. 13.

(ii) 2 nearest neighbor chromiums, plus 2 next nearest neighbor chromiums, plus 12 nearest neighbor bromine ions, a total of 16 ions. All of these ions have the desired reflection symmetry relative to plane P. The locations of these ions are indicated in Fig. 14.

(iii) The 16 ions listed in (ii) above, plus the nearest non-symmetrically located chromium ion. The location of this ion relative to the bromine site of interest is also shown in Fig. 14.

For each of these three cases, the point charge EFG tensor was calculated using a coordinates system x'y'z' which was like the xyz system of Fig. 13, but with $\psi = 0$; the z' axis coincided with the crystal c axis while the y' axis coincided with the y axis of Fig. 13. In the primed coordinates, the EFG tensors of cases (i) and (ii) have only one non-zero off-diagonal component, $\varphi_{x'z'}$. The other two off-diagonal components vanish because of the reflection symmetry, $y' \longleftrightarrow -y'$. In both these cases, the transformation to the xyz principal axis coordinates involves a single simple rotation about the y' axis through the angle ψ. We find the new xyz coordinates by requiring $\varphi_{xz} = 0$. In case (i) $\psi = 54.7^{o}$; In case (ii) $\psi = 57.5^{o}$. In both cases, our identification of the EFG z axis is found to be correct, i.e. the maximum value of φ_{ii} is along the z axis. There is one significant difference between the results for cases (i) and (ii), the value for the asymmetry parameter, η. In case (i), η is essentially zero. The inclusion of the farther neighbors in case (ii) results in a very large value, $\eta = 0.45$.

When we calculate the EFG tensor for case (iii), the only significant change from case (ii) is that we obtain small non-zero values for both $\varphi_{x'y'}$ and $\varphi_{y'z'}$. In order to evaluate the amount by which these off-diagonal components could rotate the x and z principal axes out of the symmetry plane, we first carry out a rotation about the y' axis similar to cases (i) and (ii). We rotate about y' into the xyz coordinate system in which $\varphi_{xz} = 0$. This xyz system would be the correct principal axis system if both $\varphi_{x'z'}$ and $\varphi_{y'z'}$ were zero. In this case, the angle of rotation is $\psi = 61^{o}$. In the new xyz coordinate system, the EFG tensor is

φ_{ij}	x	y	z
x	5.00	-1.20	0
y	-1.20	13.03	0.34
z	0	0.34	-18.03

$$\times \frac{e}{a^3}$$

where e is the electronic charge and a is the Cr-Cr separation.

We can estimate the effect of the remaining off-diagonal components by asking how large a rotation in the coordinate axes would be required to diagonalize each 2 x 2 submatrix. For example, the rotation δ_z about the z axis required to diagonalize the x-y submatrix is given approximately by

$$\tan \delta_z \approx \left| \frac{\varphi_{xy}}{\varphi_{xx} - \varphi_{yy}} \right|$$

In this case, $\delta_z = 8.5^{o}$. The corresponding angle, δ_x, for the rotation about x is negligibly small, about 0.5^{o}.

We think that these values of δ_x and δ_z are overestimates of the true amount by which the x or z principal axes might be rotated out of the symmetry plane. The selection of only one non-symmetrically located ion for case (iii) was extreme, in that the contributions of additional non-symmetrically located ions partially cancel the off-diagonal EFG components set up by that single ion. Also, the inclusion of additional symmetrically located ions in the model would increase the magnitude of the diagonal components of φ_{ij} relative to the off-diagonal elements. We estimate that these two effects will combine to reduce δ_x and δ_z by a factor of about 3.

A second reason for believing that our values of δ_x and δ_z are too large comes from the fact that the point charge model fails to account for the charge density in the bonds joining the bromine ion to its nearest neighbor chromium and bromine ions. Some of the "point charge" really resides in these bonds and is, therefore, closer to the bromine nucleus than the strict point charge model indicates. Since the EFG tensor components go as the inverse third power of the distance, neglect of these nearby charge densities would result in an underestimate of the magnitudes of the diagonal components of the EFG tensor. Quantitative estimates of this effect are difficult to make, but an additional factor of 2 reduction in δ_x and δ_z from this source is not inconceivable. Thus we expect $\delta_z \approx 1^o - 2^o$; $\delta_x \approx 0$.

To summarize, then, we find that to a very good approximation, the principal axes of the bromine EFG tensor are oriented as shown in Fig. 13 with the angle ψ having a value in the range $55^o - 60^o$; the

asymmetry parameter η could be as large as 0.45. The x axis might deviate from the symmetry plane by an angle on the order of 1^{o}. We shall neglect this potential deviation when analyzing the NMR data; later we will comment on how large an effect such a deviation might have on our results.

Internal Magnetic Field We next examine the internal magnetic field at the bromine site. This field, $\vec{H}_{Br}$, is primarily due to a transferred hyperfine field from the aligned spins on the nearest neighbor chromium ions. The symmetric location of these ions with respect to the x-z plane means that the resulting hyperfine field from the two ions must lie in the x-z plane as shown in Fig. 13. No hyperfine field is expected from more distant spins, but there will be dipole fields. In particular, one must ask whether the dipole fields from the spins on the non-symmetrically located chromium ions might tip the resultant internal field slightly out of the symmetry plane. A good measure of the amount of such tipping is the ratio of the total y component of the dipole field to the total magnitude of the internal field. We can obtain a conservative estimate of the maximum possible magnitude of the y component of the field by considering the y component of the dipole field set up by one spin located on the nearest non-symmetrically located chromium ion. (Contributions from other non-symmetrically located ions will partially cancel the dipole field of this single spin.) Assuming that this spin is lined up along the c axis (easy magnetization direction) and has a time average value of 3 Bohr magnetons (the saturation value at absolute zero), the y component of the dipole field at the bromine

nucleus of interest is about 200 Gauss. Anticipating our results somewhat, we know that the magnitude of the total internal field at a bromine site at absolute zero is 37.7 KGauss. The ratio of these two fields is about 0.005, meaning that the maximum angle by which the internal field could be tipped out of the symmetry plane is about 0.3^{o}. This small angle can be and will be neglected. Therefore, the direction of the internal field relative to the EFG principal axes can be specified with a single angle, θ, as shown in Fig. 13.

Note that the principal axes at the various bromine sites in the crystal are oriented differently in space. Because of this fact, it had been previously assumed[12] that the onset of a transferred hyperfine field below T_c would broaden the pure quadrupole resonances into oblivion. In fact, however, the direction of the internal field at each bromine site is fixed relative to the principal axis coordinates. Therefore, even in the presence of a large time average hyperfine field, all the bromine sites are exactly equivalent, and the resonance frequencies are well defined.

Use of the Hamiltonian Properties The general Hamiltonian of Eq. 4-18 is rewritten showing the explicit θ dependence appropriate to bromine nuclei:

$$\mathcal{H} = \frac{q}{6}\left\{3I_z^2 - \frac{15}{4} + \frac{\eta}{2}(I_+^2 + I_-^2)\right\} - \gamma H_{Br}\left\{I_z \cos\theta + \frac{I_+ + I_-}{2}\sin\theta\right\} \qquad (4\text{-}20)$$

In general, for θ different from zero, the energy levels of $\mathcal{H}$ for a particular bromine isotope look like the diagram[43] in Fig. 15. We sketch here typical eigenvalue curves, assuming $\eta = 0$, as a function of

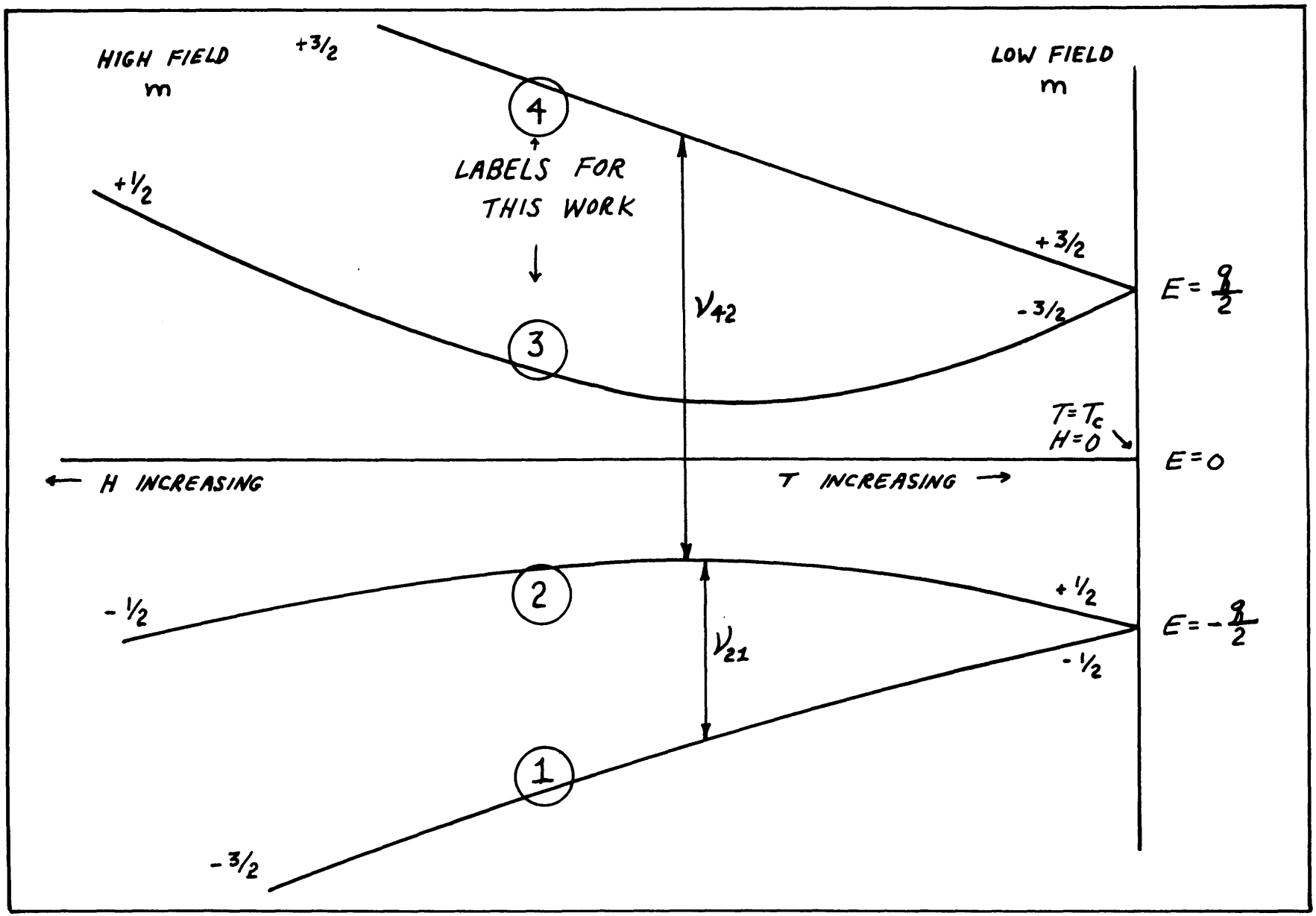

Fig. 15 Typical bromine energy levels (η = 0).

the magnitude of the hyperfine field, H_{Br}. The exact spacings between levels depends on θ as well as on q, η, and H_{Br}. Since H_{Br} is presumed to be a hyperfine field, it is a monotonically decreasing function of temperature. The point $H_{Br} = 0$ corresponds to $T = T_c$ as shown. Also shown in Fig. 15 is our numbering convention for labelling the energy levels and transitions. In general, m is not a good quantum number for the bromine levels. If η is zero, however, m is approximately a good quantum number for very large or very small fields. These approximate quantum numbers in the two limits are shown on the diagram. If η is significantly different from zero, as in $CrBr_3$, the general appearance of the energy level diagram remains the same; however, the assignment of good quantum numbers in the low field limit is no longer valid, and the $H_{Br} = 0$ energies change from $\pm\ q/2$ to $\pm\ (q/2)\ (1 + \eta^2/3)^{1/2}$.

Since m is not a good quantum number, each bromine eigenstate consists of a linear combination of several $|\ m\ \rangle$ states. As a result, transitions between any pair of levels may be possible, although certain pairs will be more probable than others.

Using general properties of the energy level diagrams for the two isotopes, we were able to prove that the two low frequency resonances came from Br^{79} and Br^{81} nuclei undergoing transitions between identically labelled states.[11] For this proof, we do not need to know the values of θ and η; nor do we need to know which pair of states is involved in the transition. The proof uses the functional form of the general Hamiltonian of Eq. 4-18. To exhibit the functional form explicitly, we "normalize" the Hamiltonian by dividing through by q:

$$\frac{\mathcal{H}}{q} = \frac{1}{6}\left\{3I_z^2 - \frac{15}{4} + \frac{\eta}{2}(I_+^2 + I_-^2)\right\} - \left(\frac{\gamma H}{q}\right)\left\{I_z \cos\theta + \left(\frac{I_+ - I_-}{2}\right)\sin\theta\right\}$$

If η and θ do not change with temperature, a very reasonable first approximation, then the entire dependence of $\mathcal{H}/q$ on either temperature or isotope appears within the ratio $(\gamma H/q)$. Therefore, the "normalized" energy levels can be written as a set of functions,

$$\frac{En}{q} = F_n\left(\frac{\gamma H}{q}\right) \qquad n = 1, 2, 3, 4$$

where $F_n(x)$ represents a function of x whose specific form is a fundamental property of the Hamiltonian. Similarly, the "normalized" transition frequencies, given by the difference between normalized energies for two levels, n_1 and n_2, can be written in terms of a second set of functions:

$$\frac{\nu_{n_1, n_2}}{q} = f_{n_1, n_2}\left(\frac{\gamma H}{q}\right) \tag{4-21}$$

To establish the identity of the two new NMR lines we proceed as follows:

i. We assume that one of the lines is due to Br^{79} and that the other line is due to Br^{81} in the same transition. That is we assume

$$\frac{\nu^{79}(T)}{q^{79}} = f_{n_1, n_2}\left(\frac{\gamma^{79} H_{Br}(T)}{q^{79}}\right)$$

$$\frac{\nu^{81}(T)}{q^{81}} = f_{n_1, n_2}\left(\frac{\gamma^{81} H_{Br}(T)}{q^{81}}\right) \tag{4-22}$$

where $f_{n_1, n_2}(x)$ is the same function for both lines.

ii. We assume that the only temperature dependent quantity is the magnitude of the hyperfine field H(T), and that its temperature dependence is given exactly by the temperature dependence of the Cr^{53} central NMR frequency, $\nu^{53}(T)$.

That is, we assume

$$H_{Br}(T) = A\,\nu^{53}(T) \tag{4-23}$$

where A is a constant. In effect, we are taking $H_{Br}(T)$ proportional to the magnetization.

iii. We recall that the quantity, q, (Eq. 4-14) is porportional to the nuclear quadrupole moment Q and to the effective field gradient q'. Kushida[24] has shown that because of the mass dependence of lattice vibration amplitudes, the average effective field gradient might differ slightly (about 0.01%) for the two isotopes. In such a case, the ratio q^{79}/q^{81} would differ by a small amount (< 0.01%) from the ratio of the quadrupole moments Q^{79}/Q^{81}. For the present discussion, we <u>assume</u> that the ratios are exactly equal:[25]

$$\frac{q^{79}}{q^{81}} = \frac{Q^{79}}{Q^{81}} = 1.19706 \tag{4-24}$$

iv. Using the NMR data on the two new lines, we choose two temperatures T_1 and T_2 such that

$$\nu^{79}(T_1) = \left(\frac{q^{79}}{q^{81}}\right) \nu^{81}(T_2) = (1.19706)\, \nu^{81}(T_2) \qquad (4\text{-}25)$$

Comparing Eq. 4-25 with Eq. 4-22, it must then follow that the arguments of $f_{n_1,\, n_2}(x)$ at the two temperatures are equal.
That is, we must have

$$\frac{\gamma^{79} H_{Br}(T_1)}{q^{79}} = \frac{\gamma^{81} H_{Br}(T_2)}{q^{81}} \qquad (4\text{-}26)$$

Writing this result in another way using Eq. 4-23, we obtain a prediction of the ratio of the Cr^{53} frequency for the two temperatures specified by Eq. 4-25:

$$\frac{\nu^{53}(T_1)}{\nu^{53}(T_2)} = \left(\frac{q^{79}}{q^{81}}\right) \times \left(\frac{\gamma^{81}}{\gamma^{79}}\right) \qquad (4\text{-}27)$$

If we use the most recent value for $\gamma^{81}/\gamma^{79} = 1.0779$,[25] we then predict that for T_1 and T_2 chosen according to Eq. 4-25,

$$\frac{\nu^{53}(T_1)}{\nu^{53}(T_2)} = (1.19706)\,(1.0779) = 1.2903 \qquad (4\text{-}28)$$

The NMR data of Tables I and II contain two sets of temperatures T_1 and T_2 which obey Eq. 4-25 well enough to permit a demonstration of the accuracy of this prediction. The results are summarized in Table IV.

Table IV

Comparison of Theory of Bromine Line Origin with Experiment

THEORY:	CONDITION			PREDICTION
	If T_1 and T_2 are chosen so that $\frac{\nu^{79}(T_1)}{\nu^{81}(T_2)} = 1.19706$			Then theory predicts $\frac{\nu^{53}(T_1)}{\nu^{53}(T_2)} = 1.2903$
EXPERIMENT:	T_1	T_2	$\frac{\nu^{79}(T_1)}{\nu^{81}(T_2)}$ from the data of Table II	$\frac{\nu^{53}(T_1)}{\nu^{53}(T_2)}$ from the data of Table I
I	23.160	28.665	1.19713	1.2905
II	25.275	29.435	1.19702	1.2905

The experimental ratios, $\nu^{79}(T_1) / \nu^{81}(T_2)$, for the two cases given in Table IV are sufficiently close to the theoretical value of 1.19706 to allow a meaningful test of the theory. And we note that the corresponding experimental ratios, $\nu^{53}(T_1) / \nu^{53}(T_2)$, match the theoretically predicted value of 1.2903 to within 2 parts in 10^4, well within experimental error. The same accuracy was found throughout the entire range of temperatures for which we could observe the Cr^{53} NMR lines (4.2°K - 29.74°K).

This accurate prediction of the temperature dependence of the Cr^{53} NMR frequency from the temperature dependence of the bromine data not only proves the correctness of our theory for the origin of the new resonances, but also justifies, to a certain degree, our assumptions about the constancy of θ and η and the proportionality between H_{Br} and $\nu^{53}(T)$.

2. Identification of Transitions

With only the NMR data for the two low frequency bromine lines and the chromium lines at our disposal, we were not able to determine uniquely which of the six possible transitions we were observing. Gossard and co-workers[14] clarified the situation considerably with the report of the resonance frequencies for a second pair of bromine lines seen by them at low temperatures. This new high frequency pair of lines turned out to have an origin similar to the low frequency lines we have been discussing. One of the new lines was due to Br^{79} nuclei, the other to Br^{81} nuclei; the labelling of the transition for the Br^{79} line was the same as for the Br^{81} line. Using calculated energy levels for the Hamiltonian of Eq. 4-18 with $\eta = 0$ together with the temperature dependence of the Cr^{53} NMR frequency,

Gossard et. al.[14] attempted to fit the four bromine NMR frequencies and their temperature derivatives at 1.48°K by varying the values of H_{Br} and θ. While it is not clear from their paper how they determined a best fit, and while their agreement between experimental and calculated frequencies is very poor (1%, while their experimental uncertainty was 0.08% or better), they do make an assignment of transitions to the two pairs of lines which is correct. The low frequency lines come from the $n = 2 \leftrightarrow n = 1$ transition (see Fig. 15); the new high frequency lines come from the $n = 4 \leftrightarrow n = 2$ transition.

After we had collected data on the high frequency lines up to $0.99\ T_c$, we carried out a third order perturbation theory analysis of the data at the highest temperatures and confirmed this assignment of the transitions. No other combination of energy levels could possibly fit the data. However, Gossard et. al. obtained values for H_{Br} and θ which were not very good, primarily because their assumption of an axially symmetric field gradient ($\eta = 0$) turned out to be a very bad assumption.

With the origin of the bromine lines now established, and with the transitions for the various bromine lines identified, we can use the Hamiltonian of Eq. 4-20 and our extensive NMR data to investigate the precise behavior of q, H_{Br}, θ and η as functions of temperature.

E. Detailed Analysis of the Bromine NMR Data

1. Scope of the Problem

We have seen that the temperature dependences of the bromine NMR frequencies can be explained quite well using the general properties of the Hamiltonian of Eq. 4-20. In the course of the analysis thus far, several explicit assumptions have been made: (i) that the magnitude of the internal field, $H_{Br}(T)$, is proportional to the Cr^{53} NMR frequency as shown below:

$$H_{Br}(T) = A\,\nu^{53}(T) \tag{4-29}$$

(ii) that the five Hamiltonian parameters, A, θ, q^{79}, q^{81}, and η, are constants; and (iii) that the ratio q^{79}/q^{81} is exactly equal to the ratio of the nuclear quadrupole moments, $Q^{79}/Q^{81} = 1.19706$.

In this section, the bromine NMR data is analyzed in more detail. The data below $29.74^{o}K$ (where $\nu^{53}(T)$ is known) are used to test the assumptions listed above, and to determine the magnitudes (and, as it turns out, the temperature dependences) of the Hamiltonian parameters. The values of the Hamiltonian parameters thus obtained are used above $29.74^{o}K$ to calculate the magnitude of $H_{Br}(T)$ from the experimental bromine NMR frequencies. Since $H_{Br}(T)$ is proportional to the magnetization, the bromine NMR data enable our determination of the temperature dependence of the magnetization to be extended up to $32.35^{o}K$, or $0.993\ T_c$.

2. Reverse Eigenvalue Problem Below $29.74^{o}K$

The experimental bromine NMR frequencies are rather

awkward quantities to work with in our study of the Hamiltonian parameters, because the value of any single NMR frequency depends in a complicated way on the values of all of the parameters. In the first step of our parameter analysis, the set of bromine NMR frequencies at each temperature is transformed into a new set of quantities which are directly related to the values of the Hamiltonian parameters.

At each of twenty temperatures between 4.2°K and 29.74°K, we have measured the resonance frequencies of four bromine lines, two for each isotope. If we allow for the possibility that the Hamiltonian parameters might be temperature dependent and that the ratio q^{79}/q^{81} might depart slightly ($< 0.01\%$) from the ratio of the nuclear quadrupole moments, there are five unknown parameters in the Hamiltonian at each temperature: A, θ, q^{79}, q^{81}, and η. The Cr^{53} NMR frequency does not alter this imbalance because $\nu^{53}(T)$ must be used in Eq. 4-29 to relate A to the strongly temperature dependent internal field.

Because of the underdetermined nature of the problem, we cannot, using the NMR data from only one temperature at a time, determine unique values for all five parameters at each temperature. We can, however, specify the value of one of the parameters and then adjust the values of the other four so as to exactly fit the four bromine NMR frequencies. Specifically, our transformation of the NMR data consists of obtaining unique values of the four Hamiltonian parameters, A, θ, q^{79}, and q^{81} as functions of the fifth parameter, η, and the temperature. For a given value of η, the values of these "calculated parameters" can be considered as experimental data since they are uniquely determined by the bromine

NMR frequencies and since the exact frequencies can be reproduced from the parameters. By carrying out this preliminary transformation of the data, we have brought into clear focus the one remaining degree of freedom in the theory; the problem is now reduced to determining the value of η to be used at each temperature.

We obtained calculated parameters at each temperature for a range of values of η. In the next step of the analysis, we examine the values of the parameters calculated at different temperatures to see whether a constant value of η can be found which results in constant values of the four calculated parameters. Before proceeding to a discussion of this step, however, a few words are in order on how these parameters were calculated from the NMR frequencies.

The calculation was carried out on the IBM 7094 high speed digital computer at the MIT Computation Center. The algorithm developed to reach the correct solution in an efficient way involved dividing the problem into two sections.

In the first section, the data for the two isotopes were treated identically, but separately. Following the specification of the value of η to be used, a sequence of test values of q^{79} was generated. For each test value, say q^{79} (i), a grid of test values of H and θ was generated and used in the Hamiltonian to calculate grids of the NMR frequencies for both transitions. Be means of two inverse interpolations, a unique pair of values, H^{79}(i) and θ^{79}(i) was found for which the calculated frequencies exactly matched the experimental frequencies $\nu_{21}^{79}(T)$ and $\nu_{42}^{79}(T)$. This same process was repeated for the Br^{81} data. Thus, at the end of these

calculations, we had two separate lists of possible solutions. We had the set $q^{79}(i)$, $H^{79}(i)$, $\theta^{79}(i)$, which when inserted in the Hamiltonian would reproduce the experimental Br^{79} frequencies; we had the similar set for the Br^{81} data, $q^{81}(j)$, $H^{81}(j)$, $\theta^{81}(j)$. These lists could be thought of as defining H^{79} as a function of q^{79}, etc. That is, we could think of these two sets of lists as defining four functions: $H^{79}(q^{79})$, $\theta^{79}(q^{79})$; $H^{81}(q^{81})$, $\theta^{81}(q^{81})$.

Physically, there can only be one value of H and one value of θ. The second section of the problem used sequential interpolation to find that unique pair of values, q_o^{79} and q_o^{81}, for which the following two conditions were simultaneously satisfied:

$$H_{Br} = H^{79}(q_o^{79}) = H^{81}(q_o^{81})$$
$$\theta_o = \theta^{79}(q_o^{79}) = \theta^{81}(q_o^{81}) \qquad (4\text{-}30)$$

The hyperfine constant, A_o, was calculated from H_{Br} using the Cr^{53} NMR frequency (Eq. 4-29). The calculated parameter solution, then, consisted of the four quantities, A_o, θ_o, q_o^{79} and q_o^{81}. To insure that no interpolation errors crept in, the correctness of the solution was always tested against the data. In every instance, the final frequencies computed from the parameter solution matched the experimental frequencies to better than ± 1 Kc/sec.

3. Use of Constant Parameters Below 20°K

It was quickly found that when values of η in the vicinity of 0.29 were used to obtain the calculated parameters from the NMR data,

the calculated parameters were very nearly constant in temperature, changing by only a few tenths of a percent between 4.2°K and 29.74°K. This result is illustrated in Fig. 16 with smoothed curves of q^{79} versus temperature obtained from the NMR data using three different values of η. We also indicate in Fig. 16 the values of q^{79} at 34.5°K (i.e., above T_c) obtained from the experimental pure quadrupole resonance frequency (Eq. 4-16) using the same three values of η. The curves of Fig. 16, and their counterparts for the other parameters, contain an enormous amount of information about both the magnitudes and temperature dependences of the Hamiltonian parameters. The two most salient features of Fig. 16 are (i) below about 20°K, constant values of both η and q^{79} appear to be compatible with the data; and (ii) the 0.3 Mc/sec discrepancy between the values of q^{79} above and below T_c strongly suggests that above 20°K, q^{79} does depend on temperature, provided that we insist η remains constant. A similar situation obtains for the values of q^{81}. In the present section (3), we shall be primarily concerned with item (i) above; in the next section (4), we shall consider item (ii).

We know from thermodynamic arguments that the values of the Hamiltonian parameters, even if they are temperature dependent, must become constants at sufficiently low temperatures. Examining the low temperature behavior of the three q^{79} curves of Fig. 16, we see that in the limit $T \to 0$, the curve for $\eta = 0.290$ has a small negative slope with temperature, the curve for $\eta = 0.295$ has essentially zero slope, and the curve for $\eta = 0.300$ has a small positive slope. The immediate conclusion based on the q^{79} values is that at least for the low temperature data, the

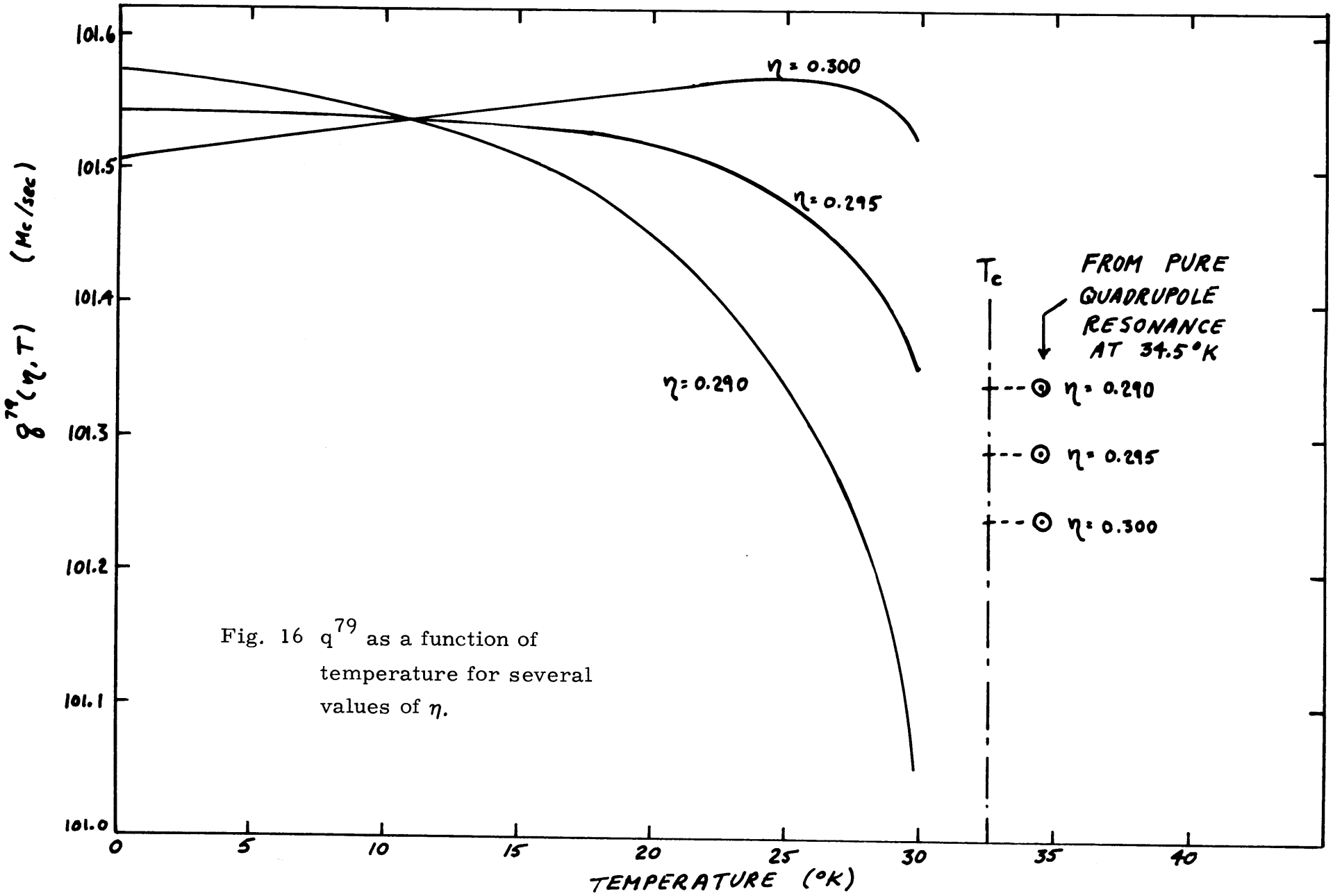

Fig. 16 q^{79} as a function of temperature for several values of η.

correct value of η must be close to 0.295.

Similar investigations of the calculated curves for the other parameters were carried out. The curves for θ showed a zero slope as $T \rightarrow 0$ at an η value of about 0.290. The corresponding zero slope values of η appropriate to q^{81} and A also fell within the range, 0.290 - 0.295.

By inspection, the value $\eta = 0.29325$ was chosen as a compromise constant. The calculated parameters obtained using this particular value of η have limiting slopes as $T \rightarrow 0$ which are very small (about -.002 (Mc/sec)/^{0}K for q^{79} and q^{81}, about +0.001 angular degree/^{o}K for θ, entirely negligible for A). In fact, with this choice of η, the total estimated change in the values of the calculated parameters between absolute zero and 20^{o}K is no bigger than the experimental uncertainty in the calculated parameters at each temperature. Therefore, to within the precision of the NMR data used to derive the values of the parameters, the low temperature values of the parameters are consistent with a set of five constant Hamiltonian parameters. The values of the constants were obtained by averaging the calculated parameters over the temperature range, 4.2^{o}K - 21^{o}K. The results are given in Table V. Also indicated in Table V is the width of the spread of the calculated parameter values over this same temperature range. This width is a conservative estimate of the precision of the constant parameter results.

4. Necessity of Using Temperature Dependent Parameters Above 20^{o}K

While the NMR data below 20^{o}K can be fit with constant

Table V

Constant Hamiltonian Parameters

Parameter	Value	Range	Units
A	0.64869	± 0.00003	KGauss/(Mc/sec)
θ	48.131	±0.015	degrees
q^{79}	101.530	±0.02	Mc/sec
q^{81}	84.815	±0.01	Mc/sec
η	0.29325	(chosen constant)	—
q^{79}/q^{81}	1.19708	±.00009	—

Hamiltonian parameters, it is impossible to fit the NMR data with constants all the way up to 29.74°K. This was demonstrated by calculating the bromine NMR frequencies at each temperature using the correct low temperature constants of Table V together with the Cr^{53} NMR data and Eq. 4-29. It was found that the calculated low frequency bromine NMR frequencies agreed quite well (to within ± 10 Kc/sec) with the experimental values from 4.2°K right up to 29.74°K. The high frequency data, however, which are much more sensitive to the values of q^{79} and q^{81}, were not fit well much above 20°K. The fit was good (± 20 Kc/sec) up to 20°K, but steadily worsened at higher temperatures. Above 29°K, the agreement between calculated and experimental frequencies was only within 100 Kc/sec. In view of the ± 10 Kc/sec experimental precision at these temperatures, this 100 Kc/sec discrepancy is significant.

This discrepancy is not surprising if one examines the q^{79} curves of Fig. 16. First, we note that the curves for constant η show definite temperature dependences above about 20°K. More significantly, we note that for any reasonable value of η in the vicinity of 0.295, the value of q^{79} at 34.5°K obtained from the pure quadrupole resonance frequency differs from the correct low temperature value of q^{79} by about 300 Kc/sec. These facts, together with the demonstrated inability of the constant Hamiltonian parameters of Table V to provide an accurate fit to the NMR data above 20°K, strongly indicate that between 20°K and 34.5°K, q^{79} and q^{81} do depend on the temperature. We must ask, however, whether these apparent temperature dependences might not be a spurious result of having used a slightly incorrect or incomplete Hamiltonian for analyzing the data below T_c.

In applying the general Hamiltonian of Eq. 4-18 to the case of the bromine nuclei, we made an assumption about the exact orientation of the internal field relative to the principal axes of the electric field gradient tensor. The assumption referred to the local reflection symmetry plane at a bromine site (P; see Fig. 13).

Specifically, we assumed that the x-z plane of the principal axis coordinate system coincided with the plane P. The point charge model, however, indicated that the correct axes might be rotated about the z axis by a small angle, $\delta_z \approx 1^o$. Since the internal field does lie in plane P, the presence of a $\delta \neq 0$ would show up in the hyperfine term of the Hamiltonian as an apparent y-component of the internal field, proportional to sin δ_z. In order to find out how large an error a non-zero value of δ_z might produce, we studied the eigenvalue problem for the full Hamiltonian (Eq. 4-18). By examining the secular equation of the Hamiltonian matrix, including the contribution from a y-component of the internal field proportional to sin δ_z, we obtained an estimate of the maximum relative shift in any calculated frequency due to changing the value of δ_z from zero to a small non-zero value:

$$\left| \frac{\Delta \nu}{\nu} \right| \leq \frac{\delta_z^2}{8}$$

For $\delta_z \approx 1^o$, this maximum shift is $\left| \nu/\nu \right| \approx 4 \times 10^{-5}$. This is much less than the experimental uncertainty in most of the NMR data. Therefore, we are entirely justified in ignoring the possibility of a small non-zero δ_z.

A more general check on the correctness of our results is the ratio q^{79}/q^{81}. We recall that in obtaining the values of the constant parameters in Table V, the values of q^{79} and q^{81} were treated as independent quantities. If the results are to be considered physically reasonable, however, their ratio should fall within about 0.01% of the ratio of the nuclear quadrupole moments (1.19706). We note that in Table V, the ratio calculated from the constant parameters is 1.19708, a number which is indistinguishable from the ratio of the quadrupole moments, given the precision of the calculation. Thus, we can find no reason to doubt the correctness either of the Hamiltonian or of the results. Accordingly, we shall accept the shifts in q^{79} and q^{81} as indicating genuine temperature dependences.

We now examine the possibility of there being temperature dependences in the other parameters. We recall that the initial data transformation from NMR frequencies to calculated parameters depended on choosing a value of η to be used at each temperature. Therefore, it is of central importance to establish whether a temperature dependent η is necessary in order to fit the NMR data. The answer can be seen immediately by examining the q^{79} curves of Fig. 16. We consider, in particular, the behavior of the q^{79} curves in the temperature region between 20°K and 34.5°K. We know that whatever the shape of the curve which represents the temperature dependence of q^{79} in this region, the value of q^{79} must be continuous across the Curie point. Therefore, for the correct value of η, the extrapolation of the q^{79} curve for that η from low temperatures up to the vicinity of the Curie point must "match up"

with the value determined at 34.5°K from the experimental pure quadrupole resonance frequency. The meaning of "match up" depends on what value is assumed for q^{79} at T_c (32.56°K). For purposes of demonstration, let us assume that $q^{79}(T_c) = q^{79}(34.5^{\circ}K)$; in other words, we assume that q^{79} is constant above T_c. Then from the experimental data, $q^{79}(T_c)$ for $\eta = 0.295$ is 101.29 Mc/sec. The extrapolated value at T_c from the low temperature $\eta = 0.295$ curve, however, is about 101.1 Mc/sec. Furthermore, the $\eta = 0.300$ low temperature curve extrapolates to a value at T_c which is greater than the 101.24 Mc/sec obtained from the pure quadrupole resonance frequency. Therefore, continuity in q^{79} near T_c requires a value of η in the range, 0.295 - 0.300. A more critical examination of the curves shows that in fact, near T_c, the possible range for η is narrower: $\eta \approx 0.297 - 0.299$. Thus while a value of $\eta = 0.293$ is needed to fit the NMR data at low temperatures, a value of $\eta \approx 0.298$ is needed to fit the data in the vicinity of T_c.

Examination of the calculated parameter curves for θ and A indicates that if η changes from 0.293 to 0.298 between 4.2°K and T_c, then θ must also be temperature dependent (total change in θ is about 0.5 degrees) while A appears to be essentially constant. Thus we find that η, θ, q^{79} and q^{81} all must be taken as slightly temperature dependent in order to fit the NMR data. We now propose a thermal expansion model to explain the presence of these temperature dependences. On the basis of the model, specific functional forms for the temperature dependences of the parameters are than suggested.

5. Thermal Expansion Anomaly - Suggested and Discussed

We propose that the observed temperature dependences are due to an anomalous peak in the $CrBr_3$ thermal expansion at the Curie point. Thermal expansion anomalies are well known at magnetic transitions.[26-28] They arise because with the onset of magnetic order, the expenditure of some elastic energy in a lattice distortion can be more than compensated for by a resulting reduction in magnetic energy (either exchange or dipole). Because of the low temperatures involved in this experiment, there is no other source of temperature dependence large enough to account for the observed shifts in q. This conclusion can be justified as follows:

In the theory of the temperature dependence of a pure quadrupole resonance, there are two sources of temperature dependence, lattice vibrations and thermal expansion.[22, 24] The lattice vibrations enter because the effective field gradient (q') includes a time average over the normal mode amplitudes, which are temperature dependent. Thermal expansion influences the effective field gradient by changing the lattice constants.

Below $35^{\circ}K$, it is not likely that the lattice vibrations produce any significant temperature dependence in the parameters. Jennings and Hansen[23] have measured the specific heat of $CrBr_3$. They found that the lattice contribution to the specific heat could be fit with a sum of two Debye functions. The lower of their two Debye temperatures was $131.3^{\circ}K$, which is about four times as large as the highest temperature encountered in our NMR experiments. Therefore, we feel that the

lattice vibrational modes are in their ground states and hence produce no temperature dependences in the parameters.

In the specific case of q^{81}, we can cite more concrete evidence. Van de Vaart[13] has measured the Br^{81} pure quadrupole resonance frequency from 77°K to room temperature. He found that the frequency changed nearly linearly from 85.652 Mc/sec at 77°K to 85.000 Mc/sec at 297°K. This observed temperature dependence includes the effects of both the lattice vibrations and the thermal expansion far away from T_c. In the absence of any magnetic anomaly, the value of q^{81} below 77°K would level off and at absolute zero, become constant. For purposes of comparison, however, if we suppose that the temperature dependence of q^{81} observed between 77°K and 297°K persisted all the way to absolute zero, then the total change in q^{81} between absolute zero and the Curie point would only be 100 Kc/sec, less than half of the observed change in q^{81}. Therefore, we conclude that there is an anomalous contribution to the total change in the form of a peak in the thermal expansion at the Curie point. The existence of this anomaly would explain why temperature dependent Hamiltonian parameters are in fact needed to fit the NMR data in detail.

This model can be elaborated further. At room temperature, the bromine ions within each three-layer Br-Cr-Br sandwich are arranged in a nearly close-packed configuration. Between the sandwiches, however, there is ample room for lattice contraction. Therefore, the largest contraction as the sample is cooled through T_c should be in the lattice parameter along the c axis which describes the spacing between the

sandwiches. We shall comment on evidence supporting the existence of this anisotropy in the thermal expansion anomaly after we have obtained the final results for the temperature dependent parameters.

Implications of a Thermal Expansion Anomaly at T_c We know the value of q^{79} at low temperatures and we know the value of q^{79} at $34.5^{o}K$. In this section, we shall use our thermal expansion model to assist in the selection of appropriate interpolation functions for obtaining the value of q^{79} at points in between. Once we have specified q^{79} at each temperature, we can work backwards, using the parameters calculated from the NMR data, and determine the value of η at each temperature and, therewith, determine the values of q^{81}, θ, and A. Our first concern, in view of the proposed thermal expansion anomaly, is to specify the shape of the interpolation functions to be used for describing the temperature dependent parts of the various parameters.

If the temperature dependences of the parameters can be related to an anomalous thermal expansion along the c axis of the crystal, then the four parameters, q^{79}, q^{81}, η, and θ, should all behave similarly with temperature. The reason for this similarity is that all four parameters should depend linearly on the change in lattice parameter, for small changes in the lattice parameter. (This is obvious for q^{79} and q^{81}, but not so obvious for η and θ. We have explicitly demonstrated the dependence on the change in lattice parameter in η and θ using our point charge model of the bromine electric field gradient; in the event that the point charge model is not entirely valid, this linearity may also follow from some more

general argument, but we have not investigated this eventuality.) Thus, the changes in q^{79}, q^{81} and η come directly from the linear dependence of the EFG tensor components on the change in lattice parameter; the change in θ, while also linearly dependent on the change in lattice parameter, comes from a small rotation of the direction of the principal axes (i.e., a change in the angle ψ of Fig. 13) to compensate for the altered charge distribution. Thus a temperature dependence in θ arises not from a change in the direction of the hyperfine field, but from a change in the orientation of the coordinate system in which that direction is specified. The anticipated similarity in temperature dependences can be stated as follows: If p(T) is one of the above four parameters, C_1 and C_2 are constants, and f(T) is some appropriate temperature dependent function, then each of the parameters should obey a relation like

$$p(T) = C_1 + C_2 f(T) \qquad (4\text{-}31)$$

The values of C_1 and C_2 are different for different parameters, but the same f(T) is used for all four parameters.

Our principal choice for the function f(T) is the reduced magnetization, m(T) = M(T)/M(O). The reduced magnetization has three desirable properties: (i) m(T) approaches absolute zero with zero slope. Thus, the parameters automatically become constant at low temperature, as required. (ii) m(T) shows anomalous behavior at T_c; i.e., its most rapid change occurs as $T \rightarrow T_c$. (iii) m(T) is a convenient "anomalous" function to use; we know its temperature dependence from the Cr^{53} NMR data.

We could equally well choose some power of m(T) as the function to represent the temperature dependent parts of the parameters. In order to see whether our results were sensitive to the assumed shape of the temperature dependent parts, we decided to fit the calculated parameters using two different functions, m(T) and $m(T)^2$, and then compare the results.

We have thus specified the shape of the curves, in particular the shape of the curve to be used for η. What we now need is a criterion for choosing the constants in Eq. 4-31. The criterion we use is somewhat indirect.

The procedure for determining η uses two facts: (i) We know q^{79} both above and below T_c. (ii) At any temperature, the same NMR data which we used to determine q^{79} if η was known can be equally well used to determine η if q^{79} is known. Since we know (Table V) the value of q^{79} at low temperatures, once we specify what value q^{79} has at T_c (see below), we can immediately draw between these two values the appropriate linear function of m(T) or $m(T)^2$. This linear function represents our final determination of $q^{79}(T)$. We then work backwards using the parameters calculated from the NMR data to find those η values required at each temperature to yield the correct behavior of $q^{79}(T)$. These η values are then fit with a linear function of m(T) (or $m(T)^2$, if appropriate). Once this linear function for $\eta(T)$ is determined, values of $q^{81}(T)$ and $\theta(T)$ are obtained from the calculated parameters and are fit with functions of the appropriate shape. Values of A are also obtained and examined for possible temperature dependence.

The one step in the procedure we have not yet decided upon is the choice of the value q^{79} is to have at T_c. Referring to Fig. 16, we know that the value of q^{79} at 34.5°K is about 101.25 Mc/sec, while the value at absolute zero is about 101.56 Mc/sec. The problem is, how much of this 0.31 Mc/sec change occurs below the Curie point (32.56°K) and how much above the Curie point. Said another way, how symmetric about T_c is the thermal expansion anomaly? A survey of the data for some other magnetic materials in which thermal expansion anomalies have been seen was inconclusive.[26,27] The best guess we can make is that if the peak is not symmetric about T_c, then the greater part of the thermal expansion takes place below T_c. This would mean that between 50% and 100% of the 0.31 Mc/sec change in q^{79} would take place below T_c. The remainder would take place between T_c and 34.5°K, since immediately above 34.5°K, NMR revealed that q^{79} was constant. This is represented schematically in Fig. 17.

In the absence of careful thermal expansion measurements on $CrBr_3$, it was decided to carry through two complete analyses which would bracket the expected correct $q^{79}(T_c)$ value. That is, we analysed the parameters twice once assuming that 100% of the change in q^{79} occurred below T_c. These two solutions are referred to as the FULL solution and the HALF solution, respectively. In both solutions, we wished to compare the results for the m(T) and $m(T)^2$ shaped curves; therefore, a grand total of four separate fits was made to the data. The results are presented in the following section.

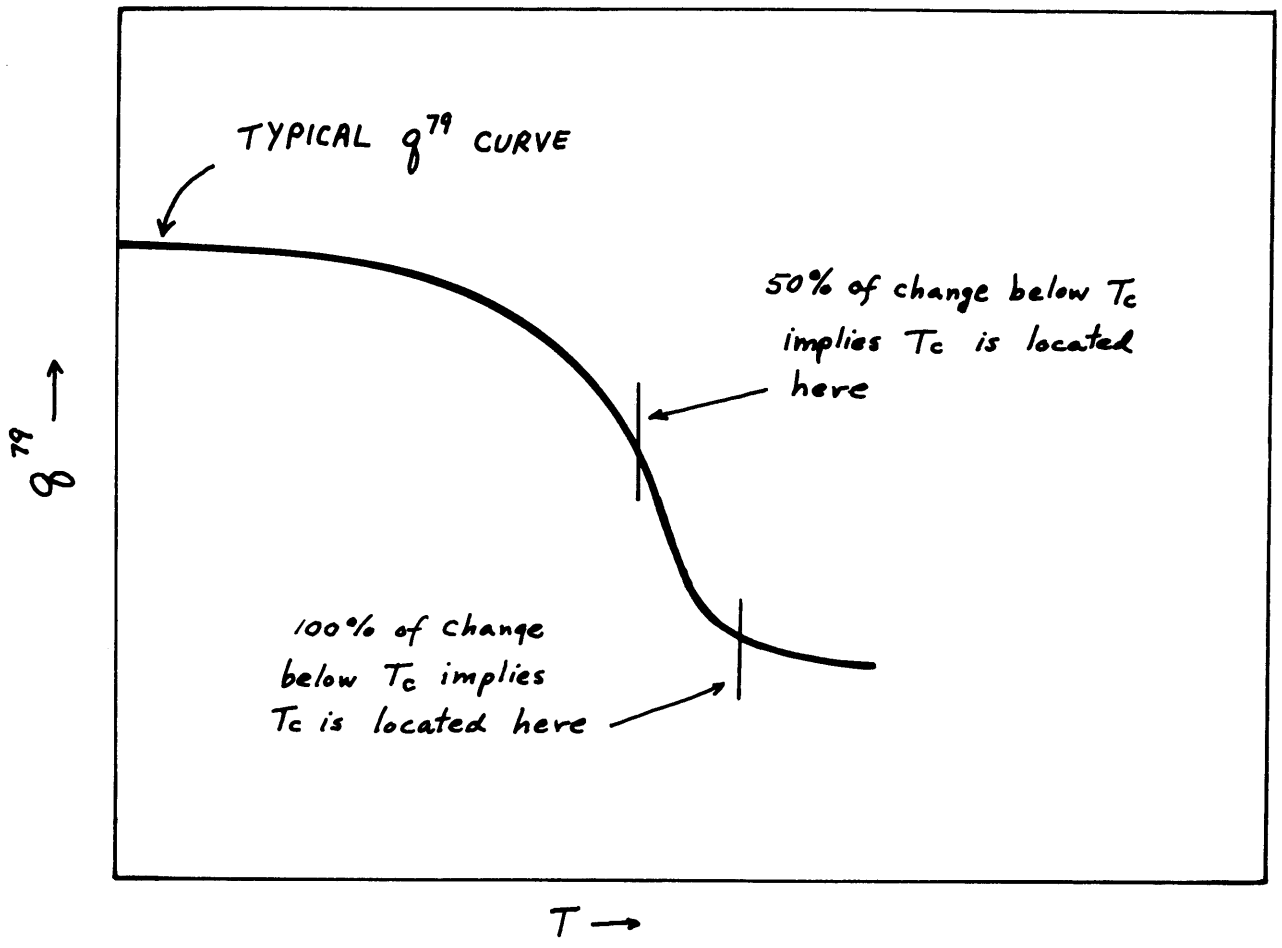

Fig. 17 Symmetry of thermal expansion peak about T_c, illustrated with q^{79}. If peak is symmetric, 50% of change occurs below T_c; if peak is totally asymmetric, 100% of change occurs below T_c.

6. Results of the Data Analysis

In this final section, we present first the temperature dependent Hamiltonian parameters obtained from our analysis; then we examine the interpretation of the parameters temperature dependences in terms of an anisotropic thermal expansion. Finally, we present our results for the temperature dependence of the magnetization from 4.2°K to 32.35°K as obtained from the chromium and bromine NMR data.

Final Temperature Dependent Hamiltonian Parameters For both the FULL and HALF solutions, two trial fits to the data were made, one using m(T) for the temperature dependent parts of the parameters, the other using $m(T)^2$. In the case of the FULL solution, the m(T) parameter curves provided a slightly better fit (about 2 Kc/sec better on the average) to the NMR frequencies than did the $m(T)^2$ curves; in the case of the HALF solution, the $m(T)^2$ curves were better. In Table VI, the two best sets of results are tabulated: the FULL solution - m(T) results; and the HALF solution - $m(T)^2$ results. Using the parameters for either solution and using the Cr^{53} NMR frequency to provide the temperature dependence of the internal field, all of the bromine NMR data between 4.2°K and 29.74°K can be fit extremely well. The low frequency lines are fit to within ±10 Kc/sec; the high frequency lines are fit to within ± 20 Kc/sec. Thus, by ascribing small, anomalous temperature dependences to the Hamiltonian parameters, the calculated frequencies can be brought into very close agreement with the experimental frequencies.

We now discuss the comparison between the results for the FULL and HALF solutions. The final Hamiltonian parameter curves are shown

Table VI

Final Temperature Dependent Hamiltonian Parameters

	FULL SOLUTION			HALF SOLUTION		
FUNCTION TYPE FOR BEST FIT	$p(T) = C_1 + C_2\ m(T)$			$p(T) = C_1' + C_2'\ [m(T)]^2$		
PARAMETER	C_1	C_2	UNITS	C_1'	C_2'	UNITS
q^{79}	101.252	0.313	Mc/sec	101.420	0.140	Mc/sec
θ	48.375	-0.325	degrees	48.435	-0.390	degrees
η	0.299	-0.007	—	0.298	-0.006	—
A	0.64870	—	KGauss/(Mc/sec)	0.64861	—	KGauss/(Mc/sec)
q^{79}/q^{81}	1.19704	—	—	1.19699	—	—

in Fig. 18a (q^{79}), Fig. 18b (η), and Fig. 18c (θ). We emphasize that in all cases, the plotted pair of curves for the FULL and HALF solutions probably bracket the correct curve. Note that in spite of the 0.1% difference between the two q^{79} curves at T_c, the two curves (FULL and HALF solutions) for each of the other parameters are <u>almost</u> identical. Examination of Table VI shows that the constants for the two θ curves agree to within 0.06 degrees, and the two sets of constants for η are within 0.001 of one another. The two values of A are essentially equal to one another <u>and</u> also equal to the constant parameter value of A in Table V (0.64869 KGauss/(Mc/sec)). As a final check on the results, we note that over the entire temperature range, the two values for the ratio, q^{79}/q^{81}, agree with one another <u>and</u> with the quadrupole moment ratio (1.19706) to well within the expected 0.01%.

In summary, then, we have determined with high precision (i) the magnitudes and temperature dependences of the components of the bromine electric field gradient tensor; (ii) the orientation of the internal field at a bromine site relative to the EFG principal axes; and (iii) the magnitude and temperature dependence of this internal field up to 29.74°K. We shall return to a further discussion of the temperature dependence of the internal field after a brief comment on the thermal expansion anomaly.

<u>Anisotropic Thermal Expansion</u> We suggested earlier that given the $CrBr_3$ crystal structure, it is reasonable to expect that most of the thermal expansion takes place in the lattice parameter along the c axis which describes the separation between the hexagonal sandwiches, while the inter-atomic spacings within one sandwich of the Br-Cr-Br sheets are

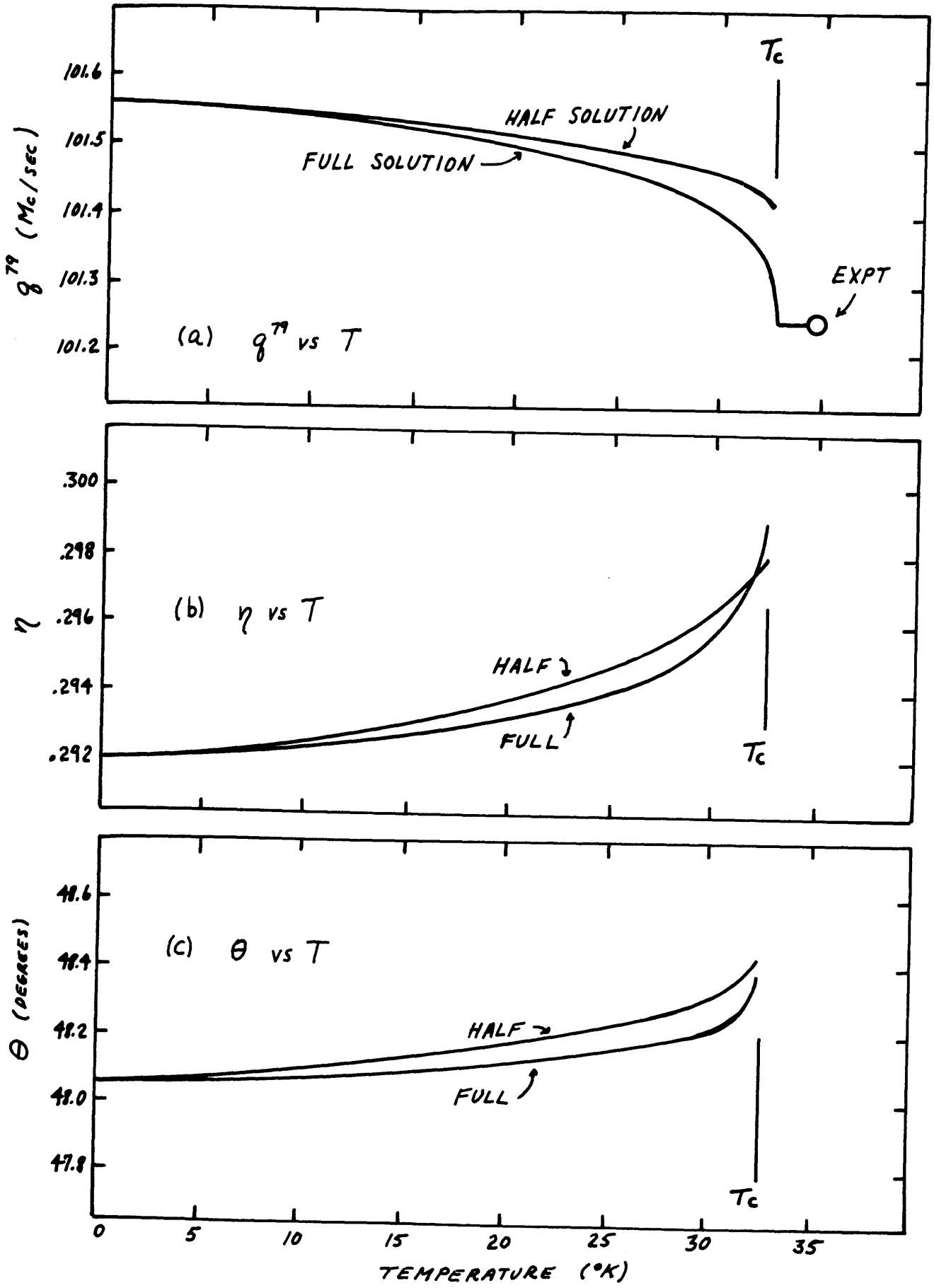

Fig. 18 Final temperature dependent Hamiltonian parameters.

constant. Highly anisotropic anomalies are not unknown. In a crystal of relatively high symmetry, MnF_2, a magnetic thermal expansion anomaly is present along one crystal axis while the lattice parameters perpendicular to this axis show almost no change.[27]

Our final Hamiltonian parameters provide two specific indications that the $CrBr_3$ thermal expansion anomaly has the described anisotropy. First, we find the value of A to be truly constant (to within a scatter amplitude of 0.05%). We recall from Eq. 4-29 that A really represents the ratio of the hyperfine field at a bromine site to the hyperfine field at a chromium site. Each of these hyperfine fields is related to the magnetization through a different mechanism; the chromium hyperfine interaction is direct while the bromine hyperfine interaction is transferred. The coefficient relating the field at the bromine site to the magnetization should be relatively sensitive to the Br-Cr nearest neighbor spacing within a sandwich. It would be a remarkable coincidence for the magnitudes of these two different hyperfine interaction mechanisms to remain exactly proportional (as indicated by the constant A) if the Br-Cr spacing were changing appreciably. Therefore, we expect that the within-the-sandwich interatomic spacings cannot be strong functions of temperature, and that the anomalous thermal expansion must not involve these particular dimensions.

A second indication of the anisotropic thermal expansion is found in a comparison of the temperature dependences of the strengths of the electric field gradients at the two sites. We recall from Table I of Chapter III that between 4.2°K and 29.74°K, the chromium quadrupole

splitting, q^{53}, decreased by about 5%. In distinct contrast, the total change in q^{79} over the entire anomalous region up to 34.5°K was only 0.3%. The chromium quadrupole interaction, because of the nearly octahedral symmetry of the nearest neighbor bromine atoms, has a relatively large contribution from the charge distributions of farther neighbors. Therefore q^{53} should depend on the between sandwich spacing more strongly than q^{79}, which has a large, dominant contribution from the charge distributions of the two nearest neighbor chromium atoms. If the lattice were expanding uniformly, we might expect the fractional shifts of q^{53} and q^{79} to be comparable; the fact that q^{53}, which is relatively more sensitive to the between sandwich spacing, is also more strongly temperature dependent supports our picture of the anisotropic thermal expansion.

Temperature Dependence of the Magnetization The reduced magnetization can be obtained from the magnitude of the hyperfine field by dividing by the magnitude of the hyperfine field at absolute zero. That is, for the hyperfine field at either a bromine or a chromium site,

$$m(T) = \frac{H(T)}{H(0)} \qquad (4\text{-}32)$$

Below 29.74°K, as we have seen repeatedly in this analysis, we obtain m(T) from the central Cr^{53} NMR frequency $\nu^{53}(T)$ by dividing by $\nu^{53}(0)$. This is equivalent to Eq. 4-32. We used Davis and Narath's[10] value for $\nu^{53}(0)$ equal to 58.099 Mc/sec to obtain the reduced magnetization between 4.2°K and 29.74°K from the Cr^{53} data. The results are

presented in the first part of Table VII.

Above 29.74°K, where the Cr^{53} line is no longer observable, we determine m(T) by calculating $H_{Br}(T)$ from the bromine NMR frequencies. The bromine NMR frequencies at a particular temperature are determined by the values of q^{79}, q^{81}, θ, η, and H_{Br} at that temperature. Since we have already determined the temperature dependences of four of these quantities, we can easily calculate the value of the one remaining quantity, $H_{Br}(T)$, from an experimental NMR frequency. Of course, the exact values of the parameters, q^{79}, q^{81}, θ, and η, depend slightly on the value of $H_{Br}(T)$ in that they depend slightly on the magnetization. Therefore we use an iterative method to obtain the exact value of $H_{Br}(T)$:

An estimate of m(T) is used to determine preliminary values of the four Hamiltonian parameters (q^{79}, q^{81}, θ, η) at each temperature. Then, since the only unknown quantity in the Hamiltonian is $H_{Br}(T)$, the calculation of $H_{Br}(T)$ from the bromine NMR frequency is straightforward. A new value of m(T) is then calculated from $H_{Br}(T)$ and $H_{Br}(0)$ (37.687 KGauss, obtained from $\nu^{53}(0)$ using the hyperfine constant A). If the new and original m(T) values differ, the calculation is repeated using the new m(T) value to determine the parameters. In practice, this procedure converged to within experimental error after one iteration.

The calculation of $H_{Br}(T)$ and m(T) was done for both the HALF solution parameters and the FULL solution parameters in order to evaluate the effect of the 0.1% difference in the two limiting values of $q^{79}(T_c)$. The results of these calculations are presented in the second part of Table VII. We also tabulate the percentage difference between these two

Table VII

Temperature Dependence of the $CrBr_3$ Magnetization

(a) Chromium Data

$$m(T) = \frac{\nu^{53}(T)}{\nu^{53}(0)} = \frac{H_{Cr}(T)}{H_{Cr}(0)}$$

$\nu^{53}(0) = 58.099$ Mc/sec[10] ; $H_{Cr}(0) = 241.48$ K Gauss

Temperature $T(^{o}K)$	Reduced Magnetization $m(T)$
0	1.00000
4.21	.98870
13.000	.91532
16.000	.87846
18.000	.85022
19.500	.82678
21.000	.80094
21.640	.78903
22.500	.77185
23.160	.75793
24.360	.73023
25.275	.70672
26.095	.68326
26.680	.66480
26.975	.65493
27.675	.62924
28.125	.61085
28.665	.5873
29.090	.5663
29.435	.5476
29.740	.5299

Table VII (Continued)

Temperature Dependence of the $CrBr_3$ Magnetization

(b) Bromine Data

$$m(T) = \frac{H_{Br}(T)}{H_{Br}(0)} \; ; \quad H_{Br}(0) = 37.687 \pm .003 \text{ KGauss}$$

TEMPERATURE ^{o}K	REDUCED MAGNETIZATION, m(T)		
T(^{o}K)	FULL Solution	HALF Solution	Difference (%)
29.970	.5152	.5149	0.06
30.085	.5076	.5074	0.04
30.360	.4878	.4875	0.06
30.550	.4733	.4730	0.06
30.760	.4556	.4552	0.09
30.915	.4415	.4413	0.05
30.946	.4387	.4385	0.05
31.003	.4332	.4329	0.07
31.039	.4296	.4293	0.07
31.085	.4253	.4246	0.16
31.140	.4192	.4190	0.05
31.188	.4141	.4139	0.05
31.234	.4090	.4088	0.05
31.279	.4045	.4036	0.22
31.323	.3988	.3986	0.05
31.350	.3957	.3947	0.25
31.797	.3359	.3334	0.75
31.898	.3191	.3164	0.85
31.996	.3011	.2981	1.0
32.046	.2926	.2893	1.1
32.098	.2811	.2776	1.3
32.147	.2691	.2653	1.4
32.198	.2567	.2527	1.6
32.245	.2440	.2398	1.7
32.294	.2304	.2259	2.0
32.349	.2130	.2080	2.4

determinations of m(T). The precision of either one of the m(T) results is about 1/5 of this difference at each temperature. Note that even at the highest temperature, 32.35^{o}K, the difference between the m(T) results for these two extreme cases is only 2.4%. We will show in the next chapter that this small uncertainty is not highly significant, even when using the data to make critical tests of various theories of ferromagnetism.

Chapter V

Critical Behavior

A. Introduction

A ferromagnet possesses long range order at low temperatures in the form of the spontaneous alignment of its spins. This alignment (i.e., the magnetization) decreases with increasing temperature until it vanishes altogether at the Curie temperature. Above the Curie temperature, there is no long range order - - the spins are oriented at random. Thus, the Curie temperature is the demarcation point between a low temperature region in which the long range order is a monotonically decreasing function of the temperature, and a higher temperature region where the long range order does not exist. Such a demarcation temperature is called a critical point.

In the vicinity of critical points, various thermodynamic quantities exhibit dramatic and sometimes anomalous behavior. There is a pattern in this "critical behavior", with analogous quantities in different systems having similar properties. In the ferromagnet, for example, the magnetization decreases rapidly to zero as $T \to T_c$, while the zero-field susceptibility and the specific heat diverge. In the liquid-vapor system, the difference between the liquid and vapor densities along the coexistence curve behaves like the magnetization, vanishing rapidly as $T \to T_c$. The isothermal compressibility, analogous to the zero-field susceptibility, diverges at T_c, as does the specific heat.

We have already encountered this critical behavior in our study of $CrBr_3$. We have seen explicitly that between $0.9\ T_c$ and T_c, the magneti-

zation decreases rapidly from over half of its saturation value to zero. The magnetic specific heat shows an anomalous peak at T_c;[23] and we have already commented in Chapter II on the enormous increase in the rf susceptibility of the samples near T_c.

None of this behavior is unexpected. The classical theories, the molecular field theory for magnetic systems, the van der Waals equation of state for the liquid-vapor system, predict such behavior; the qualitative features of these theories are quite satisfactory. Within the past few years, however, precise experimental studies of critical phenomena, using NMR and other techniques, have made it increasingly clear that the quantitative predictions of the classical theories are not correct. Also within the past few years, advances in theoretical methods, such as the method of Padé approximants,[29] have enabled theoretical calculations to be carried through for more sophisticated models. The concurrent advances on both fronts have made the study of critical phenomena an area of intense theoretical and experimental activity.

In this chapter, we shall examine the critical behavior of $CrBr_3$ in some detail. First, we attempt to fit the reduced magnetization data with various theoretically suggested expressions. The results of this analysis are discussed in the context of the present state of our knowledge of critical phenomena. Finally, an interpretation of the maximum in the rf loss near T_c is given.

B. Critical Behavior of the Magnetization -- Experimental

1. Simple Power Law

The most common expression used to describe the temperature

dependence of the reduced magnetization m(T) in the limiting case $T \rightarrow T_c$ is a simple power law.[40]

$$m(T) = D\left(1 - \frac{T}{T_c}\right)^{\beta} \tag{5-1}$$

In this expression, β, D, and T_c are constants, to be determined by fitting Eq. 5-1 to the experimental data.

The fitting procedure[18] is as follows. For a given β, estimates of T_c and D are made. Then the temperature deviations, ΔT, of the data from Eq. 5-1 are calculated from the formula

$$\Delta T = T_c \left\{\frac{1}{D} m(T)\right\}^{1/\beta} - (T_c - T) \tag{5-2}$$

If the data actually obey Eq. 5-1 as $T \rightarrow T_c$, and if the values of β, D, and T_c are the correct ones, then a plot of ΔT versus T will, as $T \rightarrow T_c$, level off at a constant value, $\Delta T = 0$. Of course, for reasonably well behaved data, virtually any power law can be made to satisfy Eq. 5-2 over a sufficiently small range of temperature. We have no a priori reasons for expecting a specific temperature range over which Eq. 5-1 must fit the data. In fact, it is convenient to treat the range which is found from the fit of the data as a measure of the extent of the "critical region". Therefore, we choose the "best fit" to be that set of β, D, and T_c which fit the data, within experimental scatter, over the widest temperature range below T_c.

This fitting procedure was carried through for the m(T) results for

both the FULL and HALF solutions (Table VIIb). The two sets of m(T) data are very nearly identical (the maximum difference between the two sets at any temperature is only 2.4%), but we wished to evaluate the maximum uncertainty in β, D, and T_c which might be introduced by our present inability to specify $q^{79}(T_c)$ to better than 0.1%. The plots of ΔT versus T for various values of β are shown in Figs. 19 and 20, and the results of the best fit analysis are presented in Table VIII.

There are several striking features to these results. First, we note that the constants, β, D, and T_c for the two solutions are almost indistinguishable. In fact, the range of uncertainty in all the quantities overlap from the FULL to the HALF solution. Therefore, the slight ambiguity in our determination of m(T) does not impede our study of the critical behavior. We can conclude that $\beta = 0.365 \pm 0.015$; $D = 1.32 \pm 0.07$; $T_c = 32.56 \pm 0.015^{\circ}K$; range is for $T/T_c \geq 0.96$ (approximate).

The value of β is in marked disagreement with the two previous determinations of β which have been made in magnetic insulators. Both determinations, using NMR techniques, were made by Heller and Benedek. In the antiferromagnet, MnF_2, they obtained $\beta = 0.333 \pm 0.003$;[7, 8] in the cubic ferromagnet, EuS, they found $\beta = 0.33 \pm 0.015$.[18] The conclusion that $\beta = 1/3$ in these two cases is almost irresistable. The departure of $CrBr_3$ from this 1/3 power law may be connected with the marked anisotropies in its crystal structure. This possibility is discussed at a later point.

The value of D obtained also departs significantly from the values found in MnF_2 and EuS. Heller and Benedek obtained 1.200 ± 0.004[7] and

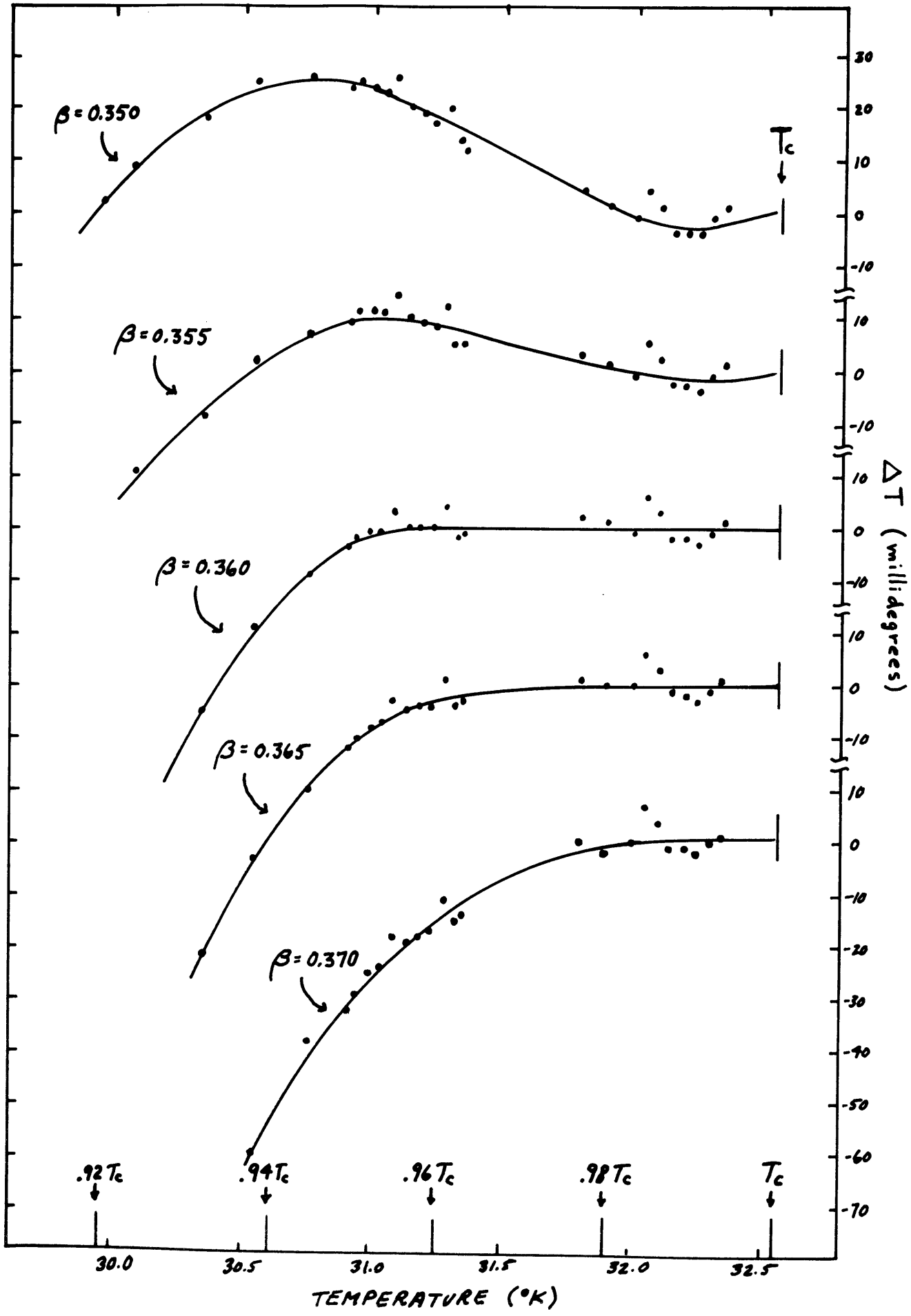

Fig. 19 Simple power law fit to reduced magnetization - FULL solution.

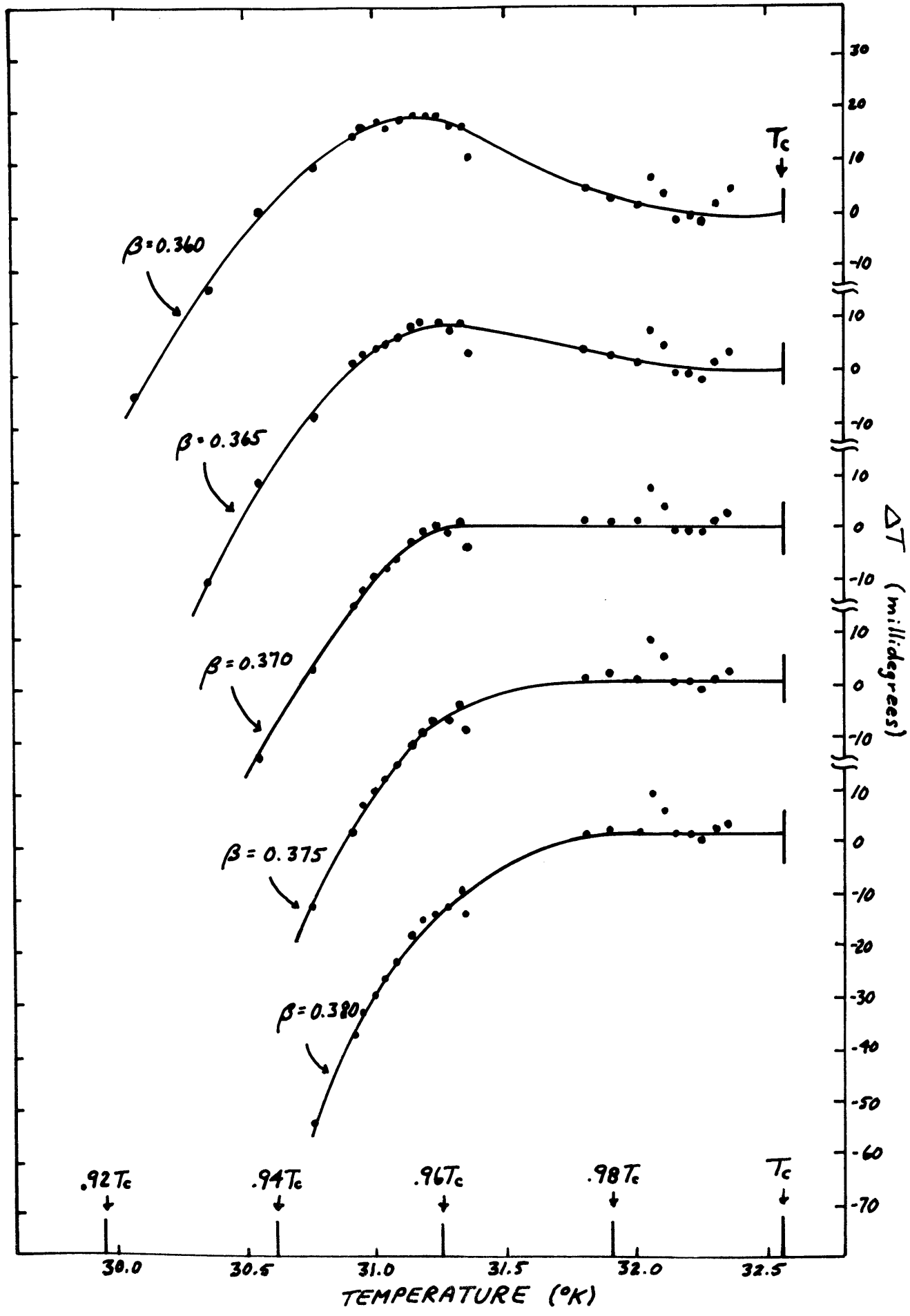

Fig. 20 Simple power law fit to reduced magnetization - HALF solution.

Table VIII

Simple Power Law Fit to Reduced Magnetization in Critical Region

	FULL Solution	HALF Solution
β	0.360 ± .010	0.370 ± .010
$T_c(^oK)$	32.565 ± .010	32.560 ± .010
D	1.29 ± .05	1.34 ± .05
Range	$0.95T_c$ -$0.993T_c$	$0.96T_c$ -$0.993T_c$

1.145 ± 0.02[18] in these two cases, while we find $D = 1.32 \pm 0.07$.

The value for T_c is in excellent agreement with the temperature at which Jennings and Hansen[23] found the maximum in the magnetic specific heat. The specific heat maximum occurs at $32.55^{\circ}K$ (no uncertainty estimate is available). We must point out that the agreement within 10 millidegrees in these two determinations of T_c may be fortuitous. It is unlikely that the two thermometer calibrations agree that closely. Nevertheless, the agreement is reassuring.

The range over which Eq. 5-1 fits the m(T) data in $CrBr_3$ ($T/T_c \geq 0.96$) is considerably smaller than the ranges in MnF_2 and EuS. In MnF_2, Eq. 5-1 was appropriate for $T/T_c \geq 0.90$, while in EuS, the corresponding figure was $T/T_c \geq 0.92$.

We must state at this time that we have published[30] a slightly different set of values for β, D, and T_c in $CrBr_3$. These values were based on our NMR data only up to $0.965\ T_c$. Using this restricted set of data, Eq. 5-1 could be fit to the m(T) data between $0.95\ T_c$ and $0.965\ T_c$ using a value of $\beta = 0.335 \pm 0.020$. Our subsequent experience with the data up to $0.993\ T_c$ has shown that the temperature range used for this result, $0.95\ T_c$ - $0.965\ T_c$, is simply too narrow to permit an accurate determination of the asymptotic behavior.

We have attempted to estimate the possible effects of a thermal expansion anomaly on our results for β and D. The theoretical form, Eq. 5-1, is expected to apply to a magnetic system of spins whose lattice separations are presumed constant as the temperature changes. A change in lattice parameter will have the effect of producing a temperature

dependent Curie point, since T_c is an implicit function of the lattice constant. We can make a very generous estimate of the amount by which the Curie temperature might shift with temperature. Assuming $\partial \ln T_c / \partial \ln V \approx 2$, where V is the volume, and assuming $\partial \ln q^{79} / \partial \ln V \approx 1$, the total observed shift in q^{79} between 4.2°K and 34.5°K would yield $\delta \ln T_c \approx 2\, \delta \ln q^{79} \approx 0.006$. Thus T_c might change by 1/2% between absolute zero and T_c. We made a huge overestimate of this effect by assuming that between $0.9\, T_c$ and T_c, the Curie temperature changed by 1%. The m(T) curve was re-analyzed using a Curie temperature changing linearly by this amount between $0.9\, T_c$ and T_c. The resulting constants, β and D, changed by less than their stated 5% experimental uncertainties. The reason for the apparent insensitivity of β and D to a temperature dependent T_c can be seen from Eq. 5-1. As long as $\partial \ln T_c / \partial \ln T << 1$, the explicit temperature dependence of m(T) represented by T is much greater than the implicit temperature dependence of m(T) represented by $T_c(T)$. As a result, even in our extreme example, where the value of $\partial \ln T_c / \partial \ln T$ was 0.1, the effect on β and D was small.

2. Buckingham's Function

Buckingham[31] has suggested that the simplest non-analytic form for the free energy of the liquid-vapor system would lead to a co-existence curve whose shape takes the form

$$\frac{x^2}{1 - \ln x} = D' (T_c - T) \qquad \text{as } T \to T_c \tag{5-3}$$

where D' is a constant, and x is the liquid-vapor density difference, suitably normalized. Edwards[33] has claimed that this function fits Heller and Benedek's magnetization data[18] on ferromagnetic EuS. We think his claim is unjustified because a 1/3 power law fits the EuS data between 0.92 Tc and 0.99 Tc, while Buckingham's functions fits the same data only above 0.97 Tc. Nevertheless, we attempted to fit the $CrBr_3$ data with an expression of the form of Eq. 5-3.

The result of this attempt was failure. For both the FULL and HALF solutions, Eq. 5-3 could fit the data only between 0.98 Tc and 0.993 Tc. This temperature range is so narrow that we can ascribe no significance whatever to the "fit". We conclude therefore, that Buckingham's function is not obeyed in $CrBr_3$.

Buckingham's function does not fit the sublattice magnetization data for MnF_2, either.[32] But it does seem to apply very well to the coexistence curves in the two kinds of liquid helium. Edwards[33] has found that Buckingham's function provides a significantly better fit than does a 1/3 or a 1/2 power law to his data[34] on the He^4 coexistence curve between 0.96 T_c and 0.994 T_c. Edwards[33] also states that Buckingham's function is appropriate for Sherman's smoothed data[35] on the He^3 coextence curve above 0.95 T_c.

Thus it appears that while Buckingham's function may be correct for the liquid-vapor systems, it is not correct for magnetic systems.

C. Critical Behavior of the Magnetization -- Discussion

In this section, we shall review briefly the state of our theoretical

understanding of the critical behavior of the magnetization in simple, symmetric spin systems. Then we shall discuss the extent to which these simple models are likely to apply to the strongly anisotropic spin system of $CrBr_3$.

1. The Heisenberg Exchange Hamiltonian and its Offspring

The force which couples together the spins in a magnetic insulating material and gives rise to long range cooperative phenomena is usually represented by the isotropic Heisenberg Exchange Hamiltonian:

$$\mathcal{H}_{Heis.} = -2 \sum_{i>j} J_{ij} \vec{S}_i \cdot \vec{S}_j \qquad (5\text{-}4)$$

The exchange constants J_{ij} are usually assumed to couple nearest neighbor spins only. If one expands the vector product of the two spins inside the sum and throws away the terms involving the x and y components of the spins, one obtains the Ising Hamiltonian:

$$\mathcal{H}_{Ising} = -2 \sum_{i>j} J_{ij} S_i^z S_j^z \qquad (5\text{-}5)$$

Finally, if one replaces S_j^z inside the sum by its time average, i. e. by the magnetization, one obtains the molecular field theory.

Of these three model Hamiltonians, calculations of the exponent β in the critical region have been performed only for the last two. The molecular field theory preducts $\beta = 1/2$; the Ising model in two dimensions

predicts $\beta = 1/8$;[36] the Ising model in three dimensions (cubic lattices) predicts $\beta = 5/16$, or 0.3125.[37]

We recall that for MnF_2 and EuS, the results strongly indicated that $\beta = 1/3$, a value which is close to but not equal to the value for the Ising model.

The results for $CrBr_3$, however, are inconsistent with every previous determination of β, either experimental or theoretical. It is important, therefore, to examine why $CrBr_3$ should behave so differently from what we might expect.

2. The $CrBr_3$ Hamiltonian

We think that the explanation for the unique critical behavior of the $CrBr_3$ magnetization may simply be that the $CrBr_3$ Hamiltonian is very different from those Hamiltonians which have been studied before. The particular features of the $CrBr_3$ Hamiltonian lacking in other Hamiltonians previously studied are: (i) There is a marked anisotropy in the strength of the $CrBr_3$ exchange coupling between different pairs of nearest neighbor spins. (ii) There is a large, strongly temperature dependent anisotropy field in $CrBr_3$; this field appears to have a non-zero value at T_c. We shall now discuss the $CrBr_3$ Hamiltonian, and these two features, in some detail.

Two central assumptions are made in writing down the $CrBr_3$ Hamiltonian. The first is a standard assumption about the basic magnetic interaction between spins. The basic magnetic interaction is assumed to be the isotropic Heisenberg Exchange Hamiltonian of Eq. 5-4. We must clarify the use of the word "isotropic" in this instance. Isotropic exchange

refers to the use of the vector product, $J(\vec{S}_i \cdot \vec{S}_j)$, to describe the interaction of a single pair of spins. All directions in the vector product are treated equivalently. Anisotropic exchange weights the z-component term in the vector product more heavily; i. e., anisotropic exchange results when one adds an Ising term to an isotropic term. The resultant pair interaction then has two terms: $J_1(S_i^z S_j^z) + J_2(S_i^x S_j^x + S_i^y S_j^y)$. While it is possible that anisotropic exchange may ultimately be recognized as being significant in the theory of magnetism, we shall restrict our attention to isotropic exchange, characterizing the interaction between a single pair of spins by one exchange constant.

The second assumption relates specifically to the crystal structure of $CrBr_3$. Following previous workers[1, 2, 10], we shall assume that the simplified magnetic lattice of Fig. 21 can be used with sufficient accuracy to describe $CrBr_3$. In the simplified lattice, the location of the planes of chromium ions has been translated (compare with Fig. 1) so that the chromium ions in each sheet are directly above and below the chromium ions in adjacent sheets. This simplified lattice has been used in the previous studies[2, 10] of spin wave theory in $CrBr_3$, and has appeared thus far to provide a sufficiently accurate representation of the spin system. The reason for making this simplification is that in the structure of Fig. 21, there are only two chromium atoms per unit cell (instead of four). The ions on the two inequivalent sites in Fig. 21 can be thought of as constituting two interlocking sublattices of indentical spins. Following Davis and Narath's notation,[10] we give the spins on the two sublattices different names, S and R, as shown in the Figure.

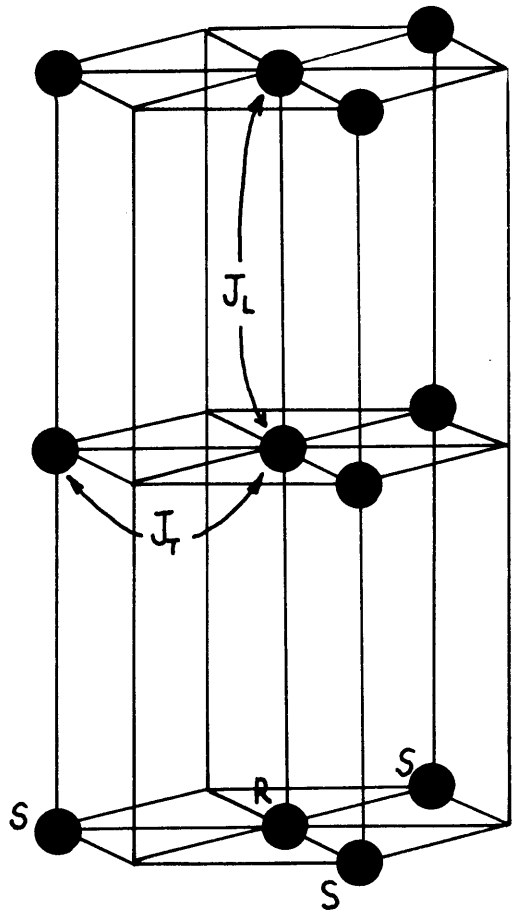

J_T, J_L ARE EXCHANGE CONSTANTS

S, R DENOTE TWO INTERLOCKING SUBLATTICES

Fig. 21 $CrBr_3$ simplified magnetic lattice.

The $CrBr_3$ Hamiltonian, with these two assumptions, is written

$$\mathcal{H}_{CrBr_3} = -2J_T \sum_{j,\epsilon} \vec{S}_j \cdot \vec{R}_{j+\epsilon} - J_L \left(\sum_{j,\epsilon'} \vec{S}_j \cdot \vec{S}_{j+\epsilon'} + \sum_{k,\epsilon'} \vec{R}_k \cdot \vec{R}_{k+\epsilon'} \right)$$

$$- g\mu_B H_A(T) \left(\sum_j S_j^z + \sum_k R_k^z \right) \qquad (5\text{-}6)$$

In the above expression, J_T and J_L are exchange constants (discussed below), ϵ denotes the vectors from a given spin site to nearest neighbors in the same hexagonal layer, ϵ' denotes the vectors to nearest neighbors in adjacent layers, and $H_A(T)$ is a magnetic anisotropy field.

Two exchange constants are used because not all pairs of nearest neighbor spins are equivalent. In particular, we distinguish between pairs lying within one plane (exchange constant J_T) and pairs situated one above the other in different planes (exchange constant J_L). This distinction, indicated schematically in Fig. 21, accounts for the two separate Heisenberg exchange sums in the Hamiltonian of Eq. 5-6. Davis and Narath[10] have determined values for the two exchange constants from a fit of their renormalized spin wave theory to the Cr^{53} NMR data up to 20^oK. They obtained $J_T/J_L = 16.6$, showing that the anisotropy in the strength of the exchange coupling is quite marked.

There is a second kind of anisotropy in $CrBr_3$, the magnetic anisotropy field, $H_A(T)$, which originates primarily in the residual spin orbit coupling.[1, 2, 41] The anisotropy is uniaxial with the crystal c axis being the easy direction of magnetization. Two independent measurements of the temperature dependence of the anisotropy field up to 40^oK have been made.[1, 41] The results of the two measurements agree in substance:

The anisotropy field is largest at absolute zero (6850 Gauss[41]), and decreases with increasing temperature. At 35°K, it appears to have a value of about 700 Gauss. Above 35°K, it continues to decrease, vanishing at about 40°K. If the temperature scales for these measurements are correct, then $H_A(T)$ has a relatively large magnitude at T_c. We shall comment below on the possible significance of this fact.

We now discuss the two basic differences between the $CrBr_3$ Hamiltonian of Eq. 5-6 and the Hamiltonians for which theoretical calculations have been made:

i. No calculations of the exponent β has yet been made for any lattice using the Heisenberg Hamiltonian. In the $CrBr_3$ Hamiltonian, the anisotropy in the strength of the exchange coupling adds one level of complexity beyond the simplest Heisenberg model. It would be interesting to see the result of an Ising model calculation for this anisotropic lattice. The success of the Padé approximant method in treating the Ising model in cubic lattices[37] suggests that such a problem might be soluble. It is indeed possible that the unique value of β found in $CrBr_3$ is simply due to its anisotropic crystal structure and its two very different exchange constants.

ii. No calculation of critical behavior has yet been made for any system which included a temperature dependent anisotropy field. In the $CrBr_3$ case, in particular, the anisotropy field is large, and if the measurements are to be believed, has a non-zero value at T_c. Such an anisotropy field tends to resemble a molecular field type of long range force. We wish to cite some recent theoretical findings which may indicate the possible significance of this anisotropy field.

Fisher[38], in a recent Letter dealing with quantum corrections to the critical point behavior of liquid-vapor systems, refers to some interesting work with the Ising model. If a small amount of a particular weak, long range interaction ("Kac potential") is added to the two-dimensional Ising Hamiltonian, then the predicted value of the exponent β changes from 1/8 to 1/2, apparently discontinuously.[39] Fisher cites other examples in which similar behavior is observed. The result of interest here can be summarized as follows: it is possible, by the addition of a small amount of a new interaction, to alter drastically the critical behavior which would be predicted by the dominant Hamiltonian, taken alone. A non-zero value of the anisotropy field in the vicinity of T_c does in fact resemble just such a new, long range interaction, and could conceivably account for the shift in the $CrBr_3$ value of β from the values observed in other systems.

In summary, then, on the experimental side, we find a definite departure of β from previously observed values. On the theoretical side, we can identify two distinct differences between the $CrBr_3$ Hamiltonian and the models treated thus far by theoreticians. The possibility that the unique exponent for $CrBr_3$ might be explained by either one of these differences should be investigated.

D. Maximum Loss Point

We have already referred to the enormous increase in the rf power absorption of the samples as $T \to T_c$. At one particular frequency (102 Mc/sec), this effect was studied closely. The maximum in the rf loss at 102 Mc/sec was found to occur 130 millidegrees above T_c; specifically $T_{max} = 32.69^{\circ}K$. A similar but smaller shift of the maximum loss point above T_c was observed in EuS.[32]

One can make a simple theory to account for the existence of this shift. The static zero-field susceptibility, χ_o, blows up right at T_c. The susceptibility to an oscillating rf magnetic field is proportional to the static susceptibility, but also includes a frequency dependent amplitude and a phase shift. Power absorption occurs only for that component of the resulting magnetization which is out of phase with the applied rf field. If the response to an applied field can be characterized by a single relaxation time, τ, then the term in the rf susceptibility which gives rise to the out of phase component is written[44]

$$\chi'' \propto \chi_o \frac{2\pi\nu\tau}{1+(2\pi\nu\tau)^2} \qquad (5\text{-}7)$$

The relaxation time, τ, gets very large also as $T \to T_c$. This can be seen qualitatively with a simple feedback model, similar to Heller's model for MnF_2.[19] If a spin configuration arises in which neighboring spins are parallel, the resulting parallel exchange field between neighboring spins tends to keep the spins lined up (the feedback). Well above T_c, the exchange field is too weak to counterect the rapid thermal fluctuations of the spins. Just above T_c, however, the exchange field is only slightly weaker than the thermal forces which tend to disorder the spins. Therefore, once the spins become lined up, the exchange field feedback prevents rapid decay to the disordered state. Thus the relaxation time tends to get very long. If one assumes that as $T \to T_c$, τ gets big faster than χ_o, it is trivial to show that for any finite frequency, there is a maximum in χ'' at a temperature slightly above the Curie point. The position of the maximum is expected to

be a very weak function of frequency. In fact, no frequency dependence of the maximum loss point was observed in EuS.[32] The frequency dependence was not studied in $CrBr_3$.

Chapter VI

Conclusions

We have discovered and identified Br^{79} and Br^{81} NMR lines in the ferromagnetic state of $CrBr_3$ which arise from the splitting of pure quadrupole resonances by a magnetic hyperfine field. From a study of these bromine NMR lines together with the Cr^{53} NMR lines we have determined the magnitudes and temperature dependences of the components of the electric field gradient tensors at both the chromium and bromine sites. We have also determined the temperature dependence of the magnetic hyperfine fields (i) at a chromium site up to 0.91 T_c, and (ii) at both bromine sites up to 0.993 T_c. From the temperature dependence of the hyperfine fields, we obtain the temperature dependence of the magnetization with high precision from 4.2°K up to 32.35°K (0.993 T_c). The data is sufficiently accurate to be valuable in testing spin wave renormalization theories to as high a temperature as may be desired. In addition, the critical behavior of the $CrBr_3$ magnetization is studied in some detail. A definite departure from the 1/3 power law is obtained. Two specific anisotropies in the magnetic coupling between chromium spins are suggested as possible origins of this departure.

We have also found that the NMR lines in ferromagnetic $CrBr_3$ are capable of being used as highly accurate, reproducible thermometers between 1.5°K and 29°K. The sensitivity is estimated to be 2 millidegrees or better over this temperature range. A preliminary calibration above 4.2°K, good to ± 0.02°K, is provided.

Finally, the temperature dependences of the bromine and chromium

electric field gradient tensor components suggest that there is an anisotropic thermal expansion anomaly at the $CrBr_3$ Curie point. Careful X-ray measurements on the crystal structure of $CrBr_3$ at temperatures near T_c would be most interesting. In concert with such measurements, determinations of the compressibility, the pressure dependence of the Curie temperature, and the pressure dependence of the pure quadrupole resonance frequencies would enable a detailed analysis of the observed electric field gradient tensor temperature dependences to be carried out.

References

1. I. Tsubokawa, J. Phys. Soc. Japan, 15, 1664 (1960).

2. A. C. Gossard, V. Jaccarino, J. P. Remeika, Phys. Rev. Lett., 7, 122 (1961); J. Appl. Phys., 33, 1187-S (1962).

3. V. Jaccarino and R. G. Shulman, Phys. Rev., 107, 1196 (1957).

4. R. G. Shulman and V. Jaccarino, Phys. Rev., 108, 1219 (1957).

5. G. B. Benedek and T. Kushida, Phys. Rev., 118, 46 (1960).

6. A concise summary of the study of the transferred hyperfine interaction in MnF_2 may be found in G. B. Benedek, Magnetic Resonance at High Pressure, (Interscience, New York, 1963) pp. 11-16.

7. P. Heller and G. B. Benedek, Phys. Rev. Lett., 8, 428 (1962).

8. P. Heller and G. B. Benedek, Proceedings of the International Conference on Magnetism, Nottingham, September 1964, (The Institute of Physics and The Physical Society, London, 1965), p.97.

9. Ralph W. G. Wyckoff, Crystal Structures, Second Ed., Vol. 2, (Interscience, New York, 1964) p. 45.

10. H. L. Davis and A. Narath, Phys. Rev., 134, A433 (1964).

11. S. D. Senturia, P. Heller, G. B. Benedek, Bull. Am. Phys. Soc., 8, 592 (1963).

12. R. G. Barnes and S. L. Segel, Phys. Rev. Lett., 3, 462 (1959).

13. H. van de Vaart, private communication.

14. A. C. Gossard, V. Jaccarino, E. D. Jones, J. P. Remeika, R. Slusher, Phys. Rev., 135, A1051 (1964).

15. G. K. White, Experimental Techniques in Low Temperature Physics, (Oxford University Press, London, 1959) p. 115.

16. G. B. Benedek and T. Kushida, Phys. Rev., 118, 46 (1960).

17. J. D. Litster, Ph.D. Thesis, MIT, 1965.

18. P. Heller and G. B. Benedek, Phys. Rev. Lett., 14, 71 (1965).

19. P. Heller, Ph.D. Thesis, Harvard University, 1963.

20. G. B. Benedek and T. Kushida, Rev. Sci. Instr., 28, 92 (1957).

21. J. Vanier, Metrologia, 1, 135 (1965).

22. T. Kushida, G. B. Benedek, and N. Bloembergen, Phys. Rev., 104 1364 (1956).

23. L. D. Jennings and W. N. Hansen, Phys. Rev., 139, A1694 (1965).

24. T. Kushida, J. Sci. Hiroshima Univ., A19, 327 (1955).

25. The values of the moments ratios used come from H. H. Brown and J. G. King, Phys. Rev., to be published.

26. F. C. Nix and D. MacNair, Phys. Rev., 60, 597 (1941).

27. D. F. Gibbons, Phys. Rev., 115, 1194 (1959).

28. D. S. Rodbell, L. M. Osika, P. E. Lawrence, J. Appl. Phys., 36, 666 (1965).

29. G. A. Baker, Phys. Rev., 124, 768 (1961).

30. G. B. Benedek, Proceedings of the Conference on Phenomena in the Neighborhood of Critical Points, National Bureau of Standards, Washington, D. C., 5-9 April 1965 (to be published).

31. M. J. Buckingham, Proceedings of the Conference on Phenomena in the Neighborhood of Critical Points (to be published).

32. P. Heller, private communication.

33. M. H. Edwards, Phys. Rev. Letters, 15, 348 (1965).

34. M. H. Edwards and W. C. Woodbury, Phys. Rev., 129, 1911 (1963).

35. R. H. Sherman, Phys. Rev. Letters, 15, 141 (1965).

36. C. N. Yang, Phys. Rev., 85, 808 (1952).

37. J. W. Essam and M. E. Fisher, J. Chem. Phys. 38, 802 (1963).

38. M. E. Fisher, Phys. Rev. Letters, 16, 11 (1966).

39. J. L. Lebowitz and O. Penrose, to be published.

40. M. E. Fisher, J. Math. Phys., 5, 944 (1964).

41. J. F. Dillon, Jr., J. Appl. Phys., 33, 1191-S (1962).

42. A more detailed discussion of the quadrupole interaction may be found in M. H. Cohen and F. Reif, "Quadrupole Effects in Nuclear Magnetic Resonance Studies of Solids", Solid State Physics, Vol. 5, Seitz and Turnbull, Ed.; (Academic Press, New York, 1957).

43. The energy level diagram of Fig. 15 has been drawn assuming that the algebraic sign of the $\gamma \vec{I} \cdot \vec{H}$ term in the Hamiltonian, $\mathcal{H}$, is positive instead of negative. This in no way changes the physical meaning of any results.

44. This result comes from a straightforward application of the Kramers-Kronig relation to a system with a simple relaxation time impulse response. A discussion of this procedure can be found in C. P. Slichter, Principles of Magnetic Resonance, (Harper & Row, New York, 1963) pp. 33ff.

Acknowledgements

In the preceeding pages, considerable use has been made of the pronoun "we". This was done partly as an editorial device, and partly as an indication of the extent of my reliance, throughout this work, on the consultation, advice, and encouragement of others.

My greatest debt is to Professor George Benedek, who suggested this problem and guided my endeavors throughout. The benefits of his insight into physics, his many suggestions and frequent encouragement, and his ability to ask the right questions, are most gratefully acknowledged.

Special thanks are also due to Professor Peter Heller, under whose tutelage I was first introduced to the art of experimental physics.

I wish to thank Dr. J. I. Harrison and Professor Alexander Smakula for kindly providing the samples so vital to our investigations. Professor John Wood wrote the preliminary computer programs, and made valuable suggestions on setting up the final data analysis method. The computations were carried out on the IBM 7094 computer at the MIT Computation Center.

I should also like to express my gratitude to my many associates, both graduate students and staff members, who have contributed to this work by providing helpful technical advice and by creating a stimulating and enjoyable environment in which to work.

The manuscript was expertly typed by Miss Carole Johnson. Her conscientious hard work is greatly appreciated.

Finally, I wish to thank the National Science Foundation for generous financial support during my graduate study.

Biographical Note

Stephen David Senturia was born in Washington, D. C., on May 25, 1940. With the exception of three years in Teaneck, N. J., he lived in Washington and attended the public schools through secondary school. In 1957, he entered Harvard College, starting out as a chemistry student, then changing his course of study to physics. In June 1961, he was graduated summa cum laude with a Bachelor of Arts in Physics. His academic honors include election to Phi Beta Kappa and Sigma Xi. From 1961 to the present, he has been a graduate student in physics at the Massachusetts Institute of Technology.

His professional experience consists of four summers as a research aide at the Johns Hopkins University - Operations Research Office, Bethesda, Maryland, a contract research agency for the Department of the Army; and two summers in the employ of the Shell Development Company, Houston, Texas, as a research physicist.

He was married to Alice Jean Werlin of Houston, Texas, on August 27, 1961. They have one son, Todd Alexander Senturia, born January 28, 1965.